Targeted Drug Delivery by Novel Polymer-Drug Conjugates
Containing Linkers Cleavable by Disease-associated Enzymes

by

Ying Chau
B.S. Cornell University, 1995
M.S. University of Pennsylvania, 1998

A dissertation submitted in partial fulfillment of the requirements
for the degree of Doctor of Philosophy
in the Department of Chemical Engineering
at the Massachusetts Institute of Technology
Cambridge, Massachusetts

MASSACHUSETTS INSTITUTE OF TECHNOLOGY
JUN 0 1 2005
LIBRARIES

Spring Term
2005
[June 2005]

Signature of author ..... May 16, 2005
Ying Chau
Department of Chemical Engineering

Certified by ..... May 16, 2005
Robert Langer
Institute Professor
Thesis Advisor

Accepted by .....
Daniel Blankschtein
Professor of Chemical Engineering
Chairman, Committee for Graduate Students

© 2005 Ying Chau

ARCHIVES

The author hereby grants to MIT permission to reproduce and to distribute publicly paper and electronic copies of this thesis document in whole or in part.

ABSTRACT

We have conceptualized a new class of polymer-linker-drug conjugates to achieve targeted drug delivery for the systemic treatment of cancer and other inflammatory diseases. The physiochemical properties of the polymer allow the conjugate to circulate longer in the body by minimizing renal and hepatic clearance, thereby improving the pharmacokinetics of the attached drugs. Traditionally, linkers are degraded by acidity or by some ubiquitous intracellular enzymes. We incorporate linkers that are sensitive to a specific extracellular enzyme whose overexpression is co-localized with the diseased tissue. The drug molecules remain inactive when attached to the polymer, thus preventing normal tissues from harmful side effects. When the conjugate is transported to the diseased area where there is a high level of the target enzyme, the linkers are cleaved to release the drugs at the specific site.

As an example, we designed and synthesized two generations of novel polymer-peptide-drug conjugates for the tumor-targeted delivery of chemotherapeutics. To allow for passive targeting and enhanced permeation and retention (EPR), dextran with a size greater than 6 nm was selected as the polymeric carrier. This biocompatible and biodegradable carrier was chemically modified to allow for conjugation with doxorubicin and methotrexate, two common chemotherapeutics with undesirable side effects. Since matrix-metalloproteinases (MMPs) are associated with a number of types of cancer and their functions are essential to disease progression, including degrading extracellular matrix, releasing angiogenic factors and activating growth factors, we explored the possibility of MMP-mediated drug release. The synthesis procedures combined solid phase and solution phase techniques to enable flexibility in the linker

design and in the charge modification of the polymer. This scaleable and robust process produced new conjugates that demonstrated excellent stability under physiological conditions and optimized sensitivity to enzymatic cleavage by MMP-2 and MMP-9.

The new conjugate, dextran-peptide-methotrexate, was assessed for its *in vivo* anti-tumor efficacy and systemic side effects. It was compared to free methotrexate and a similar conjugate, differing by an MMP-insensitive linker, at equivalent intraperitoneal dosages administered weekly. The MMP-sensitive conjugate resulted in effective inhibition of *in vivo* tumor growth in each of the two separate tumor models that overexpress MMP-2 and MMP-9 (HT-1080 and U-87). In contrast, free methotrexate resulted in no significant tumor reduction in the same models. Neither free methotrexate nor the conjugate caused any tumor inhibition in mice bearing RT-112, a slower-growing model which expresses significantly less MMP than HT-1080 and U-87 . The anti-proliferative effect of the drug contributed to the inhibition of tumor growth. Systemic side effects caused by the MMP-sensitive conjugates were tolerable. MMP-insensitive conjugates, though able to inhibit tumor growth, caused toxicity in the small intestine and bone marrow and the experiment was terminated after one injection.

We conducted a biodistribution study in HT-1080 bearing mice to investigate the targeting mechanism of the new conjugate. Independent of the linker sequence, passive targeting was evidenced by the prolonged plasma circulation and higher tissue accumulations of the conjugates in comparison with free methotrexate. The ratios of drug accumulation at the tumor versus the major site of side effects (small intestine) for both conjugates were enhanced by the EPR effects. The difference in the drug accumulation at the tumor site was insignificant between

conjugates with MMP-sensitive and MMP-insensitive linkers. We concluded that the tumor targeting effect of the dextran-peptide-methotrexate conjugate was dominantly due to passive targeting and EPR. The difference in the systemic side effects observed for the conjugates with different linkers was attributed to their varying susceptibility towards enzymes in normal tissues.

ACKNOWLEDGMENTS

I would like to express my gratitude to all who have helped me to complete my doctoral research. I am deeply indebted to my thesis advisor, Professor Robert Langer, whose inspiration, resourcefulness and confidence in me have made this thesis research possible. Throughout my years in Langer Lab, I have been benefited from the generosity and talents of numerous fellow students and postdoctoral scientists. They are also friends whom I share my joy from success and sadness from disappointment.

I am obliged to Professor Marsha Moses and Professor Dane Wittrup, my thesis committee members who have given me important inputs, in both my research project and career direction. I am thankful for the help of Dr. Sanyong Jon on the NMR analysis. I am grateful for the collaboration of Professor Robert Padera and Dr. Dipak Panigrahy in the animal studies. I have been privileged to mentor some bright undergraduate students. Particularly, the hard work of Frederick Tan and Natalie Dang has contributed significantly to this thesis. I also thank the technical support of Richard Cook of the Biopolymer Labs and the staff of Department of Comparative Medicines at MIT.

I am blessed with a wonderful family. My sister Judy and my brother-in-law Tak have encouraged me tremendously in times of despair. My parents and my in-laws have shown more than understanding, but absolute support and trust. Especially, I could not have completed my journey without my husband Philip who so patiently walks with me every day with his amazing love.

Lastly, I give thanks to God, who has given me guidance on things small and big, and has used this experience to shape me as His work.

"O Lord, you are our Father;

we are the clay, and you are our potter;

we are all the work of your hand."

Isaiah 64:8

TABLE OF CONTENTS

LIST OF TABLES

LIST OF FIGURES

LIST OF ABBREVIATIONS

Acronym	Definition of Acronym
BOC	N-t-butyloxycarbonyl
CM	varboxymethyl
DOX	doxorubicin
ECM	extracellular matrix
eq.	equivalent
FMOC	9-fluorenylmethyloxycarbonyl
H&E	hematoxylin and eosin
HPLC	high pressure liquid chromatography
HPMA	N-(2-hydroxypropyl)methylacrylamide
i.p.	intraperitoneal
i.v.	intravenous
k_{cat}	turnover rate of the substrate-enzyme complex to product
K_m	Michaelis-Menten constant
MMP	matrix-metalloproteinase
MT-MMP	membrane-type matrix metalloproteinases
MTX	methotrexate
MW	molecular weight

Acronym	Definition of Acronym
(Oligopeptides)	
GFLG	glycine- phenylalanine-leucine-glycine
GIVGPL	glycine-isoleucine-valine-glycine-proline-leucine
IPVG	isoleucine- proline-valine-glycine
IPVGLRSG	isoleucine- proline-valine-glycine-leucine-arginine-serine-glycine
LIG	leucine-isoleucine-glycine
LIGK	leucine-isoleucine-glycine-lysine
LKG	leucine-lysine-glycine
PVG	proline-valine-glycine
PVGLIG	proline-valine-glycine-leucine-isoleucine-glycine
PEG	polyethylene glycol
TIMP	tissue inhibitor of matrix-metalloproteinase

CHAPTER I : BACKGROUND

Original concept and current status of polymer-drug conjugates

The concept of a polymer-drug conjugate was first proposed by Ringsdorf in the 1970s[1]. His idea of how this drug delivery system can enhance targeting of small molecular drug molecules is illustrated in Figure I-1. With proper physiochemical characteristics, the polymer backbone can improve drug properties, for example, by enhancing drug solubility, preventing drug degradation and lowering excretory clearance. Drug molecules are attached to a polymer backbone via biodegradable linkers. Homing signals are covalently joined to the polymer to help localize the polymer-drug conjugates to the target site.

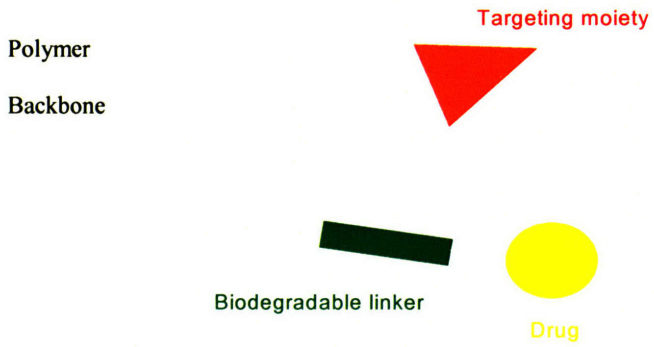

Figure I-1. Illustration of the concept of a polymer-drug conjugate proposed by Ringsdorf[1]

Since the inception of this concept, the development of polymer-drug conjugates, especially for anti-cancer targeting, has moved forwards with promising results. Notably, the idea has been popularized by the work of Kopecek's lab using HPMA as the polymeric carrier. PEG was first used to conjugate protein to increase solubility and stability, and to reduce immunogenicity. Later, PEG was useful for attaching small molecular weight chemotherapeutics for anti-cancer treatment. Listed in Table I-1 are a number of polymer-drug conjugates that have entered clinical trials. These conjugates all make use of the idea of passive targeting to achieve tumor-targeted delivery and this concept will be discussed further in a later section. In one of these conjugates, galatosamine is used as a homing signal to target to the liver tissue. Along the same line, ligands for recognizing cancer cells have been evaluated by numerous groups and the implementation of this idea will also be discussed. Last but not least, the linkage and its timely cleavage are essential for a successful application and we will explore the common linkages that have been developed in this field.

Table I-1. Polymer-drug conjugates in clinical trials as anticancer agents (adapted from source[2])

Compound	Company	Linker	Status of development
HPMA copolymer-doxorubicin	CRC/Pharmacia	Amide	Phase II
HPMA copolymer-galactosamine	CRC/Pharmacia	Amide	Phase I/II
HPMA copolymer-paclitaxel	Pharmacia	Ester	Phase I
HPMA copolymer-camptothecin	Pharmacia	Ester	Phase I
HPMA copolymer-platinate	Access Pharmaceuticals	Malonate	Phase I
Polyglutamate-paclitaxel	Cell Therapeutics	Ester	Phase II/III
Polyglutamate-camptothecin	Cell Therapeutics	Ester	Phase I
PEG-camptothecin	Enzon	Ester	Phase II

CRC, UK Cancer Research Campaign; HPMA, N-(2-hydroxypropyl)methylacrylamide; PEG, polyethylene glycol

Pharmacokinetics and drug targeting

Drug targeting is achieved when the biodistribution of drug is altered to favor its accumulation in the target tissue. This subject can be understood from the perspective of pharmacokinetics. Pharmacokinetics is the study of drug and drug carrier dynamics inside the body and includes the quantitative assessment of absorption, uptake, metabolism and elimination processes. Most relevant to our discussion is the concept of clearance, which is fundamental to pharmacokinetics. Figure I-2 presents a simple schematics showing inter-connected organs to illustrate this concept.

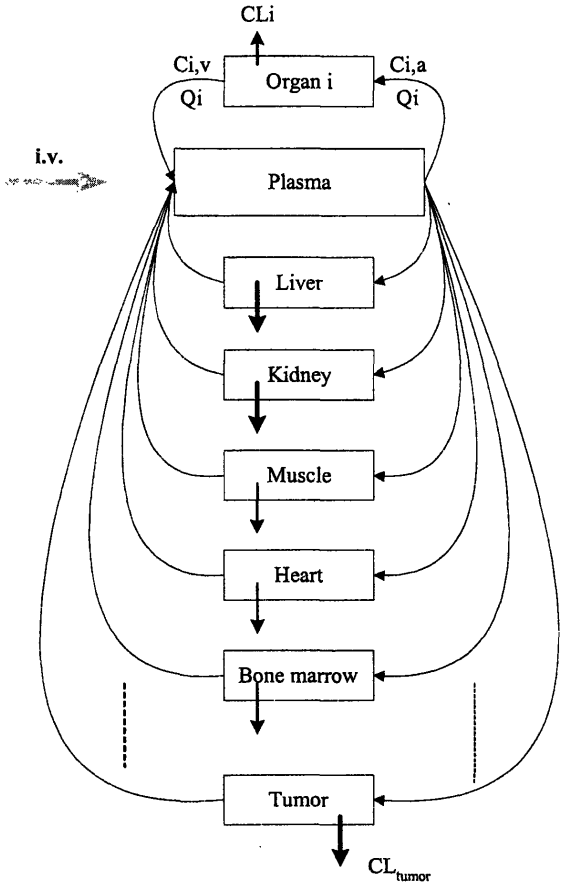

Figure I-2. Clearance concept in pharmacokinetics. Diagram is modified from the reference [3].

Clearance by a specific organ, CLi , is defined as

$$CL_i = \frac{Q_i(C_{i,a} - C_{,vi})}{C_{i,a}}$$

where Q_i is the plasma flow rate perfusing the organ. $C_{i,a}$ and $C_{i,v}$ are the drug carrier concentrations in the influent and effluent blood plasma respectively. Let α be the amount of drug molecules loaded per drug carrier, the rate of drug accumulation in a specific organ is given by

$$\frac{d X_i}{d t} = CL_i \alpha C_p$$

which, after integration is given by

$$X_i = CL_i \alpha \int_{t=o}^{\infty} C_p \, dt = CL_i \, \alpha \, AUC_p$$

Here, Xi is the total amount of drugs in a specific organ. AUC_p is called the "area under the concentration-time curve" for plasma. A useful parameter is the drug targeting ratio (F_{target}). It equals the fraction of the total dose delivered to the target site and can be calculated as:

$$F_{target} = \frac{CL_{target}}{CL_{total}}$$

When the drug targeting ratio is plotted against the two clearance terms, it is clear that a successful strategy involves maximizing CL_{tumor} while minimizing CL_{total} (Figure I-3). Physically, this means that the drug needs to be retained in the body for a long enough time to allow the drug to reach the target. Once at the target site, drugs must be taken up effectively by the target tissue.

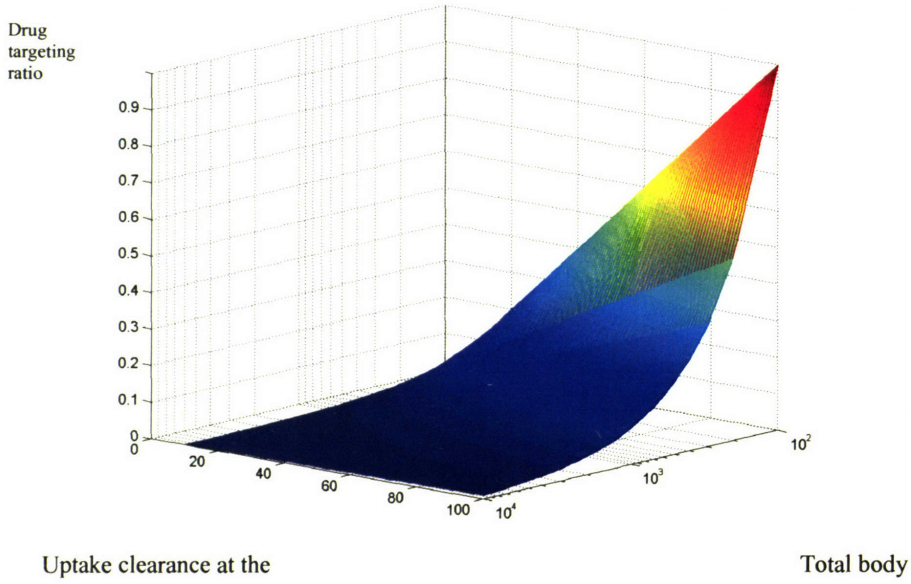

Figure I-3. Drug targeting ratio as a function of total body clearance and target site uptake clearance.

Passive targeting

The principle of passive targeting is to decrease total body clearance of the drug carrier (CL_{total}). As seen from the equation that defines drug targeting ratio in the last section, a prolonged circulation in the plasma results in a higher fraction of drug carriers distributed to the tumor tissues. The strategies to minimize body clearance have been considered for two organs, the liver and the kidney, because they are known to be the major elimination sites in the body. Hashida and Takakura reviewed the current status of the macromolecular drug delivery systems[3], relating the physiological features of these two organs to the clearance of macromolecules. The glomerular capillaries in the kidney are fenestrated, with the pores of radii estimated to be 20 –30 nm. The basement membrane acts as a size and charge barrier, which appears to hinder the transport of molecules greater than 6 nm. In the liver, the basement membrane is absent and the capillaries are characterized by having fenestrate of about 100 nm and endothelial gaps from 100 nm to 1000 nm. The passage of macromolecules is not restricted. However, cellular uptake of the drug carriers can be lowered by decreasing the interaction between the cells and the carriers . In general, cationic molecules tend to bind to the cell surface and strongly anionic species facilitate receptor mediated endocytosis. Consistent with these features, macromolecules with a size greater than approximately 6 nm (MW ≈50,000) have exhibited a marked inhibition on renal clearance. A slightly anionic carrier, for example, carboxymethyl dextran, appears to elicit the least uptake by liver cells and its hepatic clearance is similar to that of the fluid phase endocytosis (~10 μl/hr in mice).

In addition to controlling the size and the charge of a drug carrier, Kilbanov and a number of laboratories have demonstrated the benefit of a hydrophilic character using poly(ethylene-glycol) (PEG) stealths in liposomes [4], polymeric micelles [5] and nanoparticles [6, 7]. A layer of linear hydrophilic polymers surrounding the carrier in the core provides shielding effect by preventing absorption onto cell surface in the eliminating organ. With the appropriate molecular weight and density [8, 9], the PEG brush also inhibits proteins from interacting with the core through steric hindrance. These features prolong the circulation of polymeric carriers in the circulation, that is, CL_{total} is decreased.

Enhanced permeation and retention

In the targeted drug delivery for cancer treatment, the use of macromolecules as drug carriers confers one additional advantage because of tumor physiology [10]. Most capillaries in normal tissues are continuous, with small pore radii of 6.7-8.0nm and large pore radii of 20-28nm. They are found in the muscle, lung, skin, subcutaneous tissues, serous and mucous membranes. Transport of macromolecules (above approx. 7nm) across these capillaries is negligible. In contrast, tumor blood vessels are leaky and the basement membrane is absent. By observing the transvascular transport of liposomes in an implanted dorsal skin chamber of a tumor-bearing mouse, Jain's laboratory has determined the cutoff pore size of the tumor vessel to be 400-600 nm [11]. This features is attributed to the expression of angiogenic factors and various collagen degrading enzymes [12]. Large drug carriers can selectively reach malignant tissues while sparing most of the normal tissues. (Liver, bone marrow, spleen and kidney are the key exceptions.)

Maeda and coworkers observed that macromolecules are preferentially retained in tumor tissues. They conjugated the antitumor protein neocarzinostatin to a styrene and maleic acid copolymer (SMANCS) and reported a poor recovery of the conjugates in the effluent blood and lymph. This phenomenon was termed enhanced permeation and retention (EPR). The researchers explained that EPR was due to the augmented leakiness of the tumor blood vessels and the lack of a lymphatic drainage in the tumor tissue [13]. While the macromolecules could readily extravasate into the tumor tissue, their paths to return to the circulation were blocked.

Active Targeting

Active targeting is achieved by increasing the uptake clearance at the target site (CL_{target}). Using tumor targeting to illustrate this concept, the common approach is attaching specific ligands to the polymer that can bind to moieties expressed on tumor cells. Without these ligands, the conjugate is presumably internalized by tumor cells via fluid-phase endocytosis, a slow and non-specific cellular process. The targeting ligands enable the conjugate to be taken up via the route of receptor-mediated endocytosis.

There are several factors to be considered when employing this strategy. First, since tumor cells are derived from host cells, the surface antigens of tumor cells are never unique. The difference between the host and the tumor cells is the level of expression. Thus the antigen chosen should give enough selectivity between the tumor and the host tissues. Second, although a tight binding between the ligand and the antigen is essential, a high binding affinity may hinder even distribution[14]. This problem is more severe with a large polymer-drug conjugate. Jain has found that the pathophysiology of the solid tumor causes the build-up of a positive osmotic pressure[15]. The barrier to the movement deep into the tumor core increases with the size of the molecules[11]. Third, the antigen must be internalized by the tumor cells in order to facilitate receptor-mediated endocytosis. Antigen shedding has a negative impact on the effectiveness of this tumor-targeting approach.

The only polymer-drug conjugate with a targeting ligand in current clinical trial makes use of galactosamine (Table I-1)[16]. It is a molecule capable of binding to the asialoglycoprotein

receptor. The conjugate is designed to treat liver cancer. However, asialoglycoprotein receptors are not only expressed by hepatoma but also by normal hepatocytes.

Alternatively, α-fetoprotein is an example of a tumor-specific antigen. The antibody against this protein was attached to a polyglutamate-daunomycin conjugate to enhance the tumor-targeted delivery. The immunoconjugate was more effective than the polyglutamate-daunomycin conjugate in an *in vivo* study[17]. Besides using antibody or antibody fragments[18], the attachment of a metabolite represents another interesting class. Notably, Low's group has done extensive investigation in using folate as a targeting ligand. Folate is an essential vitamin for biosynthesis. Because of the rapid proliferative rate of cancer cells, folate receptors are overexpressed on their surfaces. Although HPMA-folate-fluorescein conjugates showed improved cellular uptake *in vitro*, HPMA-folate-doxorubicin conjugates were unable to show any significant targeting effect *in vivo*[19]. Other targeting ligands include transferrin, hormones, growth factors, carbohydrates and lectins.

Linkage Design

Review of linkers for intracellular release

After the polymer-drug conjugates reach the target tissues, a mechanism is needed to release covalently attached drugs such that the active components can exert their pharmacological properties. A frequently used approach relies on an intracellular drug release. The polymer-drug conjugates are presumably internalized into the cell by endocytosis. The intracellular trafficking process then proceeds to the endosomal and lysosomal pathways. The presence of proteases and the acidity of these compartments allow the design of linkers to be degraded intracellularly.

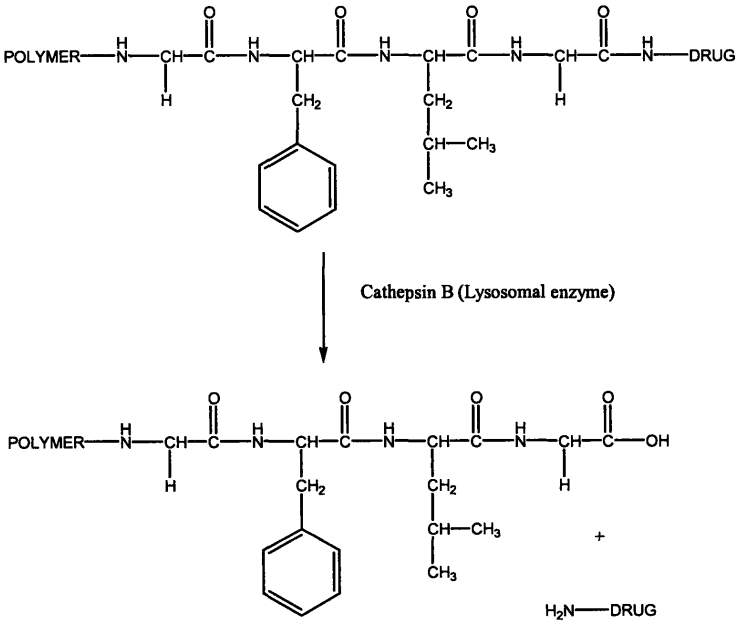

Figure I-4. A polymer-drug conjugate with a GFLG tetrapeptide linker for the lysosomal release of the attached drug[20]

A widely published tetrapeptide linker GFLG was designed by the labs of Kopecek and Duncan[20] (Figure I-4). The *in vitro* results showed that all the doxorubicin bound at the carboxyl end of tetrapeptide could be released in about 30 hours after mixing with rat liver lysosomal enzymes. The group found that cathepsin B was primarily responsible for the enzymatic cleavage[21]. The rate of cleavage depended on the composition of the peptide. In contrast to GFLG, GG is the control peptide that remained uncleaved in the presence of lysosomal enzymes[22]. Harada compared glycine-containing oligopeptides of different lengths for their susceptibility to be cleaved by lysosomal enzymes, showing that Gly-Gly-Gly was a linker that was capable of liberating bound camptothecin from the carboxymethyl dextran carrier through the action of cathepsin B. The study also indicated the dependence of enzymatic recognition on the length of the glycine sequence [23].

The pH drops from 7.5 to about 5—6 in endosomes and about 4—5 in lysosomes. This suggests an acid- sensitive linker should provide an avenue for intracellular release. The two types of linkage used in this category are the hydrazone and cis-aconityl linkers. They are both relatively stable in physiological pH and are capable of liberating the bound drugs at low pH. The mechanisms of drug release are shown in Figure I-5 and Figure I-6. The hydrazone linkage has a half-life of about 1—2 days at pH 5—6 whereas less than 20% of the linkage was broken over 30 days at pH 7.5 [24, 25]. Examples of polymer-drug conjugates containing the hydrazone linkage are HPMA-doxorubicin, PEG-doxorubicin, PEG-paclitaxel, polyglutamate-streptomycin and dextran-strptomycin[26]. The cis-aconityl linkage has a half-life of 3 hours at pH 4.0 and 96

hours at pH 7.5 [27]. Examples using this linkage include poly(aminopropyl)dextran-daunorobicin, aliginate-daunomycin, chitosan- adriamycin and HPMA-doxorubicin[26].

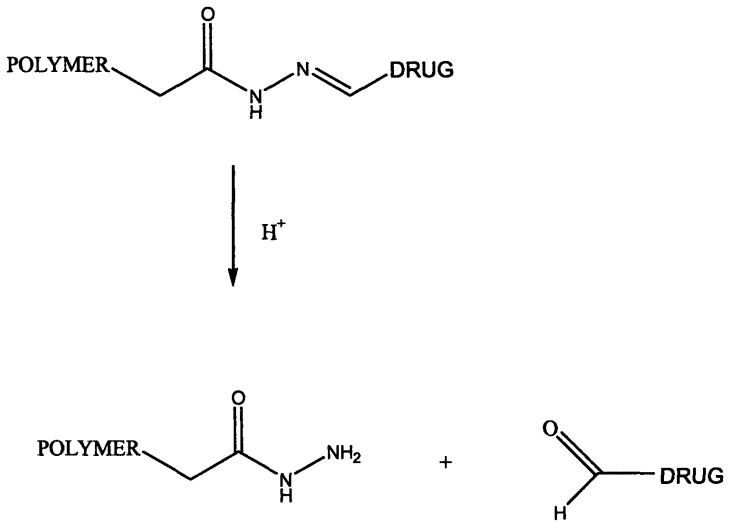

Figure I-5. Acid-triggered drug release from a polymer-drug conjugate containing a hydrazone linkage

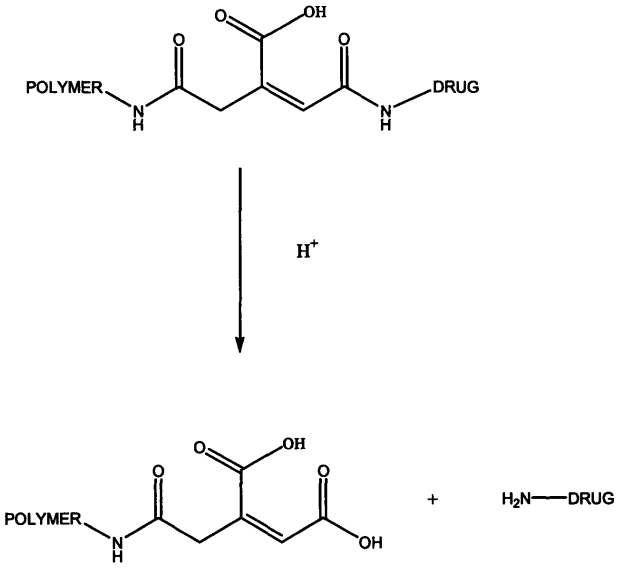

Figure I-6. Acid-triggered drug release from a polymer-drug conjugate containing an cis-aconityl linkage.

Linkers in this group only target the drugs to be released inside cells, but do not differentiate cells in the target tissue from normal tissues.

Review of linkers for extracellular release

In an approach called ADEPT (Antibody-Directed Enzyme Prodrug Therapy), drug release from polymer-peptide-drug conjugates is mediated by a foreign enzyme, which is first targeted to the tumor tissue by linking to a tumor-specific antibody [28] [29]. One limitation of this approach is the immunogenicity of the antibody-enzyme conjugate. Likewise, it is also necessary to ensure that the enzyme introduced is cleared from the blood stream prior to the injection of the polymer-drug conjugate.

A similar approach as ADEPT is termed PDEPT (Polymer-Directed Enzyme Prodrug Therapy) [30, 31]. Injection of polymer -drug conjugates is followed by the administration of polymer-enzyme conjugates. A polymer-enzyme conjugate consists of a "foreign" enzyme and tends to localize to tumor tissue due to EPR. The linker in the polymer-drug conjugate is designed for cleavage by the "foreign" enzyme. Again, the introduction of a foreign enzyme faces the potential problems of immunogenicity.

Proposal of linkers for disease-associated-enzyme-mediated release

In the design of a new polymer-drug conjugate, we explore the possibility of drug release via the mediation of an intrinsic enzyme in the extracellular space. Our idea is motivated by the fact that the microenvironment of a disease is shaped by the overexpression of extracellular enzymes, that are either secreted or membrane bound. Especially, progression of an inflammatory disease, such as cancer, arthritis and cardiovascular disease, is correlated with the proteolytic events of specific enzymes. Most of these enzymes are proteases and have preferred substrates. The substrate specificity of a particular enzyme can be deduced from the study of its natural substrates or from the screening of synthetic substrates. A peptide linker mimicking the enzyme substrate between the drug molecule and the polymeric carrier can theoretically provide a useful drug release mechanism and improve the extent of active targeting. As an example, a partial list of tumor-associated enzymes and their substrate specificities are shown in Table I-2. This information can potentially be applied for the design of a linker in a tumor-targeted drug delivery system.

Table I-2. Partial list of tumor-associated protease and their substrate specificities

Protease	Class	Substrate specificity	Comments	References
Prostate specific antigen (PSA)	Serine	HSSKLQ↓ (most selective) SS(Y/F)Y↓S(G/S) (most sensitive)	Chymotrypsin-like substrate specificity. Uniquely expressed by prostate glandular cells. Elevated level in prostate carcinoma. Secreted by PC-82 human prostate tumor model	32, 33
Human kallikrein 2 (hk2)	Serine	(Q/E)(R/K/H)R↓LXY (cleavage sites in semenogelin I and II) PFR↓	Trypsin-like substrate specificity. Uniquely expressed by prostate glandular cells. Elevated level in prostate carcinoma. Activate PSA and uPA. Cleave fibronectin	34
Urokinase-type plasminogen activator (uPA)	Serine	KKSPGR↓VVGGSVAAH (sequence of plasminogen) GPR↓ GPK↓	Chymotrypsin family. Overexpressed in a number of epithelial cancers. Involved in tumor-associated fibrolysis, associated with malignancy.	35 36 37 38
Fibroblast activating protein α (FAPα)	Serine	Collagenolytic activity-sequence specificity not determined Dipeptidyl peptidase- AP↓	Cell surface antigen of reactive tumor stromal fibroblasts in epithelial cancers or granulation tissue during wound healing. Degrade ECM. Normal tissues are FAP negative.	39
Meprin α	Metallo (Zn^{++})	RPPGF↓SPFR (sequence of bradykinin)	Expressed normally in intestinal and kidney epithelial cells. α is secreted or forms a membrane-bound tetramer with β subunits. Elevated levels of meprin observed in colon carcinoma. Degrade ECM.	40 41
Meprin β	Metallo (Zn^{++})	YEE↓EEI SNFD↓DY WM↓ DF		42
MMP-2 and MMP-9	Metallo (Zn^{++})	Pro-Leu-Gly↓Met-Trp-Ser	Extracellular proteases overexpressed in a number of epithelial cancers. Degrade type IV collagen	43
MT1-MMP	Metallo (Zn^{++})	PLP↓L	Membrane bound enzymes involved in the activation of MMP-2. Found in a number of cancer types. Constitutively activated.	44 45
Cathepsin B	Cystein	RR↓ FR↓	Lysosomal enzymes normally present intracellularly. Broad substrate selectivity. Secreted or membrane bound for some cancer cells (E.g. Cathepsin B in B16 melanoma and colon carcinoma; Cathepsin L in lung cancer cells) May degrade ECM.	46 47 48
Cathepsin L	Cystein	FR↓		49 48

Enabling technologies

To build a polymer-conjugate with a protease-sensitive linker, identifying the substrate specificity and synthesizing the peptide sequence are two major steps. Examining the natural substrates can give some information on the consensus sequence. But more direct screening

methods to yield the optimum sequences have emerged with the advance of experimental tools in molecular biology and in chemical synthesis.

Matthews and Wells have derived a method, called "substrate phage display", to perform rapid screening for a large number (on the order of 10^7) of protease substrates[50]. Using this approach, peptide substrates have been found for a number of proteases, for example, plasmin[51], tissue-type plasminogen activator[52], prostate-specific antigen[33] and membrane type-1 matrix metalloproteinase[45]. This method can be modified to select the optimal sequence for any tumor-associated enzyme of interest.

The methodology for substrate phage display is illustrated in Figure I-7. Each phagemid codes for a phage coat protein, a tether and a protease substrate sequence in between. To create a phage library, the substrate sequence is randomized by site-directed mutagenesis. Each fusion protein is displayed on the surface of a phage particle. For screening, the phage particles were incubated with the protease of interest. The entire digest is then captured by the affinity support. Phage particles with resistant sequences remain bound via the tether. The tether can be an epitope for a monoclonal antibody, a histidine tag or a protein-binding peptide. The phage with a labile peptide sequence is released. The phage with a resistant sequence can be subsequently released with elution conditions that disrupt the binding of the tether with the affinity support. Phages with desired sequences, either labile or resistant to the protease of interest, are propagated in bacteria and the cycle is repeated for enrichment. The incubation condition can be changed to vary the stringency of the screening criteria. For example, a phage that can be released at lower

protease concentration or after shorter incubation time displays a substrate sequence that is more labile.

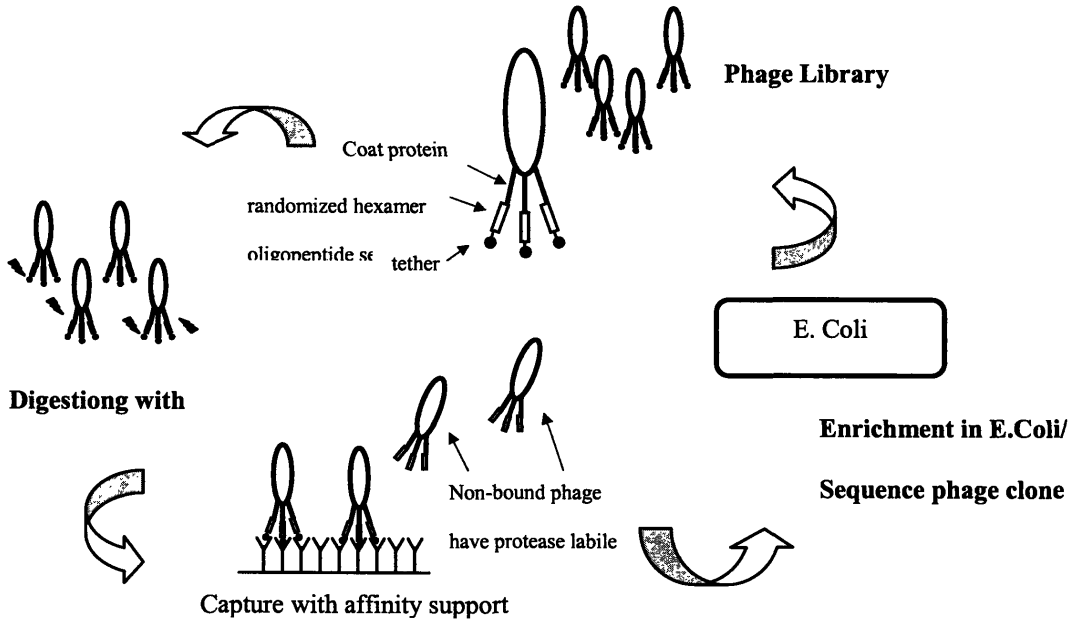

Figure I-7. Illustration of substrate phage display methodology for searching a protease-sensitive sequence

Chemical synthesis of the peptide sequence has been made more facile with the advance of solid phase peptide synthesis (SPPS). This methodology was first proposed by Merrifield in the 1960s[53]. Since then, this robust process has been improved with automation to allow the synthesis of peptides of any sequence in a short time without intensive manual labor. The most commonly employed routine nowadays uses FMOC synthesis sequence. The process flow is illustrated in Figure I-8. The keys to the success of the repeated couplings are high step yields and orthogonal protection groups. In solid phase synthesis, a large excess of reactants can be used at each chain lengthening step to force a high yield. Unreacted residues can be washed off

easily. In FMOC synthesis, the FMOC group for protecting the N-terminal is base-labile whereas the protecting groups on the side chains are acid-labile. The side groups can stay protected during the addition of a new amino acid to avoid any side reaction. At the end, the entire peptide sequence is cleaved and all side groups are deprotected using a strong acid.

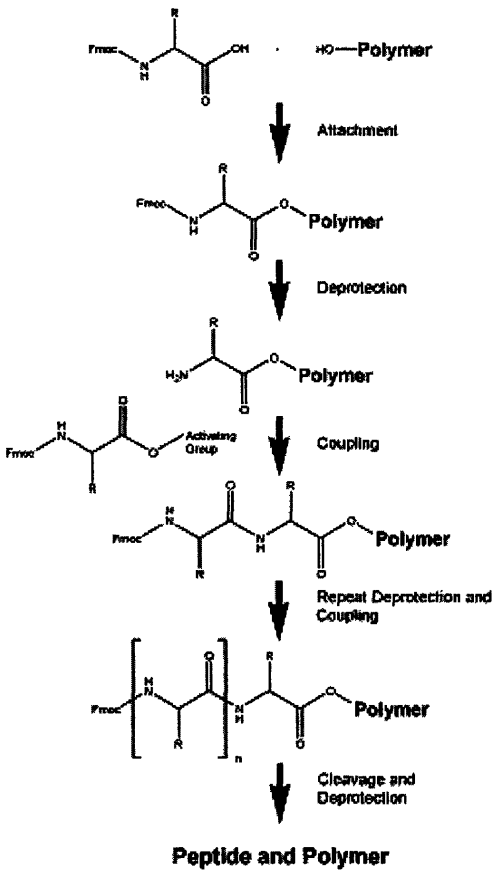

Figure I-8. A process flow chart of solid phase peptide synthesis employing FMOC chemistry. (adapted from www.anaspec.com)

In addition to synthesis of the sequence of interest, SPPS has been used as a tool in combinatorial chemistry to identify consensus sequences labile to proteases. After generating a peptide library with SPPS, Turk identified the substrate specificities of various

metalloproteinases using the methods illustrated in Figure I-9. By keeping scores of all possible amino acids at each of the substrate positions from P4 to P4', the consensus peptide sequences were found[54].

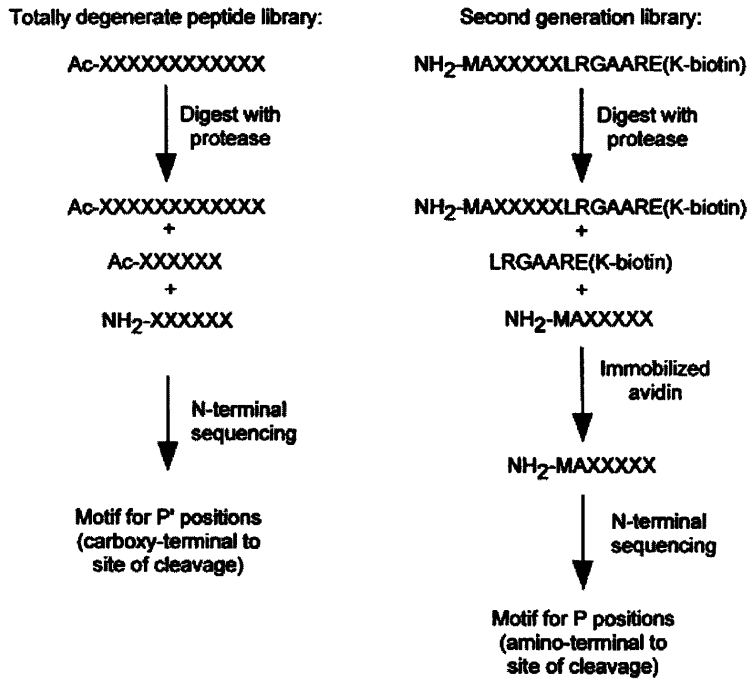

Figure I-9. Methodology for identifying protease substrate specificity from a peptide library (The chart is extracted from reference[54])

References

1. Ringsdorf H. Structure and properties of pharmacologically active polymers. *J. Polymer Sci. Polymer Symp.* 1975;51:135-53.

2. Duncan R. The dawning era of polymer therapeutics. *Nature Reviews Drug Discovery* 2003;2(5):347-60.

3. Hashida M, Takakura Y. Pharmacokinetics in Design of Polymeric Drug-Delivery Systems. *Journal of Controlled Release* 1994;31(2):163-71.

4. Klibanov AL, Maruyama K, Torchilin VP, Huang L. Amphipathic Polyethyleneglycols Effectively Prolong the Circulation Time of Liposomes. *Febs Letters* 1990;268(1):235-37.

5. Yokoyama M, Okano T, Sakurai Y, Ekimoto H, Shibazaki C, Kataoka K. Toxicity and Antitumor-Activity against Solid Tumors of Micelle-Forming Polymeric Anticancer Drug and Its Extremely Long Circulation in Blood. *Cancer Research* 1991;51(12):3229-36.

6. Gref R, Minamitake Y, Peracchia MT, Trubetskoy V, Torchilin V, Langer R. Biodegradable Long-Circulating Polymeric Nanospheres. *Science* 1994;263(5153):1600-03.

7. Gref R, Domb A, Quellec P, Blunk T, Muller RH, Verbavatz JM, Langer R. The Controlled Intravenous Delivery of Drugs Using Peg-Coated Sterically Stabilized Nanospheres. *Advanced Drug Delivery Reviews* 1995;16(2-3):215-33.

8. Gref R, Luck M, Quellec P, Marchand M, Dellacherie E, Harnisch S, Blunk T, Muller RH. 'Stealth' corona-core nanoparticles surface modified by polyethylene glycol (PEG): influences of the corona (PEG chain length and surface density) and of the core composition on phagocytic uptake and plasma protein adsorption. *Colloids and Surfaces B-Biointerfaces* 2000;18(3-4):301-13.

9. VertutDoi A, Ishiwata H, Miyajima K. Binding and uptake of liposomes containing a poly(ethylene glycol) derivative of cholesterol (stealth liposomes) by the macrophage cell line J774: Influence of PEG content and its molecular weight. *Biochimica Et Biophysica Acta-Biomembranes* 1996;1278(1):19-28.

10. Jain RK. Transport of Molecules in the Tumor Interstitium - a Review. *Cancer Research* 1987;47(12):3039-51.

11. Yuan F, Dellian M, Fukumura D, Leunig M, Berk DA, Torchilin VP, Jain RK. Vascular-Permeability in a Human Tumor Xenograft - Molecular-Size Dependence and Cutoff Size. *Cancer Research* 1995;55(17):3752-56.

12. Maeda H, Wu J, Sawa T, Matsumura Y, Hori K. Tumor vascular permeability and the EPR effect in macromolecular therapeutics: a review. *Journal of Controlled Release* 2000;65(1-2):271-84.

13. Matsumura Y, Maeda H. A New Concept for Macromolecular Therapeutics in Cancer-Chemotherapy - Mechanism of Tumoritropic Accumulation of Proteins and the Antitumor Agent Smancs. *Cancer Research* 1986;46(12):6387-92.

14. Graff CP, Wittrup KD. Theoretical analysis of antibody targeting of tumor spheroids: Importance of dosage for penetration, and affinity for retention. *Cancer Research* 2003;63(6):1288-96.

15. Jain RK. 1995 Whitaker lecture: Delivery of molecules, particles, and cells to solid tumors. *Annals of Biomedical Engineering* 1996;24(4):457-73.

16. Seymour LW, Ferry DR, Anderson D, Hesslewood S, Julyan PJ, Poyner R, Doran J, Young AM, Burtles S, Kerr DJ. Hepatic drug targeting: Phase I evaluation of polymer-bound doxorubicin. *Journal of Clinical Oncology* 2002;20(6):1668-76.

17. Tsukada Y, Kato Y, Umemoto N, Takeda Y, Hara T, Hirai H. An Anti-Alpha-Fetoprotein Antibody Daunorubicin Conjugate with a Novel Poly-L-Glutamic Acid-Derivative as Intermediate-Drug Carrier. *Journal of the National Cancer Institute* 1984;73(3):721-29.

18. Lu ZR, Kopeckova P, Kopecek J. Polymerizable Fab ' antibody fragments for targeting of anticancer drugs. *Nature Biotechnology* 1999;17(11):1101-04.

19. Lu YJ, Low PS. Folate-mediated delivery of macromolecular anticancer therapeutic agents. *Advanced Drug Delivery Reviews* 2002;54(5):675-93.

20. Duncan R, Cable HC, Lloyd JB, Rejmanova P, Kopecek J. Polymers Containing Enzymatically Degradable Bonds .7. Design of Oligopeptide Side-Chains in Poly N-(2-Hydroxypropyl)Methacrylamide Co-Polymers to Promote Efficient Degradation by Lysosomal-Enzymes. *Makromolekulare Chemie-Macromolecular Chemistry and Physics* 1983;184(10):1997-2008.

21. Rejmanova P, Kopecek J, Pohl J, Baudys M, Kostka V. Polymers Containing Enzymatically Degradable Bonds .8. Degradation of Oligopeptide Sequences in N-(2-Hydroxypropyl)Methacrylamide Co-Polymers by Bovine Spleen Cathepsin-B. *Makromolekulare Chemie-Macromolecular Chemistry and Physics* 1983;184(10):2009-20.

22. Duncan R, Hume IC, Yardley HJ, Flanagan PA, Ulbrich K, Subr V, Strohalm J. Macromolecular Prodrugs for Use in Targeted Cancer-Chemotherapy - Melphalan Covalently Coupled to N-(2-Hydroxypropyl) Methacrylamide Copolymers. *Journal of Controlled Release* 1991;16(1-2):121-36.

23. Harada M, Sakakibara H, Yano T, Suzuki T, Okuno S. Determinants for the drug release from T-0128, camptothecin analogue-carboxymethyl dextran conjugate. *Journal of Controlled Release* 2000;69(3):399-412.

24. Rodrigues PCA, Scheuermann K, Stockmar C, Maier G, Fiebig HH, Unger C, Mulhaupt R, Kratz F. Synthesis and in vitro efficacy of acid-sensitive poly(ethylene glycol) paclitaxel conjugates. *Bioorganic & Medicinal Chemistry Letters* 2003;13(3):355-60.

25. Yoo HS, Lee EA, Park TG. Doxorubicin-conjugated biodegradable polymeric micelles having acid-cleavable linkages. *Journal of Controlled Release* 2002;82(1):17-27.

26. D'Souza AJM, Topp EM. Release from polymeric prodrugs: Linkages and their degradation. *Journal of Pharmaceutical Sciences* 2004;93(8):1962-79.

27. Shen WC, Ryser HJP. Cis-Aconityl Spacer between Daunomycin and Macromolecular Carriers - a Model of Ph-Sensitive Linkage Releasing Drug from a Lysosomotropic Conjugate. *Biochemical and Biophysical Research Communications* 1981;102(3):1048-54.

28. Griffiths G, Hansen H. Methods and compositions for increasing the target-specific toxicity of a chemotherapy drug United States Patent USA, 2002.

29. Bagshawe KD, Begent RHJ. First clinical experience with ADEPT. *Advanced Drug Delivery Reviews* 1996;22(3):365-67.

30. Duncan R, Satchi-Fainaro R. Pharmaceutical compositions containing antibody-enzyme conjugates in combination with prodrugs. United States Patents USA, 2002.

31. Duncan R, Gac-Breton S, Keane R, Musila R, Sat YN, Satchi R, Searle F. Polymer-drug conjugates, PDEPT and PELT: basic principles for design and transfer from the laboratory to clinic. *Journal of Controlled Release* 2001;74(1-3):135-46.

32. Denmeade SR, Lou W, Lovgren J, Malm J, Lilja H, Isaacs JT. Specific and efficient peptide substrates for assaying the proteolytic activity of prostate-specific antigen. *Cancer Research* 1997;57(21):4924-30.

33. Coombs GS, Bergstrom RC, Pellequer JL, Baker SI, Navre M, Smith MM, Tainer JA, Madison EL, Corey DR. Substrate specificity of prostate-specific antigen (PSA). *Chemistry & Biology* 1998;5(9):475-88.

34. Lovgren J, Airas K, Lilja H. Enzymatic action of human glandular kallikrein 2 (hK2) - Substrate specificity and regulation by Zn2+ and extracellular protease inhibitors. *European Journal of Biochemistry* 1999;262(3):781-89.

35. Suzumiya J, Hasui Y, Kohga S, Sumiyoshi A, Hashida S, Ishikawa E. Comparative-Study of Plasminogen-Activator Antigens in Colonic Carcinomas and Adenomas. *International Journal of Cancer* 1988;42(4):627-32.

36. Debruin PAF, Verspaget HW, Griffioen G, Verheijen JH, Dooijewaard G, Lamers C. Plasminogen Activators in Endoscopic Biopsies as Indicators of Gastrointestinal Cancer - Comparison with Resection Specimens. *British Journal of Cancer* 1989;60(3):397-400.

37. Rijken DC, Groeneveld E. Substrate-Specificity of Tissue-Type and Urokinase-Type Plasminogen Activators. *Biochemical and Biophysical Research Communications* 1991;174(2):432-38.

38. D'Andrea MR, Saban MR, Nguyen NB, Andrade-Gordon P, Saban R. Expression of protease-activated receptor-1,-2,-3, and-4 in control and experimentally inflamed mouse bladder. *American Journal of Pathology* 2003;162(3):907-23.

39. Park JE, Lenter MC, Zimmermann RN, Garin-Chesa P, Old LJ, Rettig WJ. Fibroblast activation protein, a dual specificity serine protease expressed in reactive human tumor stromal fibroblasts. *Journal of Biological Chemistry* 1999;274(51):36505-12.

40. Kohler D, Kruse MN, Stocker W, Sterchi EE. Heterologously overexpressed, affinity-purified human meprin alpha is functionally active and cleaves components of the basement membrane in vitro. *Febs Letters* 2000;465(1):2-7.

41. Wolz RL, Harris RB, Bond JS. Mapping the Active-Site of Meprin-a with Peptide-Substrates and Inhibitors. *Biochemistry* 1991;30(34):8488-93.

42. Chestukhin A, Litovchick L, Muradov K, Batkin M, Shaltiel S. Unveiling the substrate specificity of meprin beta on the basis of the site in protein kinase A cleaved by the kinase splitting membranal proteinase. *Journal of Biological Chemistry* 1997;272(6):3153-60.

43. Netzel-Arnett S, Sang QX, Moore WGI, Navre M, Birkedalhansen H, Vanwart HE. Comparative Sequence Specificities of Human 72-kDa and 92-kDa Gelatinases (Type-Iv Collagenases) and Pump (Matrilysin). *Biochemistry* 1993;32(25):6427-32.

44. Woessner JF, Nagase H. Matrix Metalloproteinases and TIMPs. New York: Oxford university press, 2000.

45. Ohkubo S, Miyadera K, Sugimoto Y, Matsuo K, Wierzba K, Yamada Y. Identification of substrate sequences for membrane type-1 matrix metalloproteinase using bacteriophage peptide display library. *Biochemical and Biophysical Research Communications* 1999;266(2):308-13.

46. Corticchiato O, Cajot JF, Abrahamson M, Chan SJ, Keppler D, Sordat B. Cystatin-C and Cathepsin-B in Human Colon-Carcinoma - Expression by Cell-Lines and Matrix Degradation. *International Journal of Cancer* 1992;52(4):645-52.

47. Moin K, Cao L, Day NA, Koblinski JE, Sloane BF. Tumor cell membrane cathepsin B. *Biological Chemistry* 1998;379(8-9):1093-99.

48. Khalfan HA. Study of Thiol Proteases of Normal Human Skin Fibroblasts. *Cell Biochemistry and Function* 1991;9(1):55-62.

49. Heidtmann HH, Salge U, Havemann K, Kirschke H, Wiederanders B. Secretion of a Latent, Acid Activatable Cathepsin-L Precursor by Human Nonsmall Cell Lung-Cancer Cell-Lines. *Oncology Research* 1993;5(10-11):441-51.

50. Matthews DJ, Wells JA. Substrate Phage - Selection of Protease Substrates by Monovalent Phage Display. *Science* 1993;260(5111):1113-17.

51. Hervio LS, Coombs GS, Bergstrom RC, Trivedi K, Corey DR, Madison EL. Negative selectivity and the evolution of protease cascades: the specificity of plasmin for peptide and protein substrates. *Chemistry & Biology* 2000;7(6):443-52.

52. Ke SH, Coombs GS, Tachias K, Navre M, Corey DR, Madison EL. Distinguishing the specificities of closely related proteases - Role of P3 in substrate and inhibitor discrimination between tissue-type plasminogen activator and urokinase. *Journal of Biological Chemistry* 1997;272(26):16603-09.

53. Merrifield RB. Solid-Phase Synthesis (Nobel Lecture). *Angewandte Chemie-International Edition in English* 1985;24(10):799-810.

54. Turk BE, Huang LL, Piro ET, Cantley LC. Determination of protease cleavage site motifs using mixture-based oriented peptide libraries. *Nature Biotechnology* 2001;19(7):661-67.

CHAPTER II : DESIGN CRITERIA OF A NEW POLYMER-PEPTIDE-DRUG CONJUGATE

Introduction

We have conceptualized a new polymer-drug conjugate for targeted drug delivery. The new conjugate is capable of passive targeting due to the appropriate physiochemical properties of the polymer backbone. The linker of this conjugate has the potential to improve active targeting via the mediation of enzymes overexpressed in the extracellular space of the diseased tissue. As a result, the new conjugate acts as a vehicle of drugs that selectively accumulates at the diseased site and is capable of liberating active drugs in the presence of target enzymes. The conjugate consists of three parts that are covalently linked: a polymeric carrier, linkers that can be specifically cleaved the target enzymes, and drug molecules. The schematic of the new polymer-peptide-drug conjugate is shown in Figure II-1. To illustrate this concept, we will consider the design criteria for a polymer-peptide-drug conjugate intended for anticancer therapy.

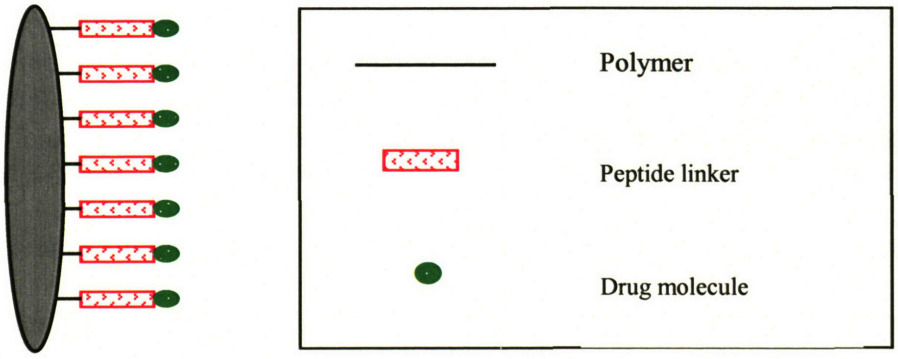

Figure II-1. Schematics of the new polymer-peptide drug conjugate

Motivation for Drug Targeting in Anticancer Therapy

Despite advances in the treatment of cancer, approximately 50% of the diagnosed cases of cancer result in death of patients. According to the estimation of American Cancer Society, approximately 600,000 Americans are expected to die of cancer in year 2005 (www.cancer.org). Surgical removal, radiation therapy and chemotherapy are the most common treatment options. Improving these treatment options will have a major impact on the future of human health.

The treatment option that uses chemicals to inhibit the spread and growth of cancerous tissues, also known as chemotherapy, has been in use since the 1950s. The application of chemotherapeutics is efficient in killing cancer cells; however, their activity can also kill normal cells. When chemotherapeutics are delivered systemically, side effects are commonly seen in the bone marrow, the hair cells and the gastrointestinal tract. Chemotherapeutics are not specific for any cell type or tissue. As a result, the dosage and extent of the treatment are limited due to drug-related toxicity and the effectiveness is compromised. Thus, difficulties in treating cancer partly stem from inadequate drug targeting. Using rational design, drug delivery devices should be able to favorably alter the pharmacokinetics of therapeutics favorably and improve the efficacy of chemotherapeutics. In this thesis research, a novel polymer-drug conjugate containing linkers cleavable by disease-associated enzymes will be constructed for the tumor-targeted delivery of chemotherapeutics.

Polymer selection

The polymer backbone needs to be biocompatible and biodegradable. It should be hydrophilic, not highly charged, and should have a size above the renal threshold limit to increase the circulation time. The large size is critical for passive targeting and selective tumor accumulation by enhanced permeation and retention (EPR). Chemically, it should provide functional sites to allow covalent attachment to create the conjugate. A number of polymers have been used in constructing polymer-drug conjugates, for example, HPMA[1], PEG[2], polyglutamate[3], albumin[4], pullulan[5], chitosan[6], dextran[7]. Previously, dextran of MW 70,000 Da was conjugated to doxorubicin via an acid-labile linkage for intratumoral delivery[8]. We selectd Dextran T40 and T70 as our polymeric carrier because of its biocompatibility [9] and biodegradability[10]. Dextran, a polymer of glucose, was first approved in 1951 as a 6% solution for use as plasma expander. Dextran 70/75 was approved by the FDA in 1953 and Dextran 40 in 1967. Its hydrophilic property and its high molecular weight should also allow for passive targeting [11]. The glomerular capillaries in kidney are fenestrated, with pores of radii estimated at 20-30nm. Their basement membranes act as a size and charge barrier which appear to hinder the transport of molecules above 6nm [12]. Our light scattering measurements indicate that dextran of 40kDa (Dextran T40) and 70kDa (Dextran T70) have a mean diameter of 9.9nm and 12.4nm respectively. These dimensions should lower renal excretion and prolong plasma circulation. The hydroxyl groups on the dextran backbone provide the necessary sites for covalent modification. In our design, we want to introduce amine-reactive functional groups to the polymeric carrier so that it can form a stable linkage with the N-terminal of the peptide linker or the N-terminal of an intermediate spacer. There are two common methods. In the first method, the hydroxyls are

oxidized by periodate to become aldehydes. The aldehyde group reacts with an amine to form a Schiff base. The relatively unstable Schiff base linkage is then reduced by sodium borohydride or sodium cyanoborohydride to form a more stable alkylamine linkage[13]. In the second method, chloroacetic acid is used to convert a hydroxyl in a base condition to an ether bond ending with a carboxymethyl group. The carboxymethyl reacts with an amine to form a stable amide linkage[13].

Linker selection

The new polymer-drug conjugate is designed to take advantage of passive targeting and EPR effect. Once the conjugate accumulates at the tumor site, we want to explore the possibility of releasing the drug in the tumor vicinity by tumor-associated enzymes. To investigate this concept, the linker between the polymer and the drug should be a substrate for an enzyme overexpressed at the tumor site. We decided to focus on two such enzymes: MMP-2 and MMP-9. These enzymes are members of the family of matrix-metalloproteinases (MMPs). MMPs are widely studied enzymes which are secreted in elevated levels in many types of human cancers [14, 15 16 17 18 19]. They help the tumor cells to survive and grow by breaking down the extracellular matrix barrier, releasing growth factors to stimulate cell proliferation and releasing angiogenesis factors to promote blood vessel formation [20].

Partly because of the interest in developing specific inhibitors against these enzymes as anti-cancer therapies, and partly because of the need to develop assays to measure their activities, their substrate specificities have been extensively studied. Netzel-Arnett examined the hydrolysis rates on over 50 octapeptides, which represent the systematic variations of a reference peptide: Gly-Pro-Gln-Gly-Ile-Ala-Gly-Gln[21]. This reference is modeled after the collagenase cleavage site in the calf/chick α1(I) chain of collagen[22, 23]. The scissile bond is Gly-Ile bond and this octapeptide covers the P4 through P4' sites (nomenclature according to Schechter & Berger[24])The key findings are:

1. Occupancy of P3 to P3' sites is required for rapid hydrolysis

2. P2 site prefers a hydrophobic residue such as Leu
3. P1 site tolerates only very small amino acid (i.e. Gly)
4. P1' site is conservative. Only substitution of Ile with Met produces a better substrate. A lot of variations in this site, including Pro, Glu, Ser, Arg and Trp, decrease the hydrolysis rate significantly.
5. P2'site prefers a large hydrophobic residue such as Trp but also accepts Arg
6. The sequence specificity for MMP-2 and for MMP-9 are similar

Assuming that the change in the reaction rate by each amino acid substitution is additive, the authors propose Pro-Leu-Gly↓Met-Trp-Ser-Arg as an optimal synthetic peptide substrate for MMP-2 and MMP-9, in which the scissile bond is between Gly and Met. (Arg is added to increase the solubility of the peptide substrate. To prevent hydrolysis by trypsin, D-Arg is used.) The kinetics for the hydrolysis of the fluorogenic heptapeptide substrate DNP-Pro-Leu-Gly↓Met-Trp-Ser-Arg was measured. At 23°C and pH 7.5, k_{cat}/K_m = 8900 and 13000 M^{-1} s^{-1} for MMP-2 and MMP-9 respectively[25].

Turk did a more comprehensive search of the optimal oligopeptide substrates for these enzymes using a combinatorial library [26]. The cleavage site motifs of MMP-2 are listed in Table II-1. He scored all amino acids at each position. His methodology was described in Chapter I. A score above 1 means that a particular amino acid is preferred at a particular position and a higher score is associated with a stronger preference. He measured the hydrolysis of the optimal sequence: Ile-Pro-Val-Ser-Leu-Arg-Ser with the scissile bond between Val and Ser. At 37°C and pH 7.4, k_{cat}/K_m = 82000 and

11500 $M^{-1}s^{-1}$ for MMP-2 and MMP-9 respectively.

Table II-1. Amino acid preference and its relative score in each substrate position for MMP-2 from the screening results of a combinatorial peptide library[26]

P4	P3	P2	P1	P1'	P2'	P3'
I (1.4)	P (1.7)	V (1.3)	S (1.9)	L (4.2)	R (1.5)	S (2.2)
V (1.3)	V (1.6)	A (1.3)	G (1.4)	M (2.8)	Y (1.5)	G (2.1)
	I (1.5)		A (1.4)	I (2.6)	I (1.4)	A (2.1)
			E (1.3)	Y (1.9)	M (1.4)	
				F (1.8)	K (1.4)	

Our linker sequence is selected from Table II-1. We assumed that the amino acid preference at each site was independent from the other sites. To simplify the synthesis procedure, we extracted the best amino acids without reactive side chains. This avoids the problem of having to dissolve the peptides with bulky protection groups and the degradation of the drug molecule in the harsh condition during the deprotection step.

Drug molecule selection

We reason that a non-specific anticancer drug molecule which causes undesirable side effects upon systemic administration can potentially benefit from the new approach, due to a better biodistribution of the polymer-peptide-drug conjugate. The drug needs to have a functional site to attach to the peptide linker. We use conventional chemotherapeutics, doxorubicin (DOX) as the model drug in our 1st generation conjugate and methotrexate (MTX) in the 2nd generation conjugate.

DOX is an anthracycline capable of intercalating DNA and thus the drug interferes with DNA synthesis. The amino ribosyl of DOX is readily available for covalent linkage. This chemotherapeutic has been used for cancer treatment for many years and is effective against leukemias, lymphomas, carcinomas of the breast, lung, endometrium, testes, prostate, cervix, head and neck, and in plasma cell myeloma. In clinical uses, major side effects are associated with the heart, bone marrow and gastrointestinal tract[27]. It has been conjugated to a polymeric carrier made of HPMA[1], dextran[8], albumin[28] and PEG[29] via both lysosomal enzyme labile sequences or acid labile linkages.

MTX is a folic acid analog that inhibits dihydrofolate reductase activity, and thus hinders the synthesis of RNA and DNA. This molecule has been used for cancer treatment for many years and is effective against a number of tumors, including lymphoblastic leukemia in children, chriocarcinoma and related trophoblastic tumors in women, osteosacroma and carcinomas of the

breast, head, neck, ovary and bladder. Chemically, methotrexate has two carboxyl groups available for covalent linkage. The limits on the clinical benefits of methotrexate are a result of the typical problems associated with most conventional chemotherapeutics: short circulation half-life and undesirable systemic side effects. Like most chemotherapeutics, it is non-specific and is toxic to all fast growing cells, with major side effects in the gastrointestinal tract and the bone marrow [27]. These problems can potentially be reduced by altering the pharmacokinetics and biodistribution using the approach of polymer-drug conjugates. Recently, there has been renewed interest in methotrexate conjugation due to the promising clinical results of albumin-methotrexate conjugates[30]. Besides albumin, studies of methotrexate conjugate with synthetic polymers such as poly(ethylene glycol)[31] and poly N-(2-hydroxypropyl)methacrylamide[32] have been carried out by different research groups.

References

1. Duncan R, Ulbrich K. Development of N-(2-Hydroxypropyl)Methacrylamide Copolymer Conjugates for Delivery of Cancer-Chemotherapy. *Makromolekulare Chemie-Macromolecular Symposia* 1993;70-1:157-62.

2. Greenwald RB, Conover CD, Choe YH. Poly(ethylene glycol) conjugated drugs and prodrugs: A comprehensive review. *Critical Reviews in Therapeutic Drug Carrier Systems* 2000;17(2):101-61.

3. Li C. Poly(L-glutamic acid) - anticancer drug conjugates. *Advanced Drug Delivery Reviews* 2002;54(5):695-713.

4. Kratz F. Drug conjugates with albumin and transferrin. *Expert Opinion on Therapeutic Patents* 2002;12(3):433-39.

5. Nogusa H, Yano T, Okuno S, Hamana H, Inoue K. Synthesis of Carboxymethylpullulan Peptide Doxorubicin Conjugates and Their Properties. *Chemical & Pharmaceutical Bulletin* 1995;43(11):1931-36.

6. Song YH, Onishi H, Nagai T. Pharmacokinetic Characteristics and Antitumor-Activity of the N-Succinyl-Chitosan Mitomycin-C Conjugate and the Carboxymethyl-Chitin Mitomycin-C Conjugate. *Biological & Pharmaceutical Bulletin* 1993;16(1):48-54.

7. Noguchi A, Takahashi T, Yamaguchi T, Kitamura K, Takakura Y, Hashida M, Sezaki H. Tumor-Localization and Invivo Antitumor-Activity of the Immunoconjugate Composed of Anti-Human Colon Cancer Monoclonal-Antibody and Mitomycin C-Dextran Conjugate. *Japanese Journal of Cancer Research* 1991;82(2):219-26.

8. Munechika K, Sogame Y, Kishi N, Kawabata Y, Ueda Y, Yamanouchi K, Yokoyama K. Tissue Distribution of Macromolecular Conjugate, Adriamycin Linked to Oxidized Dextran, in Rat and Mouse Bearing Tumor-Cells. *Biological & Pharmaceutical Bulletin* 1994;17(9):1193-98.

9. Sgouras D, Duncan R. Methods for the Evaluation of Biocompatibility of Soluble Synthetic-Polymers Which Have Potential for Bio-Medical Use .1. Use of the Tetrazolium-Based Colorimetric Assay (Mtt) as a Preliminary Screen for Evaluation of Invitro Cytotoxicity. *Journal of Materials Science-Materials in Medicine* 1990;1(2):61-68.

10. Vercauteren R, Schacht E, Duncan R. Effect of the Chemical Modification of Dextran on the Degradation by Rat-Liver Lysosomal-Enzymes. *Journal of Bioactive and Compatible Polymers* 1992;7(4):346-57.

11. Putnam D, Kopecek J. Polymer conjugates with anticancer activity Biopolymers II, vol. 122, 1995:55-123.

12. Hashida M, Takakura Y. Pharmacokinetics in Design of Polymeric Drug-Delivery Systems. *Journal of Controlled Release* 1994;31(2):163-71.

13. Hermanson GT. Bioconjugate Techniques: Academic, 1996.

14. Davies B, Miles DW, Happerfield LC, Naylor MS, Bobrow LG, Rubens RD, Balkwill FR. Activity of Type-IV Collagenases in Benign and Malignant Breast Disease. *British Journal of Cancer* 1993;67(5):1126-31.

15. Hamdy FC, Fadlon EJ, Cottam D, Lawry J, Thurrell W, Silcocks PB, Anderson JB, Williams JL, Rees RC. Matrix Metalloproteinase-9 Expression in Primary Human Prostatic Adenocarcinoma and Benign Prostatic Hyperplasia. *British Journal of Cancer* 1994;69(1):177-82.

16. Levy AT, Cioce V, Sobel ME, Garbisa S, Grigioni WF, Liotta LA, Stetlerstevenson WG. Increased Expression of the Mr 72,000 Type-IV Collagenase in Human Colonic Adenocarcinoma. *Cancer Research* 1991;51(1):439-44.

17. Naylor MS, Stamp GW, Davies BD, Balkwill FR. Expression and Activity of MMPs and Their Regulators in Ovarian-Cancer. *International Journal of Cancer* 1994;58(1):50-56.

18. Davies B, Waxman J, Wasan H, Abel P, Williams G, Krausz T, Neal D, Thomas D, Hanby A, Balkwill F. Levels of Matrix Metalloproteases in Bladder-Cancer Correlate with Tumor Grade and Invasion. *Cancer Research* 1993;53(22):5365-69.

19. Derrico A, Garbisa S, Liotta LA, Castronovo V, Stetlerstevenson WG, Grigioni WF. Augmentation of Type-Iv Collagenase, Laminin Receptor, and Ki67 Proliferation Antigen Associated with Human Colon, Gastric, and Breast-Carcinoma Progression. *Modern Pathology* 1991;4(2):239-46.

20. Egeblad M, Werb Z. New functions for the matrix metalloproteinases in cancer progression. *Nature Reviews Cancer* 2002;2(3):161-74.

21. Netzel-Arnett S, Sang QX, Moore WGI, Navre M, Birkedalhansen H, Vanwart HE. Comparative Sequence Specificities of Human 72-kDa and 92-kDa Gelatinases (Type-Iv Collagenases) and Pump (Matrilysin). *Biochemistry* 1993;32(25):6427-32.

22. Highberger JH, Corbett C, Dixit SN, Yu W, Seyer JM, Kang AH, Gross J. Amino-Acid-Sequence of Chick Skin Collagen Alpha-1(I)-Cb8 and the Complete Primary Structure of the Helical Portion of the Chick Skin Collagen Alpha-1(I) Chain. *Biochemistry* 1982;21(9):2048-55.

23. Glanville RW, Breitkreutz D, Meitinger M, Fietzek PP. Completion of the Amino-Acid-Sequence of the Alpha-1 Chain from Type-I Calf Skin Collagen - Amino-Acid-Sequence of Alpha 1 (I)B8. *Biochemical Journal* 1983;215(1):183-89.

24. Schechter I, Berger A. On the size of the active site in proteases. I. Papain. *Biochem Biophys Res Commun.* 1967;27(2):157-62.

25. Netzel-Arnett S, Mallya SK, Nagase H, Birkedalhansen H, Vanwart HE. Continuously Recording Fluorescent Assays Optimized for 5 Human Matrix Metalloproteinases. *Analytical Biochemistry* 1991;195(1):86-92.

26. Turk BE, Huang LL, Piro ET, Cantley LC. Determination of protease cleavage site motifs using mixture-based oriented peptide libraries. *Nature Biotechnology* 2001;19(7):661-67.

27. Chamber BA, Ryan DP, Paz-Ares L, Garcia-Carbonero R, Calabresi P. In: Hardman JG, Limbird LE, Gilman AG, eds. Goodman and Gilman's The Pharmacological Basis of Therapeutics: The McGraw-Hill Companies, Inc., 2001:1389.

28. Di Stefano G, Lanza M, Kratz F, Merina L, Fiume L. A novel method for coupling doxorubicin to lactosaminated human albumin by an acid sensitive hydrazone bond: synthesis, characterization and preliminary biological properties of the conjugate. *European Journal of Pharmaceutical Sciences* 2004;23(4-5):393-97.

29. Pechar M, Ulbrich K, Subr V, Seymour LW, Schacht EH. Poly(ethylene glycol) multiblock copolymer as a carrier of anti-cancer drug doxorubicin. *Bioconjugate Chemistry* 2000;11(2):131-39.

30. Hartung G, Stehle G, Sinn H, Wunder A, Schrenk HH, Heeger S, Kranzle M, Edler L, Frei E, Fiebig HH, Heene DL, Maier-Borst W, et al. Phase I trial of methotrexate-albumin in a weekly intravenous bolus regimen in cancer patients. *Clinical Cancer Research* 1999;5(4):753-59.

31. Riebeseel K, Biedermann E, Loser R, Breiter N, Hanselmann R, Mulhaupt R, Unger C, Kratz F. Polyethylene glycol conjugates of methotrexate varying in their molecular weight from MW

750 to MW 40000: Synthesis, characterization, and structure-activity relationships in vitro and in vivo. *Bioconjugate Chemistry* 2002;13(4):773-85.

32. Subr V, Strohalm J, Hirano T, Ito Y, Ulbrich K. Poly N-(2-hydroxypropyl)methacrylamide conjugates of methotrexate - Synthesis and in vitro drug release. *Journal of Controlled Release* 1997;49(2-3):123-32.

CHAPTER III : SYNTHESIS AND CHARACTERIZATION OF NEW POLYMER-PEPTIDE-DRUG CONJUGATES

Introduction

Based on the design criteria described in Chapter II, we set out to synthesize a new polymer-peptide-drug conjugate. The synthesis process should modify a polymeric carrier suitable for passive targeting and for enhanced permeation and retention (EPR). The steps should join the drug molecules to the polymeric carrier via peptide linkers. They should also be completed without degrading the drug molecules or the peptide sequences. We prepared carboxymethyl (CM)-dextran-peptide-doxorubicin as the first generation conjugate. There were three purposes in the preparation of this conjugate : 1) to investigate the stability of the delivery vehicle under physiological conditions that mimic the general circulation; 2) to examine the sensitivity of the linker towards MMPs; 3) to find out important aspects for improving the conjugate in our next design.

The experimental results from the first generation conjugate gave us some feedback on how to improve the sensitivity of the conjugate towards MMP-2 and MMP-9. We switched the model drug from doxorubicin to methotrexate because the potency of methotrexate was potentially more tolerable to the covalent modification on the drug at its gamma carboxyl site[1]. This change could also facilitate the coupling step between the drug and the peptide. By using a carboxyl instead of an amino group to conjugate to the peptide linker, the drug molecule can form an amide linkage with the peptide chain on a solid phase resin (which has an exposed

amino terminal), thereby simplifying the coupling and the purification steps. In developing the second generation conjugate, dextran-peptide-methotrexate, we had three goals in mind: 1) to produce an optimized conjugate capable of releasing drugs by the enzymatic cleavage of MMPs that is stable in serum containing conditions; 2) to characterize the physiochemical features of the conjugates; 3) to develop a robust and scalable process in order to prepare materials for further evaluation in animal studies. In laying out the synthesis route for the second generation conjugate, we also placed an emphasis on flexibility. The procedures are easily modified to prepare conjugates with different peptide linkers and different backbone charges. By tuning these parameters, a polymer-peptide-drug conjugate can be tailored to a wide variety of disease-associated enzymes.

We describe here the methods to synthesize two generations of dextran-peptide-chemotherapeutic conjugates. These conjugates were well characterized by various analytical tools, measuring the product purity, chemical identity, degree of modification of the dextran backbone, drug loading density and charge potential. Their stability was assessed by size exclusion chromatographic methods. The rate of drug release in the presence of MMPs was measured assuming that the enzymatic digestion followed Michaelis Menten kinetics model.

Experimental Procedures

Materials

Dextran T-40 with a nominal weight of 40,000 Da and T-70 with a nominal molecular weight of 70,000 Da were ordered from Pharmacia. 1-ethyl-3-(3-dimethylamino propyl)carbodiimide hydrochloride (EDC) and ethanolamine were obtained from Alfa Aesar. O-Bis-(aminoethyl)ethylene glycol trityl resin, 2-(*tert*-Butoxycarbonyloxyimino)-2-phenyl-acetonitrile (Boc-on), 1-Hydroxybenzotriazole hydrate (HOBT), (Benzotriazol-1-yloxy)tripyrrolidinophosphonium hexafluorophosphate (PyBop) and triisopropylsilane (TIS) were obtained from Nova Biochem. Glutamic acid-α-OtBu was purchased from Bachem. Trifluoroacetic acid (TFA), dimethylformamide (DMF), dimethylsulfoxide (DMSO), dioxane, acetonitrile (ACN), ethyl acetate, ether and 10X phosphate buffered saline were obtained from EM Science. Methanol, sodium chloride and sodium phosphate were from Mallinckrodt. Tris was purchased from Boehringer Mannheim. Chloroacetic acid, 4-amino-4-deoxy-N^{10}-methylpteroic acid (APA), benzotriazol-1-yloxytris(dimethylamino)phosphonium (BOP), *N-N'*-diisopropylethylamine (DIPEA), diaminopropionic (DPA), 2-Ethoxy-1-ethoxycarbonyl-1,2-dihydroquinoline (EEDQ), *N,N,N',N'*-Tetramethyl-*O*-(7-azabenzotriazol-1-yl)uronium hexafluorophosphate (HATU), triethylamine (TEA), pyridine, doxorubicin hydrochloride, methotrexate and calcium chloride and phorbol 12-myristate 13-acetate (PMA) were from Sigma. Concanavalin A (ConA) was ordered from Calbiochem. mPEG-NHS (methoxy polyethyleneglycol- N-hydroxysuccinimide ester) of nominal weight of 20,000 was from

Shearwaters. Peptides were synthesized in the Biopolymer Lab at the Massachusetts Institute of Technology using standard solid phase techniques and FMOC chemistry (Chapter I).

Purified active human MMP-2 and MMP-9 were purchased from Calbiochem. Precast protein gels with 10% gelatin and reagents for gelatin zymography were obtained from Biorad. Plasmocin was ordered from Invivogen. All other cell culture media and reagents as well as EDTA solution pH 8.0 were ordered from Gibco. Human tumor cell lines HT-1080 and BT-20 were obtained from American Type Cell Culture.

Synthesis procedures of the 1st generation conjugate: CM-dextran-peptide-doxorubicin

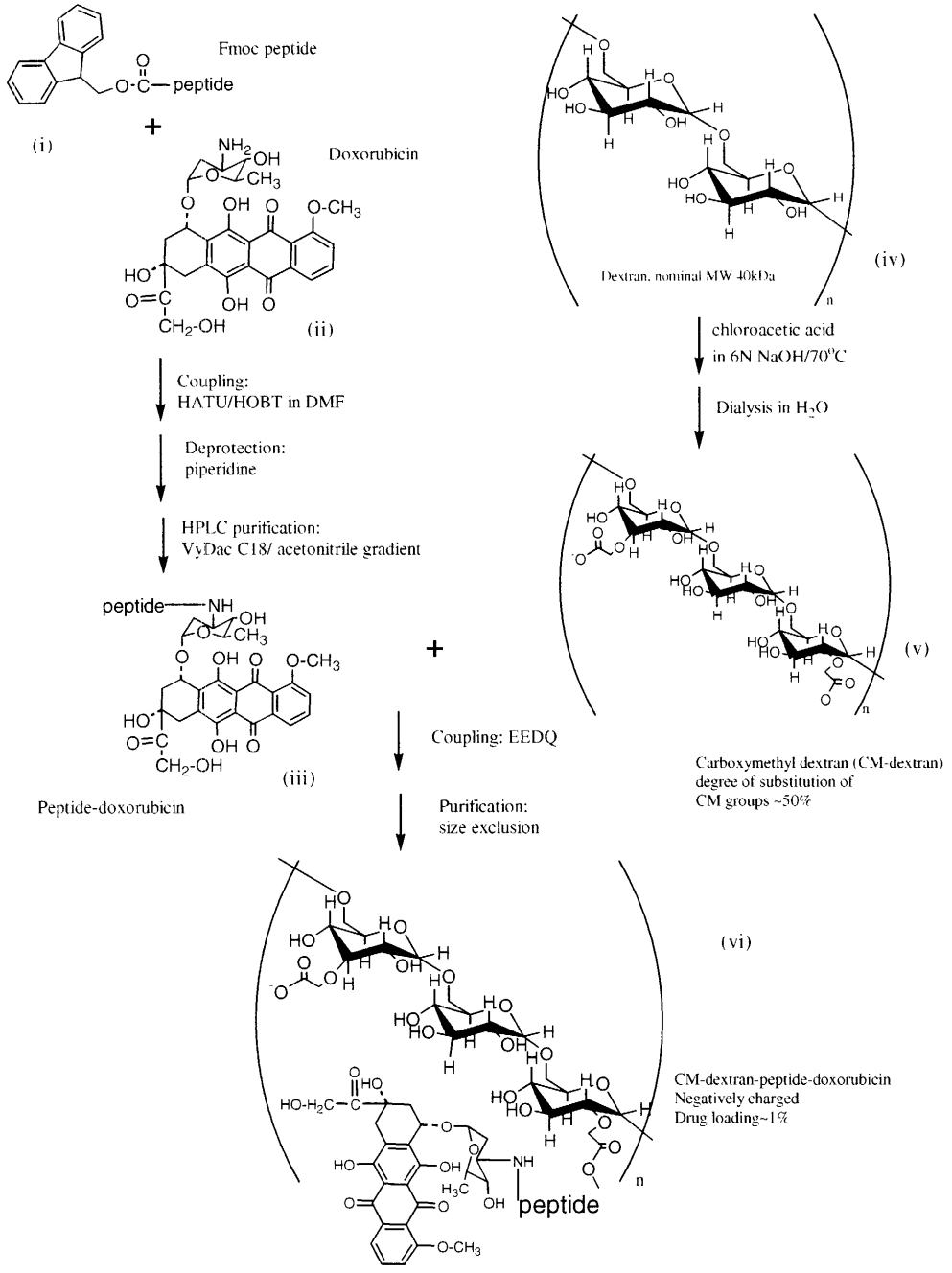

Figure III-1. The reaction scheme for synthesizing the first generation conjugate: carboxymethyl dextran-peptide-doxorubicin.

Preparation of carboxymethyl dextran (CM-dextran) (structure v, ***Figure III-1****)*

This procedure was based on the method by Nogusa for activating pullulan[2]. Dextran T-40 (10g) was dissolved in 100ml of 6N sodium hydroxide solution. Chloroacetic acid (30.2g) was added to the solution and was held at 70°C for 2--3 hours. Elevated temperature was necessary for this reaction. The reaction mixture was removed from heat and checked for pH. Acetic acid was used to neutralize the pH if necessary. The solution was then dialyzed against DI water using Spectrapor regenerated cellulose membrane with molecular weight cutoff at 3000-8000 for 2 days at 4°C and lyophilized for storage. Degree of carboxymethyl substitution was determined by analysis of sodium content. Atomic absorption analysis to determine sodium content was performed by Quantitative Technologies Inc. (Whitehouse, NJ). The degree of substitution was consistently at 50% (±2%).

Synthesis and purification of peptide-doxorubicin (structure iii, ***Figure III-1****)*

N-terminal protected FMOC-peptide was condensed with doxorubicin in DMF using PyBop and HOBT as coupling reagents. Two eq. of FMOC-peptide was mixed with 1.9eq. of HATU and 6 eq. of HOBT in DMF. After adding 15 eq. of DIPEA, the mixture was reacted with 1 eq. of doxorubicin hydrochloride pre-dissolved in DMF. The reaction was held at room temperature overnight. The volume of reaction was approximately 0.8mL per 10mg of doxorubicin hydrochloride. The resulting product was FMOC-peptide-doxorubicin. The FMOC group was removed by treating in 10%v/v piperidine for 5 minutes at room temperature. The mixture was then neutralized on ice by a quenching solution containing TFA/pyridine/DMF

(3:7:20). Peptide-doxorubicin was purified by HPLC on a 20ml C18 preparative scale column (Grace Vydac, Hesperia, CA) using a gradient from 20—100% acetonitrile with 0.2% TFA. The organic solvent in the product fractions was removed by rotoevaporation and the purified material was subsequently lyophilized. Product purity was confirmed to be ≥ 95% and the amount was quantified by the analytical scale reversed-phase HPLC. The average retention factor was: 6.24 (pure Dox), 6.57 (IPVG-Dox), 6.90 (IPVGL-Dox), 7.19 (IPVGLI-Dox), 7.19 (IPVGLIG-Dox). The identity of the intermediate product was confirmed with mass spectroscopy: Calc: 910.2 Found: 909.5 (IPVG-Dox); Calc: 1023.5 Found: 1022.9 (IPVGL-Dox); Calc: 1136.3 Found: 1135.8 (IPVGLI-Dox); Calc: 1193.5 Found: 1192.8 (IPVGLIG-Dox).

Synthesis and purification of CM-dextran-peptide-doxorubicin (structure vi, ***Figure III-1****)*

To couple peptide-doxorubicin to CM-dextran, peptide-dox (2 μmole) dissolved in 1:1 DMF:water (100 μl) was combined with CM-dextran (10.7 mg) dissolved in 1:1 DMF:water (200 μλ). EEDQ (33 μmole) was added to the mixture. The reaction was held for 2 hours at room temperature. The material was purified with a size exclusion column (HR 26/10 column with Sephadex 75 from Pharmacia) using water as the eluent. After purification, the product was lyophilized for storage. The product purity was confirmed to be ≥ 99% by the size exclusion HPLC analytical assay. The drug loading density was estimated by HPLC to be at about 1.0 (mole % per glucose unit).

Synthesis and purification of PEG-peptide-doxorubicin

Two eq. of mPEG-NHS was reacted with 1 eq. of peptide-dox in the presence of 3 eq. of DIPEA. ACN was used as the solvent and a volume was used such that the concentration of PEG was 10% w/v. The reaction was held at room temperature overnight. After the completion of the reaction, PEG-peptide-doxorubicin was purified by HPLC on a 20ml C18 ptreparative scale column (Grace Vydac, Hesperia, CA) using a gradient from 20—100% ACN with 0.2% TFA. The organic solvent was removed by rotoevaporation and the purified material was subsequently lyophilized. Product purity was confirmed to be ≥ 90% and the amount was quantified by the analytical scale reversed-phase HPLC.

Synthesis and purification of peptide-cisplatin

Boc-protected diaminopropionic (Boc-DPA) acid was prepared by reacting 1.1 eq. Boc-on with 0.5 eq. DPA in the presence of 1.5 eq. TEA in 1:1 dioxane/water for 3 hours at room temperature. Boc-DPA (1 eq.) was then conjugated to the lysine side chain or the amino terminal of the peptide (1.1 eq.) using PyBop (1.5 eq.) in DMF containing TEA (2 eq.) at room temperature for 4 hours. After drying the solvent, Boc was removed by treating with TFA/TIS/water (95:2.5:2.5) for 1.5 hours. The intermediate product, peptide-DPA, was purified by HPLC on a 20ml C18 preparative scale column using a gradient from 0—100% ACN with 0.2% TFA. Potassium tetrachloroplatinate (II) was added in aliquots to peptide-DPA in water. The reaction was held for 3 hours and room temperature. The final product, peptide-cisplatin, was purified with a similar HPLC method as above and the platinum content was measured by inductively coupled plasma analysis, performed at Quantitative Technologies Inc.

Synthesis procedures of the 2nd generation conjugate: dextran-peptide-doxorubicin

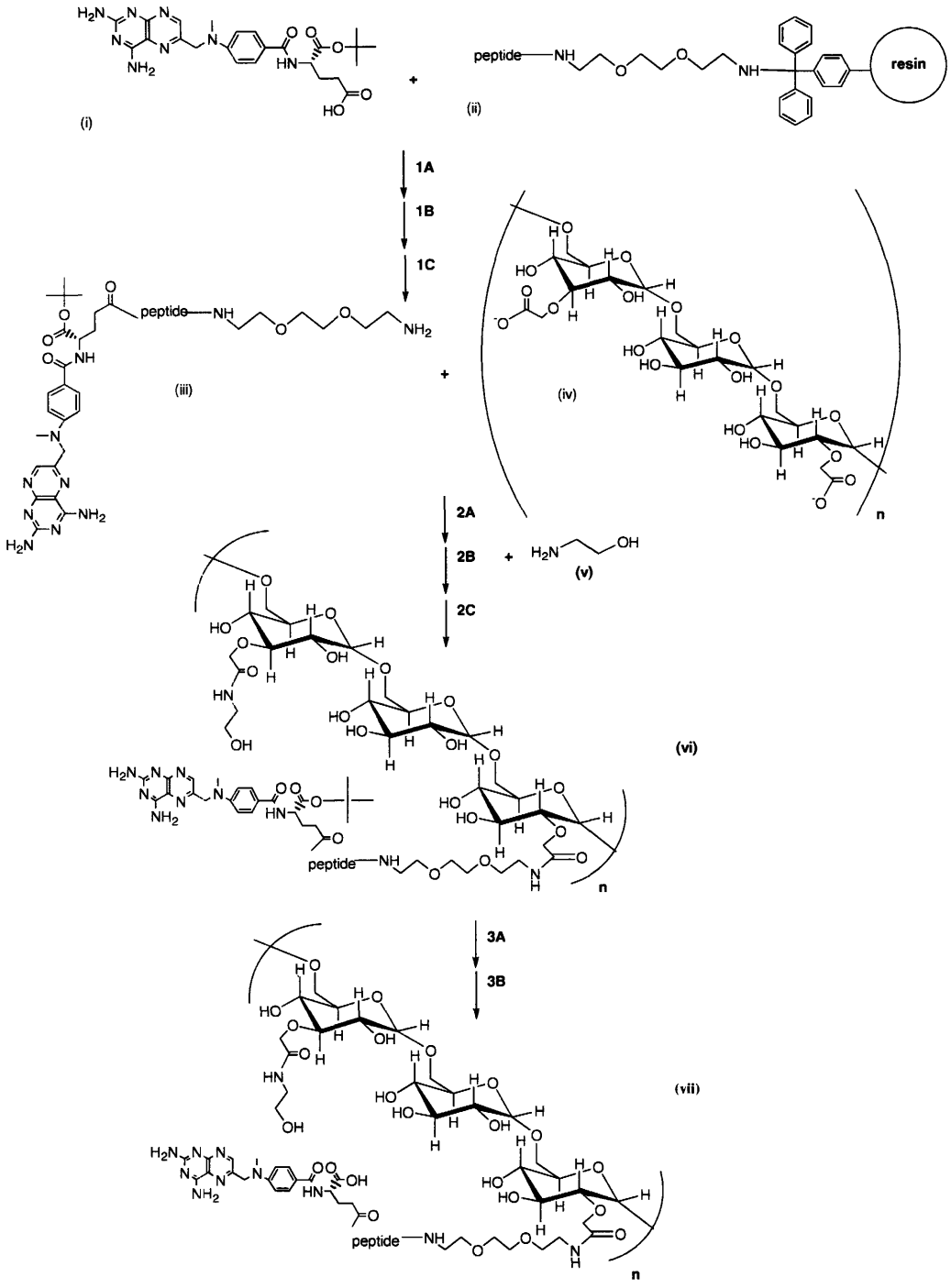

Figure III-2. The reaction scheme for synthesizing the 2nd generation conjugate: dextran-peptide-methotrexate. Reactants and scales: (i) methotrexate with alpha carboxyl protected (MTX(OtBu)); typical scale = 1.25mMole MTX equivalent = 2.5 molar excess of peptide. (ii) peptide on O-Bis-(aminoethyl)ethylene glycol trityl resin (iii) Jeffamine-peptide-MTX(OtBu); typical scale= 0.35 mMole MTX eq. (iv) Carboxymethyl dextran with degree of substitution of

CM groups at ~50% and nominal MW 70,000. (v) Ethanolamine. (vi) modified Dextran-peptide-MTX(OtBu) with degree of modification at ~50% and degree of drug loading at ~1%; typical scale = 0.14mMole MTX eq. (vii) modified Dextran-peptide-MTX with degree of modification ~50% and with degree of drug loading~1%; typical scale = 0.11mMole MTX eq. Reaction conditions and step yields: 1A: PyBop / HOBT / DIPEA coupling in DMF; 1B: dilute trifluoroacetic acid cleavage from resin.; 1C: reversed phase HPLC purification; typical yield for step 1= ~70% yield. 2A: coupling with EDC in H2O; 2B: charge neutralization by EDC / ethanolamine in excess; 2C: methanol precipitation; typical yield for step 2 = ~40%. 3A: strong trifluoroacetic acid cleavage to deprotect tert-butyl group from MTX; 3B: diafiltration against DI water; typical yield for step 3 = ~80%.

Preparation of carboxymethyl dextran (CM-dextran) (structure iv, ***Figure III-2****)*

This procedure was similar to the preparation of structure v in Figure III-1 except that Dextran T-70 instead of T-40 was used as a starting material. The degree of substitution was consistently at 50% (±2%).

Synthesis and purification of methotrexate-alpha-OtBu (structure i, ***Figure III-2****)*

Methotrexate-alpha-OtBu (MTX(OtBu)) was prepared from 4-amino-4-deoxy-N^{10}-methylpteroic acid (APA) and glutamic acid-α-OtBu using BOP as the conjugating reagent, following the procedure of Nagy[3]. Crude MTX(OtBu) was precipitated by centrifugation in a 1:1 mixture of cold ether/ethyl acetate. The material was further purified by HPLC on a 95ml C18 preparative scale column (Grace Vydac, Hesperia, CA) using a gradient from 0—100% ACN with 0.2% TFA. The organic solvent in the product fractions was removed by rotoevaporation and the purified material was subsequently lyophilized. Product purity was confirmed to be ≥ 95% and the amount was quantified by the analytical scale reversed-phase HPLC. The average retention factor was 6.14.

Synthesis of jeffamine-peptide-methotrexate(OtBu) (structure iii, ***Figure III-2****)*

Standard FMOC peptide synthesis in solid phase was carried out on O-Bis-(aminoethyl)ethylene glycol trityl resins. As in the conventional solid phase peptide peptide synthesis, the peptide chain grew from the carboxyl to the amino terminals. After the last amino acid was loaded to the chain, FMOC was removed and the peptide with a free amino terminal was exposed whereas the carboxyl remained attached to the solid resin via a short 6-carbon polyethylene oxide spacer.

To couple MTX-α-OtBu to the amino terminal of the peptide chain, MTX-α-OtBu (2.5 equivalent to the amount of peptide) was dissolved in DMF containing DIPEA (2.5 equivalent). PyBop (2.5 equivalent), HOBT (2.5 equivalent) and additional DIPEA (2.5 equivalent) were used to activate the γ-carboxyl of MTX-α-OtBu for about 15 minutes. More DMF was added such that the final concentration of MTX-α-OtBu was about 0.1 M. The mixture was combined with the resins loaded with peptide and stirred at room temperature overnight. The reaction was confirmed for completeness the next day by ninhydrin test. Excessive reactants were washed away from the resins with DMF, DCM and methanol. The resins were then dried thoroughly.

Jeffamine-peptide-MTX(OtBu) was cleaved from trityl resins by suspending the resins in DCM containing 2% TFA for 10 minutes. This step was repeated 3 times. To collect all the cleaved product, the resins were further washed with DCM and methanol and the step was

repeated until no further yellow color was observed (the yellow color was indicative of the presence of the MTX(OtBu) containing product). Organic solvent was subsequently removed by rotoevaporation from the collected product. The crude material was resuspended in water and purified by HPLC over a 0—100% acetonitrile gradient with 0.2% TFA using a 95ml C18 preparative column. Product fractions were lyophilized after the organic solvent was removed by rotoevaporation. Product purity was found to be ≥ 95% and the amount was quantified by analytical scale reversed phase HPLC.

The average retention factor on HPLC for MTX(OtBu)-Pro-Val-Gly-Leu-Ile-Gly-jeffamine was 6.71. Mass spectroscopy confirmed the identity of this intermediate product (structure iii in Figure III-2): Calc: 1177.3; Found: 1177.7. [^{1}H NMR (400 MHz, D_2O): δ 8.59 (s, H-7 of methotrexate, 1H), 7.62 (d, 3',5'-H of methotrexate, 2H), 6.81 (d, 2'6'-H of methotrexate, 2H), 4.86 (s, H-9 of methotrexate, ~2H, overlapping with H_2O), 4.33 (m, Hα of methotrexate, ~1H, overlapping with H-2 of Pro) 1.8—2.0 (m,Hβ of methotrexate, 2H, overlapping with 3,4-H of Pro), 2.6 (m, Hγ of methotrexate, ~2H), 1.41 (s, CH_3 of tert-butyl, ~9H, overlapping with 3,4-H of Leu), 3.21 (s, CH_3-11 of methotrexate, 3H, overlapping with Jeffamine EDR 148), 3.18—3.74 (m, H of Jeffamine EDR 148, ~12H, overlapping with H-5 of proline and CH_3-11 of methotrexate), 4.33 (m, H-2 of Pro, ~1H, overlapping with Hα of methotrexate), 3.87--- 4.35 (m, H-2 of Val, Gly, Leu, Ile, Gly, 7H), 3.4—3.6 (m, H-5 of Pro, ~2H, overlapping with Jeffamine EDR 148), 2.1—2.3 (m, 3-H of Val, 3H of Ile, 2H), 1.8—2.1 (m, 3,4-H of Pro, 4H, overlapping with Hβ of methotrexate), 1.2---1.54 (m, 3,4-H of Leu, ~3H, overlapping with CH_3 of tert-butyl), 0.78 – 0.93 (m, 3',4-H of Val, 4'5-H of Leu, 3'4,5-H of Ile, 20H)]

The average retention factor of MTX(OtBu)-Gly-Ile-Val-Gly-Pro-Leu-jeffamine on our reversed-phase HPLC assay was 6.59. Mass spectroscopy confirmed the identity of this intermediate product (structure iii in scheme 1): Calc: 1177.3; Found: 1177.1 [^{1}H NMR (400 MHz, D_2O): δ 8.59 (s, H-7 of methotrexate, 1H), 7.60—7.62 (d, 3',5'-H of methotrexate, 2H), 6.78—6.80 (d, 2'6'-H of methotrexate, 2H), 4.85 (s, H-9 of methotrexate, ~2H, overlapping with H_2O), 4.35 (m, Hα of methotrexate, ~1H, overlapping with H-2 of Pro), 1.7—2.1 (m, Hβ of methotrexate,~2H, overlapping with 3,4-H of Pro), 2.45 (m, Hγ of methotrexate, 2H), 1.41 (s, CH_3 of tert-butyl, ~9H, overlapping with 3,4-H of Leu), 3.20 (s, CH_3-11 of methotrexate, 3H, overlapping with Jeffamine EDR 148), 3.16—3.74 (m, H of Jeffamine EDR 148, ~12H, overlapping with H-5 of proline and CH_3-11 of methotrexate), 4.35 (m, H-2 of Pro, 1H, overlapping with Hα of methotrexate), 3.84--- 4.25 (m, H-2 of Val, Gly, Leu, Ile, Gly, 7H), 3.3—3.5 (m, H-5 of Pro, ~2H, overlapping with Jeffamine EDR 148), 2.1—2.3 (m, 3-H of Val, 3H of Ile, 2H), 1.7—2.1 (m, 3,4-H of Pro, ~4H, overlapping with Hβ of methotrexate), 1.1--- 1.7 (m, 3,4-H of Leu, ~3H, overlapping with CH_3 of tert-butyl), 0.74 – 0.88 (m, 3',4-H of Val, 4'5-H of Leu, 3'4,5-H of Ile, 20H)]

Synthesis of jeffamine-methotrexate(OtBu) (structure iii', structure not shown)

The procedure was similar to above for the synthesis of (iii) except that no peptide was loaded onto the resin. MTX-α-OtBu was directly coupled to O-Bis-(aminoethyl)ethylene glycol trityl resin using the same protocol. Product found to be ≥ 95% by reversed-phase HPLC. The

average retention factor of jeffamine-MTX(OtBu) was 5.81. Mass spectroscopy confirmed the identity of this intermediate product (iii'): Calc: 640.6; Found:640.6.

Synthesis and purification of Dextran-peptide-MTX (structure vii, ***Figure III-2****)*

To couple jeffamine-peptide-MTX(OtBu) to CM-dextran, jeffamine-peptide-MTX(OtBu) (0.5 mMol) dissolved in DI water (1.9 ml) was combined with CM-dextran (4g) dissolved in DI water (6.7ml). EDC (4.7g) was added to the mixture while stirring. The reaction was held overnight at room temperature. Another aliquot of EDC (4.7g) was added the next day and the reaction was held overnight to form CM-Dextran-peptide-MTX(OtBu) (structure vi of Figure III-2).

To block the unreacted carboxymethyl groups on the dextran backbone, ethanolamine (30ml) was first neutralized to pH 6—7 using 5N HCL in dibasic phosphate buffer on ice. This mixture was added to (vi) followed by the reaction with EDC (47g). It was held stirring at room temperature overnight. The modified Dextran-peptide-MTX(OtBu) was precipitated by centrifugation in methanol.

To remove the protection group OtBu, modified Dextran-peptide-MTX(OtBu) was resuspended in 40ml strong trifluroacetic acid by vigorous stirring and held at room temperature for 3 hours. This deprotection step was quenched by diluting the acidic mixture with 0.1M phosphate buffer and neutralizing the pH with 5N sodium hydroxide on ice. Extensive diafiltration was performed using Pellicon XL membrane cassettes of regenerated cellulose with 10,000 MWCO (Millipore, Billerica, MA) to remove excessive reactants and byproducts of the reaction. After purification, the product in the retentate was concentrated and then lyophilized for

storage. The product purity was confirmed to be ≥ 99% by size exclusion HPLC. The drug loading density was estimated by HPLC to be at 1.0 ± 0.2 % (mole % per glucose unit).

Synthesis and purification of Dextran-MTX (structure vii', structure not shown)

This procedure comprised of steps similar to those for the synthesis and purification of dextran-peptide-MTX (structure vii of Figure III-2), with the exception that jeffamine-MTX(OtBu) was used instead of jeffamine-peptide-MTX(OtBu).

Zeta potential measurement

Dextran and dextran-peptide-MTX conjugates were dissolved in DI water at 10mg/ml. Measurement was performed with Zeta-analyzer (Brookhaven Instruments Co., Holtsville, NY).

Measurement of kinetics parameters for MMP-2 and MMP-9 digestion of conjugates

The kinetics of enzymatic digestion of the conjugates by MMP-2 and MMP-9 was modeled by the classical Michaelis Menten equation:

$$\frac{1}{Vi} = \frac{1}{k_{cat} E_{total}} + \left(\frac{K_m}{k_{cat} E_{total}}\right)\frac{1}{S_o}$$

where V_i is the initial reaction velocity, S_o is the substrate concentration and E_{total} is the total enzyme concentration, including both bound and non-bound forms. K_m is the Michaelis-Menten constant and k_{cat} is the turnover rate of the substrate-enzyme complex to product. The ratio k_{cat} / K_m is widely used in literature, termed as specificity constant, as a measure of how fast enzymatic digestion occurs. Conjugates of interest were dissolved in assay buffer (10mM $CaCl_2$, 0.2M NaCl in 50mM Tris pH 7.5) at various concentrations: 5, 10, 20, 50 and 100μM. For each substrate concentration, active MMP-2 or MMP-9 at a final concentration of 10nM was added and the mixture was incubated at 37°C. At specific time points, the reaction mixture was quenched with EDTA solution at a final concentration of 20mM. The mixture was assayed by 2-column size exclusion HPLC (assay details are included in the next paragraph) and the cleavage product peak was quantified to calculate the reaction rate. Initial rate was defined as the rate for the cleavage of the first 20% of the conjugate. Linear regression was performed on a double reciprocal plot of $1/V_i$ versus $1/S_o$ to determine the specificity constant k_{cat}/K_m.

HPLC Analytical Methods

Reversed phase analytical assay for online monitoring of process yield and product purity

A silica C18 0.21mmID x 25cmL column (Grace Vydac, Hesperia, CA) was connected to a HPLC solvent delivery system equipped with a UV detector (1100 series, Agilent Technologies, Palo Alto, CA). The method was run at 0.5ml/min with mobile phase A as 0.2% trifluoroacetic acid (TFA) in water and mobile phase B as 0.2% TFA in acetonitrile. A sample of 10 µL was injected onto a pre-equilibrated column followed by 5 minutes of wash with mobile phase A. A gradient ramped from 0%B to 100%B in 20 minutes. Detection for doxorubicin-containing moieties and methotrexate-containing moieties was made by their UV absorbance at 495 nM and 307nM respectively. A calibration curve was constructed correlating the peak areas in the chromatograms and the concentrations of the free drugs.

One-column size-exclusion assay for online monitoring of process yield and product purity

A PW3000 7.8mmID X 30cmL column (Tosohaas) was connected to a HPLC solvent delivery system equipped with a UV detector (Agilent Technologies). The method consisted of an isocratic elution with 20% ACN and 3.6X phosphate buffered saline in water at 0.8ml/min. Detection for doxorubicin-containing and methotrexate-containing moieties was made by their UV absorbance at 495nM and 307nM respectively. The default sample injection volume was set at 10 µL. A calibration curve was constructed correlating the peak areas in the chromatograms

and the concentrations of methotrexate standards. The enzymatic kinetics for polymer conjugate with bound doxorubicin was also measured with this assay.

Two-column size-exclusion assay for enzyme kinetics study of dextran-peptide-methotrexate

A PW3000 7.8mmID X 30cmL column followed by PW2000 7.5mmID x30cmL column (Tosohaas, Montgomeryville, PA) were connected to a HPLC solvent delivery system equipped with a UV detector (Agilent Technologies).The method consisted of an isocratic elution with 20% acetonitrile and 3.6X phosphate buffered saline in water at 0.8ml/min. Methotrexate-containing moieties were detected by their UV absorbance at 307nM or 390nM. The default sample injection volume was set at 10 μL. A calibration curve was constructed correlating the peak areas in the chromatograms and the concentrations of methotrexate standards.

Maintenance of cell culture

Human tumor cells HT-1080 and BT-20 were maintained using DMEM low glucose media supplemented with 2mM L-glutamine, 1X glutamine-penicillin-streptomycin (GPS), 25 μg/ml plasmocin and 10% fetal bovine serum.

Zymography of cell conditioned media

HT-1080 and BT-20 were grown to about 70% confluent before the growth media was exchanged to the serum-free media (DMEM low glucose containing 2mM L-glutamine, 1X GPS and 12.5 ng/ml of PMA) The culture was grown in serum-free media for another three days.

Cell-conditioned media were analyzed with gelatin zymography according to a previously described procedure [4,5]. Briefly, samples were separated with electrophoresis in a 10% polyacrylamide gel containing gelatin. After renaturing the gel in 2.5% Triton X-100 solution, it was incubated overnight in a development buffer to allow the digestion of the gelatin by MMP-2 or MMP-9. White clear bands in a blue background after Coomassie Blue staining indicated the presence of the enzymes.

In vitro digestion experiments of conjugates

To assess the stability of the conjugate MTX-PVGLIG-Dextran (PVGLIG is the shorthand notation of the peptide Pro-Val-Gly-Leu-Ile-Gly) in serum-containing conditions, it was incubated at 37°C and 5% CO2 with various media for 24 hours. The percentage cleavage of the conjugate was determined by the two-column size exclusion HPLC assay.

To demonstrate that the specificity of release of peptidyl drug from the conjugate in cell culture was MMP-2 and MMP-9 dependent, HT-1080 and BT-20 were grown in 12-well-plates to about 80% confluent and growth media was exchanged to serum-free media containing 12ng/ml of PMA or 10μg/ml of ConA. PMA and ConA were used to activate pro-MMP-2 and pro-MMP-9 to their active forms. After two days, the conjugate MTX-PVGLIG-Dextran was added to the cell culture and incubated for 6 hours. Media samples were analyzed by two-column size exclusion HPLC assay to determine the percentage peptidyl drug released from the conjugate.

Cytotoxicity assay

(3-(4,5-dimethylthiazol-2-yl)-2,5-diphenyl-2H-tetrazolium bromide) assay (MTT assay) was used to measure the drug cytotoxicity according to a previously described procedure with modifications[6]. Cells were seeded in serum-containing growth media to 96-well-plates at 10,000 cells/well. After 1 day, the growth media was exchanged to serum-free media and the drug solutions at specified concentrations were added. After another 2 days of drug exposure, MTT solution was added and the plates were incubated at 37°C for 2 hours, followed by overnight incubation with extraction solution (10% SDS in DMF/H_2O pH 4.7). Plates were read at 570nM and the readings of the absorbance corresponded to the number of living cells. Percentage survival was calculated using the formula listed in the website of National Cancer Institute (http://dtp.nci.nih.gov/branches/btb/ivclsp.html):

[(Ti-Tz)/(C-Tz)] x 100 for concentrations for which Ti ≥ Tz

[(Ti-Tz)/Tz] x 100 for concentrations for which Ti < Tz

Where Tz is the reading at time zero prior to the addition of drug solutions, Ti is the reading at the assay end-point at each of the drug concentration level, and C is reading at the assay end-point for the control growth (with no drug addition).

Growth inhibition of 50 % (GI50) was calculated from [(Ti-Tz)/(C-Tz)] x 100 = 50, which was the drug concentration resulting in a 50% reduction in the net increase in the number of viable cells (as measured by MTT assay) compared to control growth.

Results and Discussion

1st generation conjugate: CM-dextran-peptide-doxorubicin

Synthesis of the new conjugates

Following the scheme in Figure III-1, we successfully prepared the 1st generation conjugate. The synthesis of CM-dextran-peptide-doxorubicin required dextran modification, solid phase peptide synthesis and coupling techniques in solution phase. To help us monitor and optimize the synthesis process, we have established a reversed-phase and a size-exclusion HPLC assay. The dextran polymer, 40 kDa, was modified to carry carboxymethyl groups such that they can form stable amide linkages with the peptides. Preparative chromatographic methods were developed to purify the intermediate products and the final conjugates. Analytical HPLC methods were developed to analyze the conjugate purity, measure its stability and characterize its drug loading. Drug loading density of the conjugate was about 1% (mole/mole of sugar units). Empirically, we found that the use of HATU, HBTU or PyBop as the coupling reagent between the peptide (structure i in Figure III-1) and doxorubicin (structure ii in Figure III-1) could achieve a significantly higher yield than the more traditional reagent DCC. At first we employed BOC chemistry in the peptide synthesis. After coupling the protected peptide with doxorubicin, the BOC group was removed by the treatment with TFA. Dox was degraded in this acidic environment and this problem was solved by replacing BOC chemistry with FMOC chemistry. Using HPLC, we confirmed that doxorubicin was stable in 10% piperidine, the deprotection

condition to remove FMOC. In purifying the conjugate in the last step, we used a size exclusion column. This method, however, was throughput limited and was therefore difficult to scale up.

To summarize, we learnt some important lessons from the synthesis of the first generation conjugates: 1) a good choice of coupling reagents is essential to form the amide linkage between the drug and the peptide; 2) the drug liability in the harsh deprotection conditions should be tested in the early phase during the development of a synthesis procedure; 3) an alternative purification process is needed for scaling up.

Stability in serum

To achieve passive targeting, it is important that the conjugate remains uncleaved in the circulation prior reaching the tumor site. We assessed the stability of the conjugate in the serum at the physiological temperature (Figure III-3). Serum alone did not cause any significant release of peptidyl-doxorubicin from the conjugate.

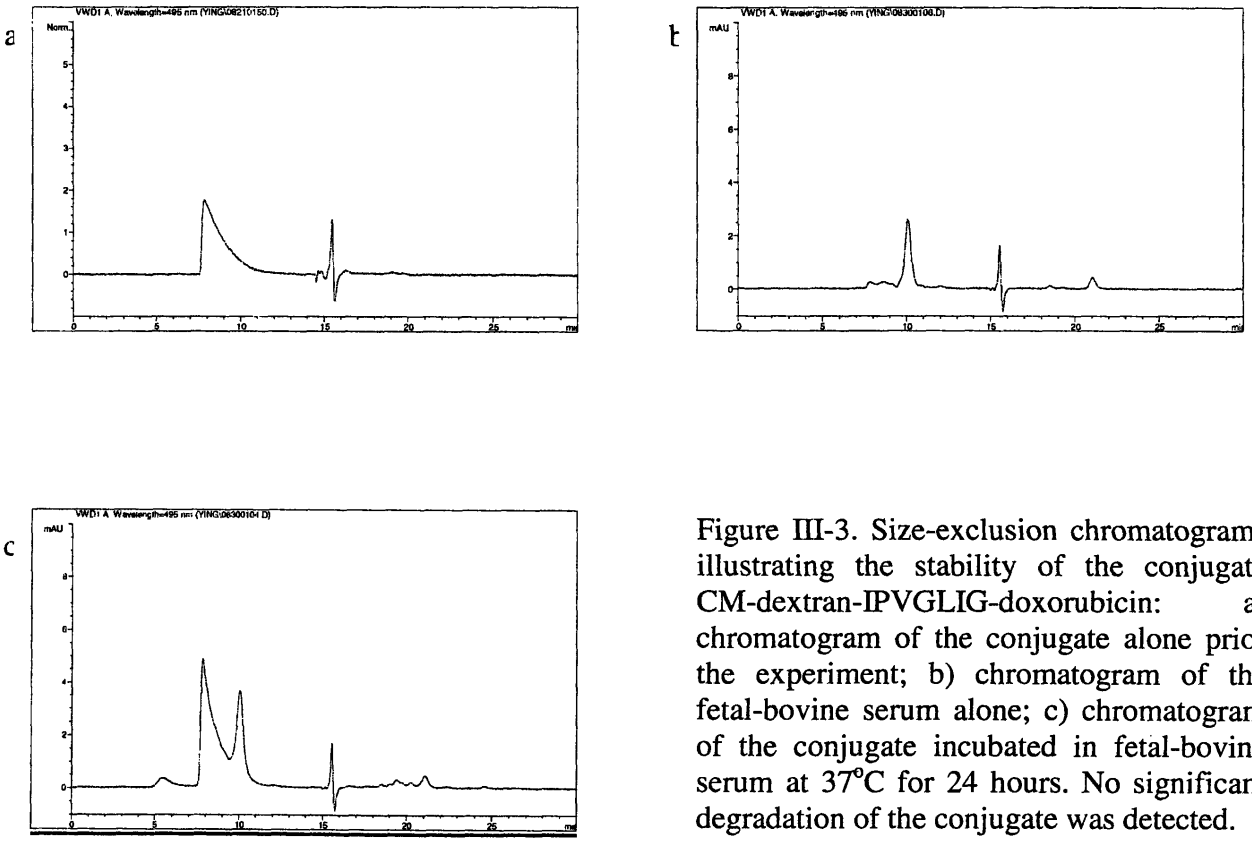

Figure III-3. Size-exclusion chromatograms illustrating the stability of the conjugate CM-dextran-IPVGLIG-doxorubicin: a) chromatogram of the conjugate alone prior the experiment; b) chromatogram of the fetal-bovine serum alone; c) chromatogram of the conjugate incubated in fetal-bovine serum at 37°C for 24 hours. No significant degradation of the conjugate was detected.

MMP-mediated release is dependent on the peptide sequence

Oligopeptides of 4 to 7 amino acids were evaluated as the peptide linkers (Table III-1). The sequences were based on the work of Turk[7]. A combinatorial pool of octapeptides was screened and the probability of each amino acid at each position was counted. The optimal sequence determined by this method for MMP-2 was IPVSLRSG. The presence of the reactive side chains on serine and arginine may pose a problem since doxorubicin is labile to the acidic conditions required to remove the protection groups put on these amino acids during solid phase synthesis. As a result, the second best amino acids with non-reactive side chain were selected in synthesizing the polymer-peptide-drug conjugate.

Table III-1. Oligopeptide sequences used as peptide linkers in the 1st generation conjugates. The potential cleavage position for MMP-2 and MMP-9 is between P1 and P1'

P4'-P3'-P2'-P1'---P1-P2-P3
Ile-Pro-Val-Gly
Ile-Pro-Val-Gly—Leu
Ile-Pro-Val-Gly—Leu-Ile
Ile-Pro-Val-Gly—Leu-Ile-Gly

We confirmed the release of peptidyl-doxorubicin from the new conjugates, and showed that the sensitivity of the linker towards MMP-2 to follow this order: IPVGLIG > IPVGLI > IPVGL > IPVG (Figure III-4). The rate of the cleavage depends on the length of the oligopeptide. After 3 hours, more than 90% of peptidyl-dox was released from CM-dextran-IPVGLI-dox, less than 15% was released from CM-dextran-IPVGLI-dox ,

and no significant amount of peptidyl-dox was liberated from CM-dextran-IPVGL-dox or CM-dextran-IPVG-dox. The results were consistent with the reports in the literature about the necessity to include the optimal amino acids in 3 positions proximal and distal to the cleavage site[8]; we concluded that a linker consisting of amino acids from P3' to P3 should be used in the conjugate of the next design.

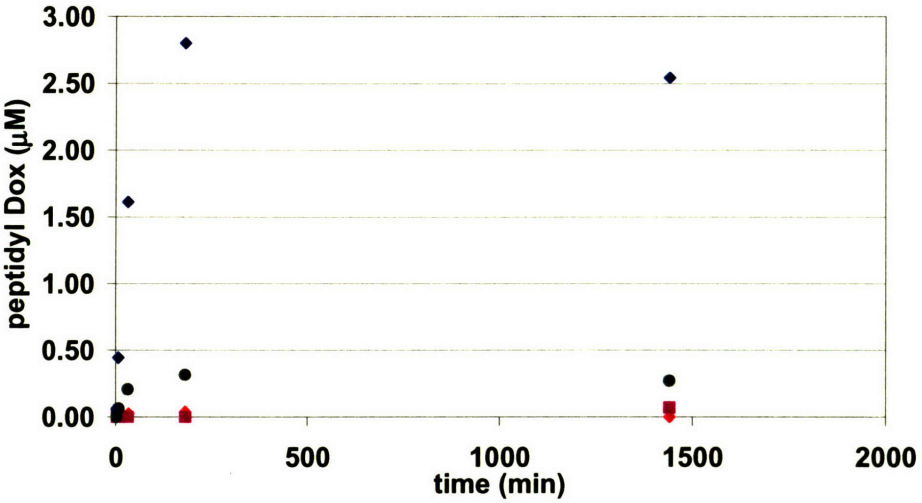

Figure III-4. Release of peptidyl-doxorubicin from CM-dextran-peptide-doxorubicin conjugates with different peptide linkers in the presence of MMP-2. Peptide linkers are: IPVGLIG (♦), IPVGLI (●), IPVGL (■) and IPVG (▲).Digestion conditions: [MMP-2] =100nM and [Doxorubicin eq.] = 3.2μM in 50mM Tris, 0.2M NaCl, 2mM CaCl2, pH 7.5

CM-dextran backbone interferes with enzymatic drug release by MMP-2

We measured the kinetics of enzymatic digestion of the new conjugate with the optimal linker, CM-dextran-IPVGLIG-Dox, and compared the result with the peptide-doxorubicin and the optimal peptide cleavable by MMP-2 (Table III-2). We found that the specificity constant (k_{cat} / K_m) of the CM-dextran-peptide-dox conjugate was two orders of magnitude lower than the optimal peptide. On the other hand, the value of the

specificity constant of the peptide-doxorubicin was comparable with that of the optimal peptide. It appeared therefore that covalent attachment to the CM-dextran backbone caused some hindrance to the enzymatic digestion. Furthermore, the enzymatic cleavage rate was not lowered when the peptide-doxorubicin was conjugated to methoxy PEG in a 1:1 ratio. There are two differences between CM-dextran and mPEG: 1) CM-dextran carries a negative charge because of the unreacted carboxymethyl groups, whereas mPEG is neutral; 2) peptide-doxorubicin is grafted along the dextran backbone (Figure II-1), whereas the attachment occurred at the terminal end of the long and flexible mPEG polymer (Figure III-5). These comparison suggested to us that either the enzymatic digestion by MMP-2 was affected by the configuration of how peptide-doxorubicin was tethered to the polymer, or by the electrostatic charge of the polymer.

Table III-2. Michaelis-Menten specificity constants of MMP-2 sensitive peptide, peptide-doxorubicin, CM-dextran-peptide doxorubicin and mPEG-peptide-doxorubicin

	k_{cat} / K_m (M-1 s-1)
Peptide: IPVSLRSG	$0.82 \times 10^5 \pm 6000$ *
Peptide-Dox: IPVGLIG-Dox	1.40×10^5
Polymer-peptide-Dox: CM-Dextran-IPVGLIG-Dox	1.77×10^3
Polymer-peptide-Dox: mPEG-IPVGLIG-Dox	1.78×10^5

*Value obtained from reference[7]

Figure III-5. Schematic representation of mPEG-peptide-doxorubicin

If the negative charge on the carboxymethyl-dextran backbone poses a electrostatic repulsion between the conjugate and MMP-2, we should observe a phenomenon consistent with Debye-Hückel theory, which states that:

$$\log (k/k_o) = 1.018\, z_A z_B \sqrt{I}$$

where k is the rate constant at ionic strength I, k_o is the rate constant at zero ionic strength, z_A and z_B are the charges of the reactants.

If z_A and z_B have the same signs, the theory predicts that as ionic strength in the digestion environment increases, the kinetics of the cleavage improves. This is because the charges of the reactants are more efficiently screened by the media. We observed this trend in a salt titration experiment (Table III-3) and concluded that the electrostatic repulsion between CM-dextran and MMP-2 significantly hampered the enzymatic digestion. As a result, we decided to experiment with blocking the excessive negative charge on the CM-dextran backbone in the next design.

Table III-3. Effect of salt concentration on the rate of enzymatic digestion of the conjugate CM-dextran-IPVGLIG-doxorubicin. The assay buffer contains 50mM Tris, 2mM CaCl2, pH 7.5 and varying amount of NaCl as indicated.

Salt concentration (Molar of NaCl) in assay buffer	**k_{cat} / K_m ($M^{-1} s^{-1}$)**
0.01	7.50×10^1
0.1	1.15×10^2
0.2	1.09×10^3
0.5	4.47×10^3

Cytotoxicity of doxorubicin is neutralized by amino acid attachment

The product released by MMP-2 from the most sensitive 1st generation conjugate, CM-dextran-IPVGLIG-dox,was confirmed by mass spectroscopy to be LIG-Dox (Calc: 826.8 , Found: 826.1). The potency of cytotoxicity of doxorubicin dropped by two orders of magnitude when LIG was covalently attached the drug (Figure III-6). This is probably because the ribosyl amino group on doxorubicin participates in the hydrogen bonding with the intercalated DNA. Thus the blocking of this group reduces the drug's efficiency in inhibiting DNA replication.

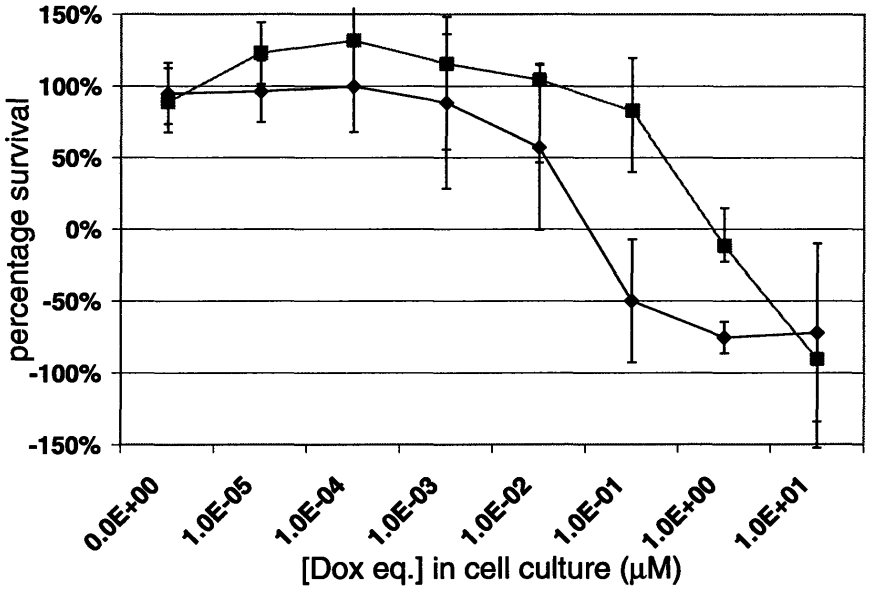

Figure III-6. Comparison of cytotoxicity of free doxorubicin (♦) and Leu-Ile-Gly-Dox (■) on HT-1080 fibrosacroma culture. LIG-Dox is the product released from CM dextran-IPVGLIG-Dox by MMP cleavage.

This prompted us to investigate the possibilities of other drug candidates: cisplatin and methotrexate (Figure III-7). The literature contained information about their structure-activity-relationship which suggested possible modifications without the sacrifice of the drug potency[1]. Analogs of peptide-coupled drugs, which represent the possible cleavage products by MMP digestion, were compared with free drugs for their cytotoxicity in cell culture (Figure III-8). The results from cisplatin were disappointing, showing a complete neutralization of the drug potency with peptide attachment. The results of methotrexate were more promising, though the peptide attachment still reduced drug activity. We decided to use methotrexate as the next drug candidate, also because its gamma-carboxyl group is available for coupling and should allow us to attach the drug to the peptide with a more facile method (further discussed in the synthesis of 2nd generation conjugate).

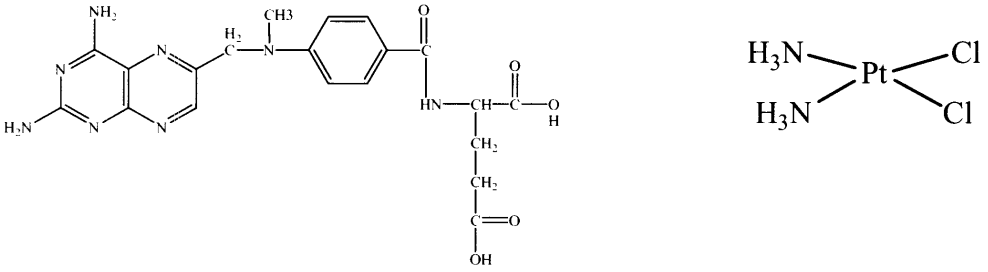

Figure III-7. Chemical structure of metotrexate (left) and cisplatin (right)

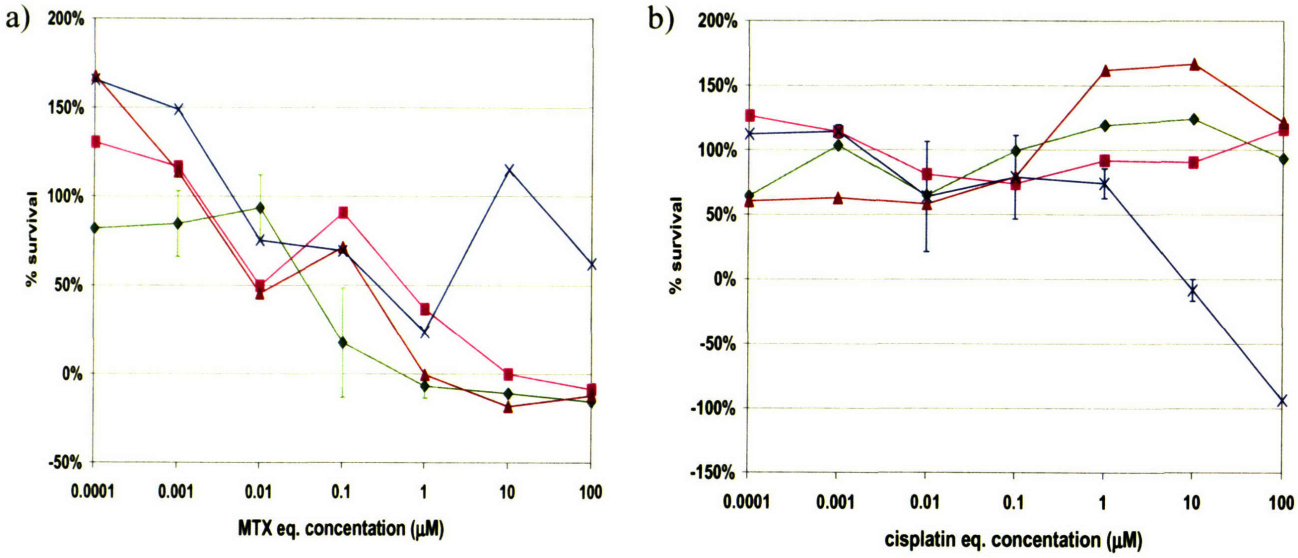

Figure III-8. Comparison of cytotoxicity of free drug and peptide-drug of methotrexate and cisplatin: a) methotrexate [♦], MTX-PVG [■], MTX-IPVG [▲] and LK(MTX)G [×]; b) cisplatin [×], cisplatin-PVG [♦], LK(cisplatin)G [■] and LIGK(cisplatin) [▲].

2nd generation conjugate: dextran-peptide-methotrexate

Synthesis of the new conjugates

We have developed a robust, adaptable and scalable process to prepare the 2nd generation conjugate. The process flow chart for synthesizing and purifying dextran-peptide-methotrexate conjugates is shown in Figure III-2. The reversed phase and size exclusion HPLC assays used for analyzing the 1st generation conjugate were modified to analyze the 2nd generation conjugate.

The drug molecule to be attached to the new conjugate, methotrexate, has some bulk tolerance at the γ-carboxyl group. It is important that the α-carboxyl, the less tolerable functional group, is protected throughout the synthesis process. Thus methotrexate-alpha-(OtBu) (structure i, Figure III-2) was prepared from APA. This protected methotrexate was first conjugated to the peptide in a solid phase reaction. Trityl resins were chosen as the solid-phase supports since the products synthesized on the resins could be released using a dilute acid thus leaving the tert-butyl group on methotrexate unaffected. This protection group was eventually removed in the last reaction step (step 3A, Figure III-2).

We have combined solid phase and solution phase synthesis to make the process more flexible. Peptide synthesis on solid supports is now a highly automated process and peptide sequences of varying length or composition can be readily prepared in a short time (Chapter I). The advance of this current technology lets us readily accommodate any change in the peptide sequence as the conjugate's linker. This is valuable when we expand the current approach to target other tumor-associated enzymes, which are made up of a diverse group of proteases. A few examples include prostate-specific antigens [9], urokinase-type plasminogen activator [10] and cathepsin-L [11]. On the solid support, the peptide chain grows from the carboxyl terminal and a free amino terminal is exposed after the last prolongation step. Since methotrexate has a gamma-carboxyl, it can be covalently joined to the amino end of the peptide in a solid phase reaction (step 1A, Figure III-2). Using an excess amount of reactants is feasible and this enables the conjugation step to have high yield. Afterwards, the unreacted species can be washed off while jeffamine-peptide-methotrexate remains attached to the solid support. This results in a reasonable purity of the intermediate product (structure iii, Figure III-2).

We have chosen a special trityl resin, O-Bis-(aminoethyl)ethylene glycol trityl resin (structure ii, Figure III-2), as the solid support. This enables the peptide to be attached to jeffamine, a short polyethylene oxide chain. After detaching from the solid support, the peptide remains attached to jeffamine. Jeffamine aids in the coupling between the peptide-drug and carboxymethyl dextran (structure iv, Figure III-2). Our MMP-recognizable peptide sequence is composed of hydrophobic amino acids (Pro-Val-Gly-Leu-Ile-Gly). The protected drug MTX-α-(OtBu) also has limited aqueous solubility. On the other hand, carboxymethyl dextran is hydrophilic. In our attempts to couple peptide-drug to carboxymethyl dextran in the presence of EDC, we have found that the concentration of the amine component and the concentration of the carboxyl component are critical factors in determining conjugation yield.

Table III-4 lists the conjugation yield when we varied the amine or the carboxyl concentration in the coupling step, keeping all other reaction conditions identical. This observation is explained by the relatively short half-life of the EDC-activated carboxyl. If unable to encounter an amine component for reaction, the active ester becomes inactivated [12].Because of the hydrophilic character of the jeffamine spacer that improves aqueous solubility, higher concentration of jeffamine-peptide-MTX(OtBu) (structure iii, Figure III-2) can be attained and the conjugation in aqueous phase results in a reasonable yield (Step 2A, Figure III-2).

Table III-4. Conjugation yield of the reaction step between carboxymethyl dextran and jeffamine-peptide-MTX(OtBu), varying the amine and the carboxyl concentration

Amine concentration (M)	Carboxyl concentration (M)	Conjugation yield (%)
0.02	0.66	76
0.02	0.18	41
0.02	0.09	29
0.02	0.02	15
0.01	0.66	25

Stability in serum-containing conditions

Our new conjugates are intended for systemic delivery. To be able to passively target the tumor sites and achieve enhanced permeation and retention, the conjugates must remain stable in the blood circulation and the drug molecules should stay attached to the polymer backbone prior reaching the tumor tissues. We used fetal bovine serum and serum spiked with active human MMP-2 and MMP-9 to approximate the physiological conditions encountered by the conjugates in systemic circulation. The MMP addition was intended to mimic the circulation environment when tumor growth is present in the body. When tumor tissues overexpress MMP-2 and MMP-9, the enzyme levels are also elevated in the blood stream [13]. However, protease activities of these MMPs in the systemic circulation are greatly reduced because of the inhibition by serum proteins. One of these inhibitors is α2-macroglobulin, a large serum protein with molecular weight of about 800kDa that offers the proteases a bait region. Once the bait region is cut, α2-macroglobulin changes shape to entrap the MMP [14]. We demonstrated that the conjugates were satisfactory in meeting the stability criteria(Figure III-9). While the conjugate MTX-PVGLIG-

Dextran was sensitive to MMP-2 or MMP-9 in assay medium that was serum free, releasing a significant amount of peptidyl methotrexate, it remained uncleaved in the serum. This inhibitory effect of the serum on MMP activity was also evident. There was no significant release from the conjugate in the serum spiked with same concentrations of MMPs.

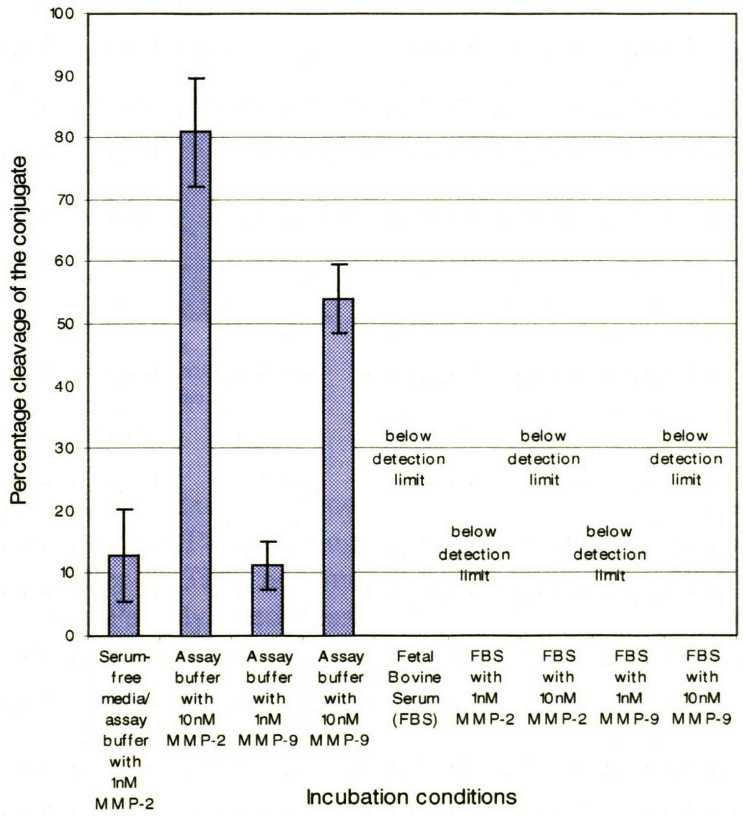

Figure III-9. Stability of conjugate MTX-PVGLIG-Dextran in various media conditions. Conjugates were incubated with the specified conditions for 24 hours at 37°C and assayed by size exclusion HPLC to determine the percentage cleavage of the conjugate. The conjugate released peptidyl drug in serum-free conditions but remained intact in all the serum-containing conditions. The average values from 3 replicates with standard deviations as error bars are shown.

MMP-mediated drug release requires an optimized peptide linker

We have prepared three different conjugates: 1) MTX-PVGLIG-Dextran, with the peptide linker composition optimized for MMP-2 recognition; 2) MTX-GIVGPL-Dextran, with a scrambled peptide linker; 3) MTX-Dextran, without a peptide linker. The extents of drug release from these conjugates in the presence of MMP-2 and MMP-9 were compared in Figure III-10 and Figure III-11.

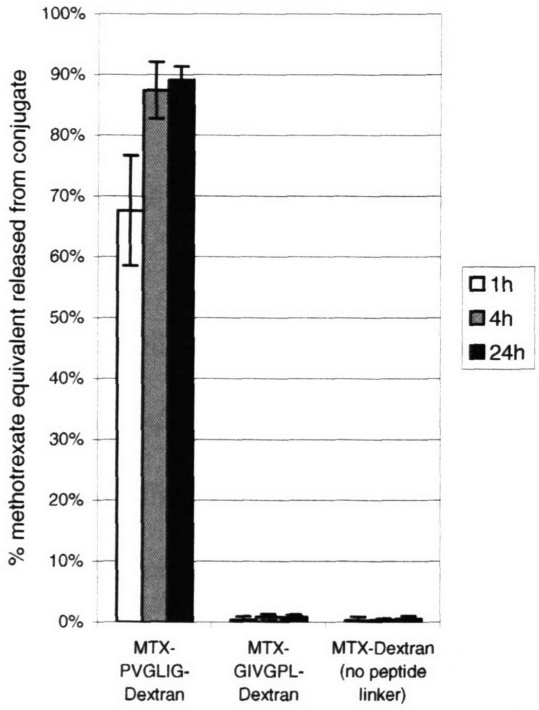

Figure III-10. Extent of methotrexate equivalent released from different conjugates in the presence of MMP-2. Conjugates of different linkers were incubated with 10nM of MMP-2 in assay buffer at 37°C and measured for percentage cleavage at specified time points by size exclusion. Peptidyl methotrexate analogs were the expected products released from the dextran-peptide-methotrexate conjugates upon cleavage. Methotrexate was the expected product released from the dextran-methotrexate conjugate upon cleavage. Cleavage of the conjugate by MMP-2 was dependent on the linker composition.

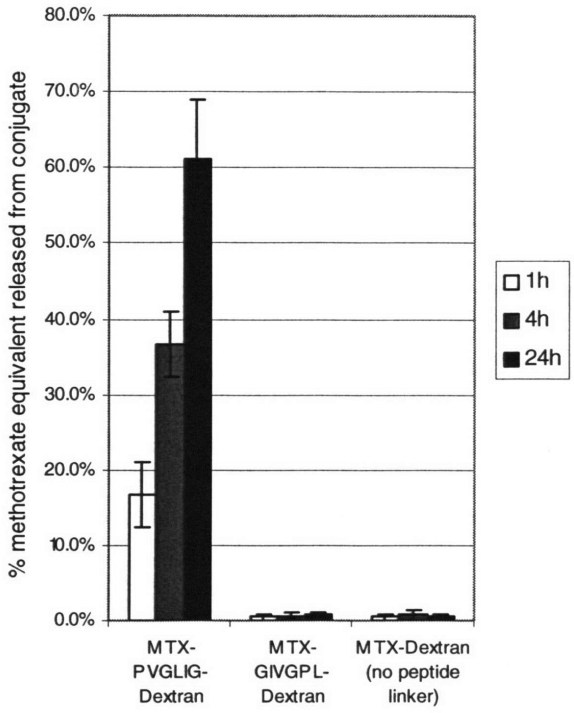

Figure III-11. Extent of methotrexate equivalent released from different conjugates in the presence of MMP-9. Conjugates of different linkers were incubated with 10nM of MMP-9 in assay buffer at 37°C and measured for percentage cleavage at specified time points by size exclusion. Peptidyl methotrexate analogs were the expected products released from the dextran-peptide-methotrexate conjugates upon cleavage. Methotrexate was the expected product released from the dextran-methotrexate conjugate upon cleavage, if any. Cleavage of conjugate by MMP-9 was dependent on the linker composition.

Similar trends were observed for both MMP-2 and MMP-9. MTX-PVGLIG-Dextran conjugate released 89% of peptidyl methotrexate in the presence of MMP-2 and 61% in the presence of MMP-9 after 24 hours. In contrast, conjugates without any peptide linker or carrying the scrambled peptide linker did not show any significant release. Without the MMP recognizable peptide linker, the conjugate was stable even in the presence of a high concentration of MMP-2 or MMP-9. We isolated the small molecular weight cleavage product from the digest of MTX-PVGLIG-Dextran on size exclusion column and analyzed the product

fraction by mass spectroscopy. The molecular weight found was 707.5 and was consistent with the notion that methotrexate-Proline-Valine-Gly (MTX-PVG) was the released product. This can be predicted by the scissile site of MMP-2 and MMP-9 on the peptide[7].

We want to explore the possibility of releasing the active drug molecules from the conjugates in the presence of the tumor-associated enzymes MMP-2 and MMP-9. A peptide linker labile to the enzymatic digestion is important to achieve this purpose. For the optimal linker, we selected the most preferable amino acids with non-reactive side chains from Turk's work [7] to fill the substrate positions from P3 to P3'. From our experience in the 1st generation conjugate, these six positions are necessary for the recognition by MMP-2. We showed that the cleavage of the new dextran-peptide-methotrexate conjugate depended on the composition of the peptide linker. Although PVGLIG shows a high cleavage rate by MMP-2 and MMP-9, this peptide is not sensitive exclusively to these two enzymes. Because of the similarity among members in the family of matrix-metalloproteinases [7, 14] , this peptide is expected to be cleavable by other MMPs albeit with lower rates.

Preparation of conjugates with varying backbone negative charges

To investigate the effect of the net charge on the dextran backbone, we prepared different conjugates by reacting the excess carboxymethyl with ethanolamine using different conditions. Ethanolamine is a simple, neutral and hydrophilic molecule (structure v and step 2B, Figure III-2). The charges on the resulting conjugates were characterized by its zeta potential. We first experimented with just carboxymethyl dextran (structure iv, Figure III-2) and found that the

negative charge could be partially or fully neutralized using appropriate reaction conditions (Table III-5). We have therefore devised a method to modify the magnitude of the negative charge on the dextran backbone, a factor other than the peptide composition that can be tailored to different enzymes of interest for optimizing conjugate sensitivity.

Table III-5. Zeta potentials of dextran and modified dextran samples

Sample	Zeta potential (mV)
Dextran T70 (neutral)	-6.6
Carboxymethyl dextran CM-Dextran (degree of substition ~50% determined by atomic absorption sodium analysis)	-47.4
Ethanolamine neutralized CM-Dextran A (EDC at 2 fold excess and ethanolamine at 10 fold excess of glucose units present on dextran)	-36.25
Ethanolamine neutralized CM-Dextran B (EDC at 10 fold excess and ethanolamine at 20 fold excess of glucose units present on dextran)	-1.06

By tuning the amount of EDC and ethanolamine, we prepared MTX-PVGLIG-Dextran conjugates with varying negative charges and examined the charge effect on the kinetics of digestion by MMP-2 and MMP-9 (Table III-6). Recall that in our experience with the 1st generation conjugate, we observed that the rate of MMP-2 cleavage increased with higher ionic strength in the digestion media. In accordance with Debye-Hückel theory, we reasoned that this phenomenon could be explained by the electrostatic repulsion between the enzyme and the

negatively charged conjugate. Here, we confirm this hypothesis by showing that the charge on the conjugate backbone has a significant effect on the rate of MMP-2 cleavage. The value of k_{cat}/Km is varied by an order of magnitude depending on the charge. The conjugate most sensitive to MMP-2 (Conjugate C) has its excess carboxymethyl groups completely masked by ethanolamine and is neutral in charge. It has a similar kinetics constant towards MMP-2 digestion as the optimal peptide found by Turk[7]. (In his report, Ile-Pro-Val-Ser-Leu-Arg-Ser was reported to have a k_{cat}/Km value of 0.82E5 $M^{-1}s^{-1}$.) On the other hand, the kinetics of enzymatic digestion by MMP-9 was much less sensitive to the charge difference on our conjugate backbone. Taken together, the conjugate with its carboxymethyl groups masked and hence least negatively charged has the highest sensitivity towards MMP-2 and MMP-9.

Table III-6. MTX-PVGLIG-Dextran conjugates with varying negative backbone charge show significantly different sensitivity towards MMP-2 cleavage but similar sensitivity towards MMP-9

Conjugate I.D.	Backbone negative charge masked with ethanolamine?	Zeta potential (mV)	k_{cat}/K_m (M^{-1} s^{-1}) by MMP-2 digestion[a]	k_{cat}/K_m (M^{-1} s^{-1}) by MMP-9 digestion[b]
A	None	-43.7	2.12E4 ± 3.33E2	7.09E3 ± 5.52E2
B	Partially	-27.8	1.10E4 ± 9.66E2	3.09E3 ± 5.04E2
C	Fully	-12.2	1.21E5 ± 4.11E3	3.60E3 ± 4.14E2

[a,b] The average values and standard deviations of 3 replicates are reported

The difference in charge effect on MMP-2 and MMP-9 digestion kinetics is interesting considering that these two enzymes are very similar in structure. Both have three repeats of fibronectin type II domain [14]. Categorized together as gelatinases, they are also reported to have

similar biological substrates and specificity [8].We compared the amino acid sequences of the active form of human MMP-2 and MMP-9, taken from the Swiss-Prot database (P08253 and P14780 for their precursors). The net charge of MMP-2 is 10 times more negative than MMP-9. This discrepency is consistent with our current experimental observation that MMP-2 exhibits significantly more electrostatic repulsion towards the negatively charged dextran backbone.

Specificity of release in tumor cell culture

HT-1080 is a human fibrosacroma cell line that is known to express MMP-2 and MMP-9. BT-20, a human breast cancer cell line, expresses a lower amount of MMP-2 compared to HT-1080 and has no detectable level of MMP-9. These features were confirmed by zymography of the cell conditioned media from these cell lines (Figure III-12). In HT-1080 cell conditioned media, prominent bands are observed at at 92kD, 86kD, 72kD and 68D. These molecular weights are consistent with the values of latent MMP-9, active MMP-9, latent MMP-2 and active MMP-2 respectively. In BT-20 conditioned media, only a faint band is present at 72kD indicating a relatively small amount of latent MMP-2.

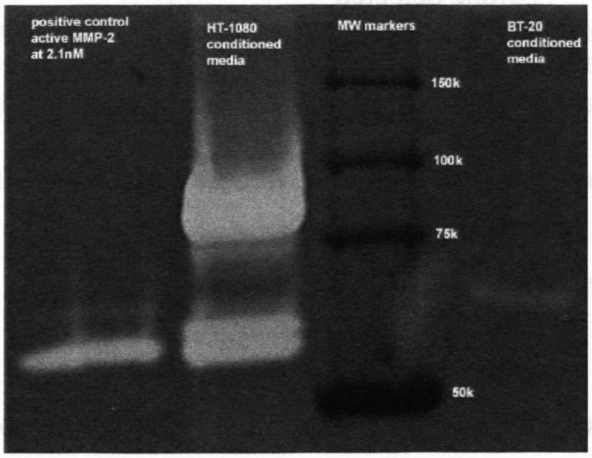

Figure III-12. Gelatin zymography of HT-1080 and BT-20 cell conditioned media. The white bands in the dark backgrounds indicate the presence of MMPs. Latent and active MMP-2 (72kD and 68kD) and latent and active MMP-9 (92kD and 86kD) were expressed by HT-1080. Only a faint band of pro-MMP-2 (72kD) was found in BT-20. All conditioned media samples were normalized to the same cell number.

The conjugates MTX-PVGLIG-Dextran were incubated for 6 hours with these two types of cell culture. The digest showed no detectable cleavage of the conjugates in BT-20 culture. In contrast, 14% cleavage was observed in HT-1080 culture (Table III-7). The *in vitro* experiments provided evidence that the conjugates were able to be cleaved in the tumor culture and the extracellular release of peptidyl drug was due to the presence of MMP-2 and MMP-9. In these cell cultures, no serum was present. The absence of serum protein was intended to mimic the conditions in the tumor vicinity *in vivo*. Because of the large sizes of the serum protease inhibitors such as α2-macroglobulin, they are unable to cross the capillary endothelium and therefore are absent in the interstitial fluid. In the tumor tissues, the activities of MMP-2 and MMP-9 are not inhibited by serum proteins although they are regulated more specifically by tissue inhibitors of metalloproteinases (TIMPs) [14].

Table III-7. Susceptibility of the MTX-PVGLIG-Dextran conjugate to cleavage in tumor cell conditioned media

Cell culture	Expression of active MMP-2	Expression of active MMP-9	Percentage cleavage of the conjugate[a]
HT-1080	+++	+++	14.2% ± 0.07%
BT-20	+	-	None detected

[a] The average value of 2 experiments and the standard deviation are reported

Cytotoxicity of the released peptidyl drugs towards tumor cells

Because of the requirement of P3 to P3' sites for substrate recognition by MMP-2 and MMP-9, the released product from the conjugate contains three amino acids attached to the free

drug. Although methotrexate exhibits some bulk tolerance at the gamma-carboxyl site, we are concerned about the therapeutic effect of the released product. The released product from the new conjugate is a peptidyl methotrexate analog (MTX-PVG). The cytotoxicity of MTX-PVG was measured and compared with free methotrexate using MTT assay. For both tumor cell lines, HT-1080 and BT-20, peptidyl methotrexate was cytotoxic with GI50 on the order of 10μM. Compared to free methotrexate, the potency of the drug was lowered by two orders of magnitude (Figure III-13).

Cytotoxicity assays showed that the released product was still effective in inhibiting the proliferation of tumor cells but the potency was lower than the free methotrexate. This is the biggest concern of the current approach, namely, the drug is not released in the original free form. However, the loss in cytotoxicity *in vitro* may not translate to the loss in anti-tumor efficacy *in vivo*. The capability of remaining stable in the systemic circulation, as well as the sensitivity of the new conjugates to the tumor-associated enzymes MMP-2 and MMP-9, suggest that the new conjugates can passively target the tumor tissue and potentially have localized drug release by MMPs. We predict that these qualities will improve both the circulation half life of the conjugate and the percentage dose accumulated in the tumor tissue. While these effects can bring about improvement in anti-tumor efficacy *in vivo* but cannot be measured in cell culture assays, further investigation in animal models is warranted.

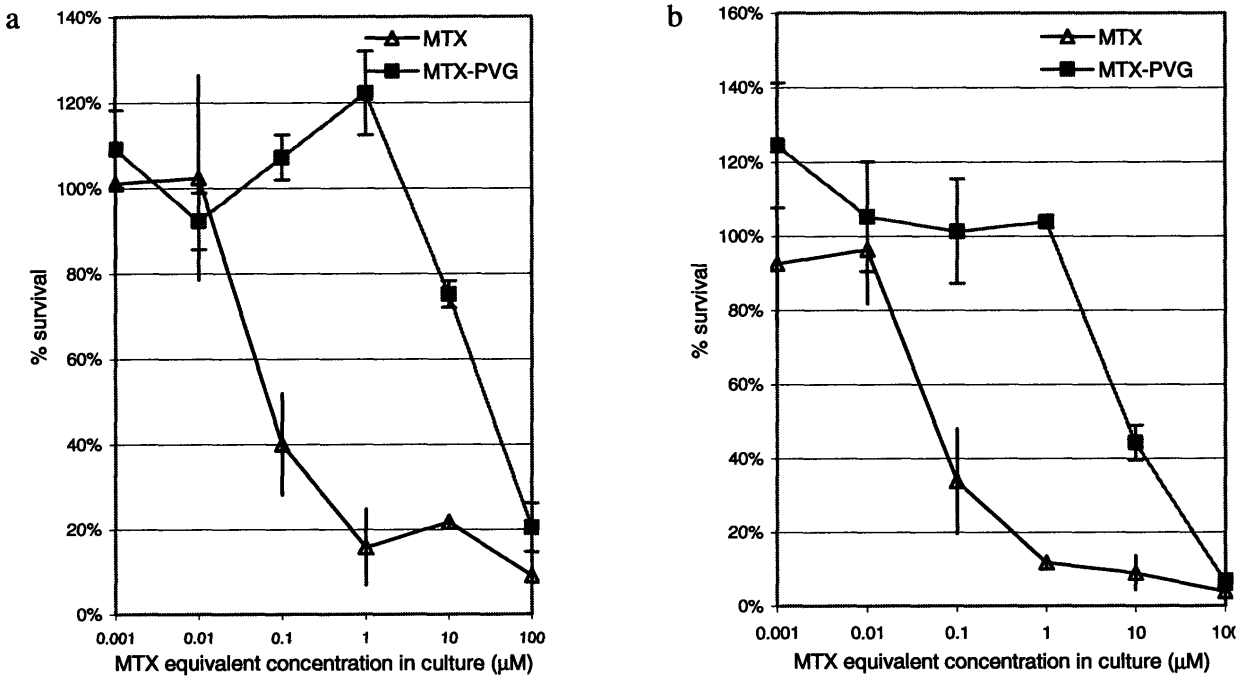

Figure III-13. Cytotoxic effect of methotrexate and methotrexate-Pro-Val-Gly by MTT assays on cell culture : a) HT-1080 and b) BT-20. The average values of 3 replicates with standard deviations as error bars are shown.

References

1. Rosowsky A, Forsch R, Uren J, Wick M. Methotrexate Analogs .14. Synthesis of New Gamma-Substituted Derivatives as Dihydrofolate-Reductase Inhibitors and Potential Anticancer Agents. *Journal of Medicinal Chemistry* 1981;24(12):1450-55.

2. Nogusa H, Yano T, Okuno S, Hamana H, Inoue K. Synthesis of Carboxymethylpullulan Peptide Doxorubicin Conjugates and Their Properties. *Chemical & Pharmaceutical Bulletin* 1995;43(11):1931-36.

3. Nagy A, Szoke B, Schally AV. Selective Coupling of Methotrexate to Peptide-Hormone Carriers through a Gamma-Carboxamide Linkage of Its Glutamic-Acid Moiety - Benzotriazol-1-Yloxytris(Dimethylamino)Phosphonium Hexafluorophosphate Activation in Salt Coupling. *Proceedings of the National Academy of Sciences of the United States of America* 1993;90(13):6373-76.

4. Hibbs MS, Hasty KA, Seyer JM, Kang AH, Mainardi CL. Biochemical and immunological characterization of the secreted forms of human neutrophil gelatinase. *Journal of Biological Chemistry* 1985;260:2493-500.

5. Braunhut SJ, Moses MA. Retinoids Modulate Endothelial-Cell Production of Matrix-Degrading Proteases and Tissue Inhibitors of Metalloproteinases (Timp). *Journal of Biological Chemistry* 1994;269(18):13472-79.

6. Denizot FL, R. Rapid colorimetric assay for cell growth and survival. Modifications to the tetrazolium dye procedure giving improved sensitivity and reliability. *J. Immunol. Meth.* 1986; 89:271.

7. Turk BE, Huang LL, Piro ET, Cantley LC. Determination of protease cleavage site motifs using mixture-based oriented peptide libraries. *Nature Biotechnology* 2001;19(7):661-67.

8. Netzel-Arnett S, Sang QX, Moore WGI, Navre M, Birkedalhansen H, Vanwart HE. Comparative Sequence Specificities of Human 72-kDa and 92-kDa Gelatinases (Type-Iv Collagenases) and Pump (Matrilysin). *Biochemistry* 1993;32(25):6427-32.

9. Denmeade SR, Lou W, Lovgren J, Malm J, Lilja H, Isaacs JT. Specific and efficient peptide substrates for assaying the proteolytic activity of prostate-specific antigen. *Cancer Research* 1997;57(21):4924-30.

10. Marutsuka K, Suzumiya J, Kataoka H, Komada N, Koono M, Sumiyoshi A. Correlation between Urokinase-Type Plasminogen-Activator Production and the Metastatic Ability of Human Rectal-Cancer Cells. *Invasion & Metastasis* 1991;11(4):181-91.

11. Heidtmann HH, Salge U, Havemann K, Kirschke H, Wiederanders B. Secretion of a Latent, Acid Activatable Cathepsin-L Precursor by Human Nonsmall Cell Lung-Cancer Cell-Lines. *Oncology Research* 1993;5(10-11):441-51.

12. Hermanson GT. Bioconjugate Techniques: Academic, 1996.

13. Kuyvenhoven JP, van Hoek B, Blom E, van Duijn W, Hanemaaijer R, Verheijen JH, Lamers C, Verspaget HW. Assessment of the clinical significance of serum matrix metalloproteinases MMP-2 and MMP-9 in patients with various chronic liver diseases and hepatocellular carcinoma. *Thrombosis and Haemostasis* 2003;89(4):718-25.

14. Woessner JF, Nagase H. Matrix Metalloproteinases and TIMPs. New York: Oxford university press, 2000.

CHAPTER IV : *IN VIVO* ANTI-TUMOR EFFICACY OF NEW DEXTRAN-PEPTIDE-METHOTREXATE CONJUGATES

Introduction

We have developed and characterized a new conjugate that is stable under physiological conditions and is capable of drug release by the enzymatic digestion of MMPs. The ultimate goal of this conjugate is to achieve targeted drug delivery to the tumor site, resulting in an improved anti-tumor efficacy and decreased systemic side effects. Although *in vitro* models provide convenient settings for experimentation, with well defined and controllable variables, they lack the complexity of the actual disease environment. Furthermore, we intended our design to favorably alter the pharmacokinetics and biodistribution of the chemotherapeutics. These potential benefits can only be observed in an *in vivo* model, in which tissues are interconnected and mechanisms are in place for drug clearance and metabolism. In the field of polymer-drug conjugates, it has been emphasized that *in vivo* but not *in vitro* results are useful as basic indicators of any clinical potential. Some published records of polymer-drug conjugates in treating tumor-bearing animals are listed in Table IV-1. These findings can be used as a benchmark for gauging our *in vivo* results.

Table IV-1. In vivo anti-tumor effect of polymer-drug conjugates from a number of laboratories

Compound	Antitumor effect	Animal model and therapeutic experiment	Reference
Free MMC	No inhibitory effect on tumor growth	Subcutaneous SW 1116 tumor bearing mice; 2 x i.v. injection at LD_{50} dose; Measured tumor growth of treated group (T) versus control group (C)	1
MMCDan (T-70)	Tumor growth : T/C = 65%		
Mab (Specific)-MMCDan	Tumor growth: T/C= 26%		
Dox	Mean survival: T/C = 125%	Subcutaneous M5076 tumor bearing mice; 3 x i.v. injection Measured mean survival of treated (T) versus control group (C)	2
HPMA-Dox	Mean survival: T/C = 319% with long term survivors (>=120 days)		
Dox	Mean survival: T/C = 133	Subcutaneous B16 melanoma bearing mice; 3x i.p. injection Measured mean survival of treated (T) versus control group (C)	
HPMA-Dox	Mean survival: T/C = 320 with long term survivors (>=30 days)		
Dox	ED_{50} = 0.44 mg/kg	Intramuscular Walker 256 bearing rats; 1xi.v. injection Measured mean survival of treated (T) versus control group (C). Deduced ED_{50}	3
CMPul-DXR	ED_{50} = 1.1 mg/kg		
MMC	Inhibitory effect on tumor growth = 52% at 5mg MMC/kg; toxic death at 10 mg/kg	Subcutaneous B16 melanoma bearing mice; 1xi.p. injection Measured inhibitory effect on tumor growth= % decrease of tumor weight at end point compared to initial weight At least 2 fold increase in MTD by conjugation with chitin / chitosan. Note: i.p. administration of conjugates was less effective than free MMC against i.p. L1210 leukemia model in mice	4, 5
CM-chitin-MMC (carboxymethyl-chitin of MW 600,000 conjugated to MMC via amide linkage subjected to chemical hydrolysis with half life=6.2hr)	Inhibitory effect on tumor growth = 54% at 5 mg eq MMC/kg Inhibitory effect on tumor growth = 100% at 10 mg eq MMC/kg		
Suc-chitosan (N-succinyl chitosan of MW 300,000 conjugated to MMC via amide linkage subjected to chemical hydrolysis with half life=180hr)	Inhibitory effect on tumor growth = 28% at 5 mg eq MMC/kg Inhibitory effect on tumor growth = 83% at 10 mg eq MMC/kg		
Dox	Mean survival: T/C = 147%	i.p. L1210 leukemia bearing mice 1xi.p. injection Measured mean survival of treated (T) versus control group (C) at same equivalent dose (5mg/kg)	6
PGA-Dox (poly(α-L-glutamic acid) of MW 236,000 conjugated to doxorubicin via lysosomal degradable GGGL peptide linker)	Mean survival: T/C = 148%		

There are three main goals in our *in vivo* studies: 1) to measure the anti-tumor efficacy of the new conjugates and compare the results to the free drugs; 2) to evaluate drug-related side effects in normal tissues; 3) to estimate the role of MMP-mediated release in the targeting ability of the new conjugate. For these purposes, we performed experiments in three tumor-bearing mouse models: HT-1080, U-87 and RT-112. RT-112 contrasted the other two models by its lack of MMP-expression. The MMP-sensitive conjugate, MTX-PVGLIG-dextran, was compared with free methotrexate and the MMP-insensitive conjugate, MTX-GIVGPL-dextran, at an equivalent dosage. The two forms of conjugates are similar, differing only by the peptide sequences in their linkers.

Materials and Methods

Materials

Methotrexate was purchased from Sigma-Aldrich. The two conjugates, MTX-PVGLIG-dextran and MTX-GIVGPL-dextran, were synthesized and purified as described (Chapter III) [7]. The four methotrexate-peptide analogs: MTX-G, MTX-GI, MTX-GIV and MTX-PVG were prepared using the reported methods with slight modifications: 1) different amino acid sequences were synthesized on the solid-phase resins and 2) the HPLC purification of these methotrexate-peptide analogs was performed on a smaller 20mL column. Human tumor cell lines HT-1080 and U-87 were grown from seed vials purchased from American Type Cell Culture. RT-112 was a gift from Dr. Marsha Moses at the Children's Hospital (Boston, MA). The cell lines were maintained as described (Chapter III) [7] and tested negative for murine pathogens and mycoplasma prior being used in animal study.

Animal Models

Six-week old female SCID mice were obtained from Charles River Laboratory. Animal studies were conducted in accordance with an approved protocol by the Department of Comparative Medicine at the Massachusetts Institute of Technology. One to two million tumor cells were injected subcutaneously at the mid-dorsal level. Treatment was initiated after the tumor was allowed to grow to about 100 mm^3on the back of the mouse. This experimental protocol is intended to mimic the clinical situation when treatment begins after a tumor has already been established in a patient. Free methotrexate, MTX-PVGLIG-dextran and MTX-GIVGPL-dextran were injected intraperitoneally (i.p.) once a week. The dosage was normalized

according to the body weight of the mouse. In the control group, each mouse was injected with 0.5mL of phosphate buffered saline. Up to three injections were performed for HT-1080 and RT-112 and two injections for the fastest growing U-87. For all three models, the groups receiving MTX-GIVGPL-dextran were sacrificed after the first injection because of severe weight loss. Weight and tumor size were monitored three times a week. Tumor size was calculated with the formula: size = width^2 x length x 0.52.

Histology and Immunochemistry

Tissues were fixed in 10% buffered formalin overnight, and were processed for paraffin embedding and sectioning using standard histological procedures. For bone marrow sections, femurs were decalcified after fixation. Tumor sections were stained with hematoxylin and eosin for general morphologic evaluation, with MMP-2 and MMP-9 antibodies for the expressions of the two enzymes, with Ki67 for proliferating cells, and with CD34 for blood vessels.

Preparation of Tumor Extract and Measurement of MMP concentrations

The procedure of preparing tumor extract was adopted from the Moses Laboratory at the Children's Hospital (Boston, MA) [8]. Samples of dialyzed tumor extract were analyzed for their MMP-2 and MMP-9 concentrations using ELISA kits (Calbiochem) according to the manufacturer's instructions. Gelatin zymography of the tumor extract was performed as described in Chapter III.

Results

Design of animal study

We used subcutaneous tumor models in mice for the *in vivo* studies. These types of rodent models are most common in literature, as exemplified in Table IV-1, and they can be readily set up. Since our design and characterization of the conjugates are associated with human-form MMPs, we selected three tumor cell lines of human origin: HT-1080 human fibrosacroma, U-87 human glioblastoma and RT-112 human bladder tumor. HT-1080 and U-87 are known to overexpress MMP-2 and MMP-9 [9-12]. RT-112 was selected to contrast the other two cell lines by its absence of MMP overexpression to assess whether the treatment efficacy of the new conjugate would depend on the expression of MMP in the tumor model. The level of enzyme expression of the tumor lines were assessed in cell-conditioned media using gelatin zymography (data not shown) and in *in vivo* tumor extracts by ELISA (Table IV-2). The concentration of MMP-2 was 10-fold higher and the concentration of MMP-9 was 50-fold higher in HT-1080 and U-87 tumors than in the RT-112 tumor. Immunohistochemical staining of tumor sections harvested from the mice also indicated that HT-1080 and U-87 were MMP-2 positive and RT-112 was MMP-2 negative (Figure IV-1). MMP-9 staining was positive for all cell lines but the staining was significantly weaker in RT-112 (Figure IV-2).

Table IV-2. ELISA measurement of MMP-2 and MMP-9 in extracts from tumors harvested from the three mice tumor models

	HT-1080	U-87	RT-112
MMP-2 concentration (ng/ml)	17.0 ±6.3	16.1 ±12.4	1.5 ±1.1
MMP-9 concentration (ng/ml)	5.2 ±1.7	5.0 ±1.0	0.1 ±.01

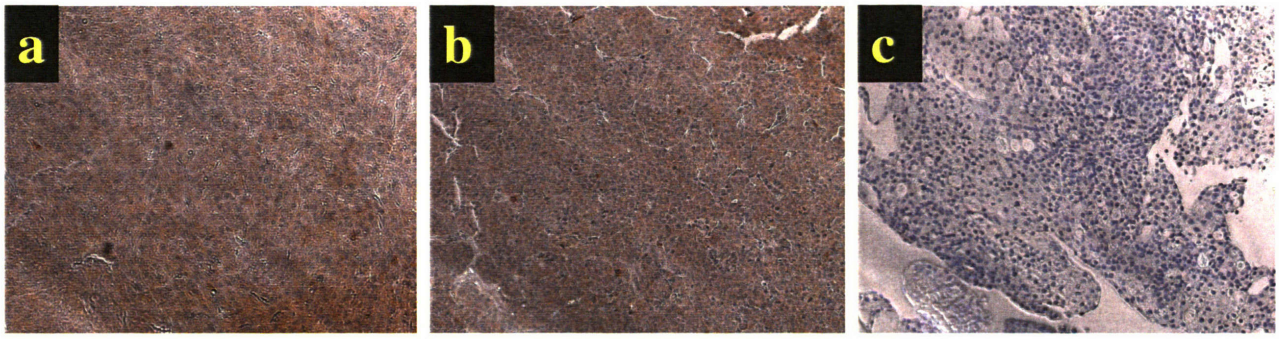

Figure IV-1. Tumor sections harvested from tumor-bearing mice stained against MMP-2 antibody. a) HT-1080; b) U-87; c) RT-112. Brown coloration indicates that the presence of MMP-2.

Figure IV-2. Tumor sections harvested from tumor-bearing mice stained against MMP-9 antibody. a) HT-1080; b) U-87; c) RT-112. Brown coloration indicates that the presence of MMP-9.

Although we used BT-20 to investigate the *in vitro* properties of the conjugate in the absence of MMP over-expression, we did not complete the *in vivo* study with this cell line. We performed one preliminary experiment in BT-20 bearing mice but later observed that the tumor model could not be established reproducibly. The problem failed to be resolved by implanting

more tumor cells, restarting cell passage from existing seeds, or using fresh new seeds from the source company. At that point, we decided to use RT-112 as our best alternative.

Pilot studies were performed in HT-1080 bearing mice to assess the maximum safe dose of the free drug and the conjugate (MTX-PVGLIG-dextran), which was 50mg/kg/week; the results are summarized in Table IV-3. Three weekly dosages were injected by the end of the pilot study when the tumor burden reached the maximally bearable size in the control group. The mice in the conjugate group had slightly more weight loss compared to the saline-treated control group but generally remained healthy and active. The conjugate did not cause any toxic death at this dosage whereas free methotrexate caused an average about 20% death rate for two pilot studies. There was more variability in the death rate in the free methotrexate-treated group, which could not be attributed to drug-related toxicity with full certainty because symptoms such as severe hypoactivity and sharp weight loss were absent. In addition to the weekly injection study, a twice-weekly dosing study was performed with 50mg/kg free methotrexate or MTX-PVGLIG-dextran. Doubling the injection frequency resulted in severe and acute toxicity in both treatment groups, so the subsequent studies were carried out with weekly injections of 50 mg methotrexate eq./mouse body weight and a maximum of three injections were administered.

Table IV-3. Tolerance of tumor bearing mice on different dosage regimes of free methotrexate, dextran-methotrexate and dextran-peptide-methotrexate found in pilot studies

Dosage form	**i.p. dosage per week (mg methotrexate eq. /kg of mouse body weight)**	**% weight drop at the end of the study**	**Number of deaths due to drug-related toxicity**
Free methotrexate	12.5	8%	0/3
	25	20%	0/3
	50	16%;15%	2/5*;0/5
	100	24%	0/4
MTX-dextran conjugate	6.25	13%	0/4
	12.5	16%; 12%	1/3; 0/3
	25	19%	3/3**
	50	27%	3/3**
MTX-PVGLIG-dextran conjugate	12.5	1%	0/3
	25	12%	0/3
	50	13%; 10%	0/3; 0/4
	100	19%	3/4 **
Saline control	0	3%;11%;8%;9%	0/3;0/3;0/3;0/3

* deaths are of unknown causes; drug-related toxicity was suspected
** only 2 weekly injections were performed because of severe toxic response and serious weight loss

In the pilot study, we noted an unexpected phenomenon with MTX-dextran though this dosage form would not be used in the subsequent efficacy study. The maximum tolerable dosage for this conjugate was 12.5mg/kg, 4 fold lower than free methotrexate. Without a peptide linker, we did not expect this conjugate to be cleavable. However, the severe toxicity observed at

25mg/kg, in contrast to the mild weight drop (10-13%) in MTX-PVGLIG-dextran treated group, suggested that there was release of active methotrexate from MTX-dextran.

For the anti-tumor efficacy study, we decided to use MTX-GIVGPL-dextran instead of MTX-dextran to contrast the targeting conjugate MTX-PVGLIG-dextran. MTX-GIVGPL-dextran bears more similarity to MTX-PVGLIG-dextran. They are identical apart from the order of the amino acids in the peptide linkers. The difference in their sensitivity towards MMPs would let us explore the role of the enzymes in the targeting capability of the conjugates.

In summary, we concluded that the subsequent efficacy and side-effect studies would be performed in HT-1080, U-87 and RT-112 bearing mice. The three dosage forms: free methotrexate, MTX-PVGLIG-dextran, MTX-GIVGPL-dextran would be compared at equivalent dosage of 50mg methotrexate eq./kg of body weight. This dosage would be administered via i.p. injection on a weekly basis up to three times. Phosphate-buffered saline injections would serve as the control in these experiments.

Measurement of anti-tumor efficacy

The anti-tumor efficacy in the full-scale study was measured by monitoring the tumor volume after treatment and by histological examination of the tumor tissues. Figure IV-3 showed the results for HT-1080 bearing mice. Three weekly i.p. injections of free methotrexate at 50mg/kg caused only a slight reduction in tumor size. The difference in the tumor size was not significant ($p=0.194$, two-tailed t-test) compared to the control group treated with phosphate-

buffered saline. A week after the third injection, the study was terminated because the tumor size in the control group exceeded 10% of the mouse body weight and the mice needed to euthanized per the guidelines of the animal care committee at our institute. At this point, the tumor size of the group treated with MTX-PVGLIG-dextran at an equivalent dosage (3 x 50mg of methotrexate eq./kg of body weight) averaged only 16.8 ±3.6 % of that of the control group. The inhibition on tumor growth was statistically significant ($p= 1.86x\ 10^{-4}$, one-tailed t-test). The study with MTX-GIVGPL-dextran was terminated prematurely, after the first injection on day 6, because of severe toxicity. Nevertheless, this conjugate was effective in suppressing the tumor growth with tumor size averaging 37.5 ±9.0 % of that of the control group on day 6 (p=0.00056, two-tailed t-test).

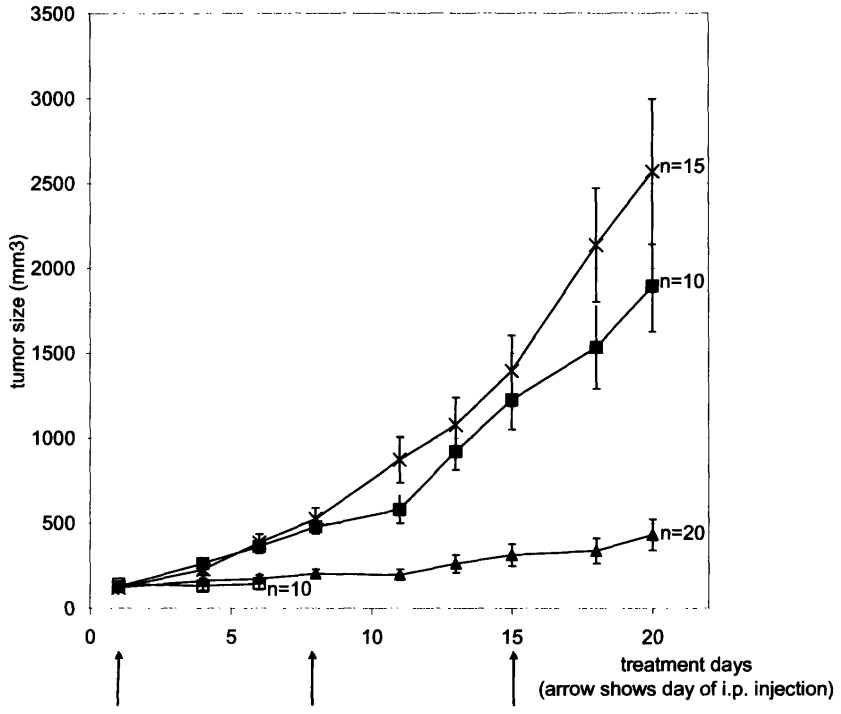

Figure IV-3. Tumor progression in HT-1080 bearing mice with different treatments: free methotrexate (■), MTX-PVGLIG-Dextran (▲), MTX-GIVGPL-Dextran (□) and phosphate buffered saline control (×).Equivalent dosage of methotrexate at 50 mg/kg of mouse body weight was used at each i.p. injection.

The HT-1080 fibrosarcoma in the control and free methotrexate groups consisted of hypercellular sheets of a monomorphic population of oval to spindle shaped cells with coarse chromatin, prominent nucleoli and a moderate amount of eosinophilic cytoplasm. There were numerous mitotic figures (Figure IV-4a, b). In contrast, the tumor in the group treated with MTX-PVGLIG-dextran was much less cellular, had fewer mitotic figures and contained an infiltrate of foamy histiocytes, likely as a response to the treatment (Figure IV-4c).

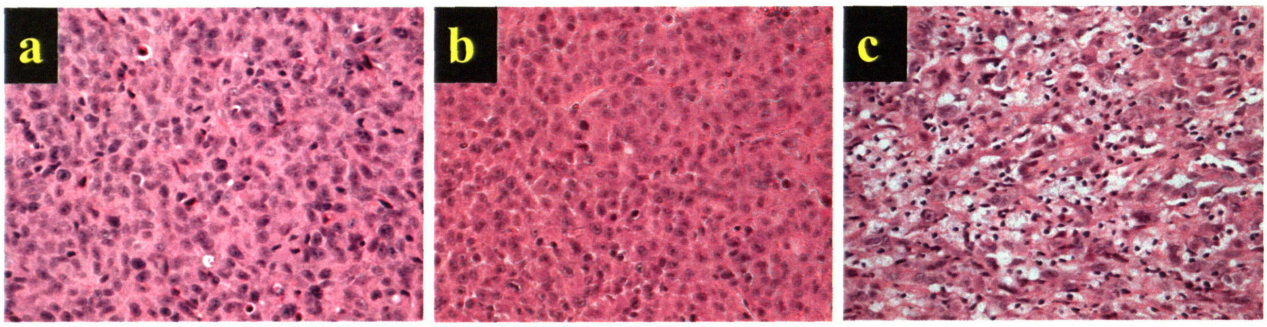

Figure IV-4. Histological examination of H&E stained tumor sections from HT-1080 bearing mice. Tumors were harvested a week after the third injection from mice treated with : a) saline (control); b) free methotrexate ; c) conjugate MTX-PVGLIG-dextran.

The anti-tumor effect from the conjugate MTX-PVGLIG-dextran was also evident by the measurement of the proliferative index using Ki67 stain, a marker for dividing cells. The tumor sections in the saline control and free methotrexate treated group had a much higher proliferative index than the conjugate treated group (Figure IV-5). We also examined the tumor sections stained with CD34, a marker for blood vessels (Figure IV-6). However, we were not able to draw a definite conclusion about the effect of different treatments on the blood vessel density. Further experiments are needed to determine whether the conjugate has any anti-angiogenesis property.

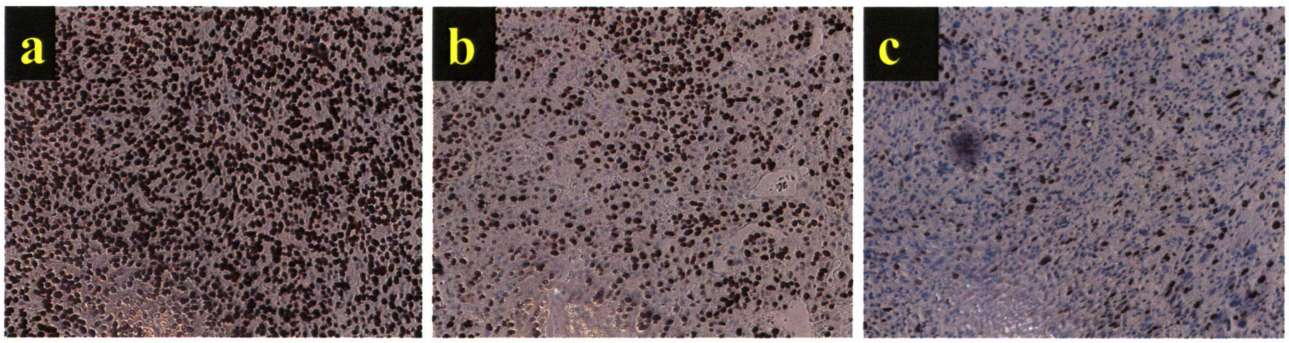

Figure IV-5. Histological examination of Ki67 stained tumor sections from HT-1080 bearing mice. Tumors were harvested a week after the third injection from mice treated with : a) saline (control); b) free methotrexate ; c) conjugate MTX-PVGLIG-dextran. Brown colorations indicate the presence of proliferative cells.

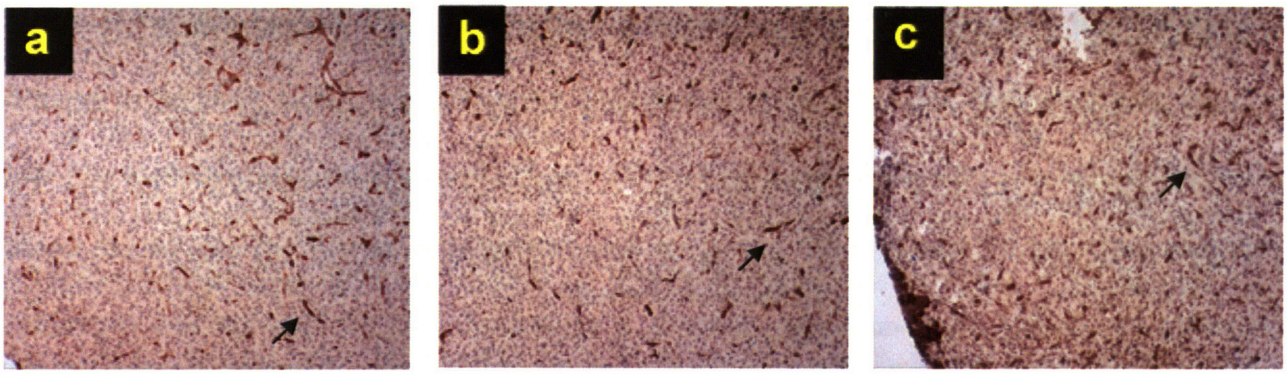

Figure IV-6. Histological examination of CD34 stained tumor sections from HT-1080 bearing mice. Tumors were harvested a week after the third injection from mice treated with: a) saline (control); b) free methotrexate ; c) conjugate MTX-PVGLIG-dextran. Examples of brown stained blood vessels are pointed by arrows.

The results were similar in the U-87 bearing mice (Figure IV-7), whose tumor cells have a higher growth rate than HT-1080. The animal study was terminated a week after the second i.p. injection to avoid excessive tumor burden in the control group. Treatment using free methotrexate at 50mg/kg did not have any effect on the tumor size. ($p=0.48$ compared to the tumor size of the control group using a two-tailed t-test). In contrast, the tumor growth was significantly inhibited in the MTX-PVGLIG-dextran group, with the tumor size averaging 17.2±3.7% of the size of the control group ($p= 1.52 \times 10^{-4}$, two-tailed t-test). Similar to the case in

HT-1080, the study with MTX-GIVGPL-dextran was terminated prematurely on day 6, because of severe toxicity. The conjugate appeared effective in suppressing the tumor growth with tumor size averaging 28.9 ±5.6 % of that of the control group on day 6 (p=0.0026, two-tailed t-test).

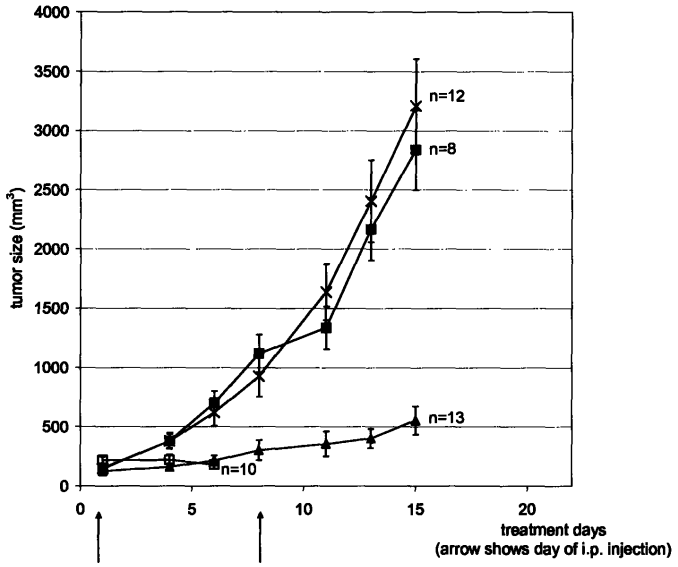

Figure IV-7. Tumor progression in U-87 bearing mice with different treatments: free methotrexate (■), MTX-PVGLIG-Dextran (▲), MTX-GIVGPL-Dextran (□) and phosphate buffered saline control (×).Equivalent dosage of methotrexate at 50 mg/kg of mouse body weight was used at each i.p. injection.

The U-87 glioblastoma in the control and free methotrexate groups consisted of hypercellular sheets of large pleomorphic tumor cells with marked nuclear atypia, prominent nucleoli, and abundant eosinophilic cytoplasm. There were numerous mitotic figures. In contrast, the tumors in the group treated with MTX-PVGLIG-dextran were much less cellular, had fewer mitotic figures and contained an infiltrate of foamy histiocytes, similar to that observed in the HT-1080 treatment group (Figure IV-8).

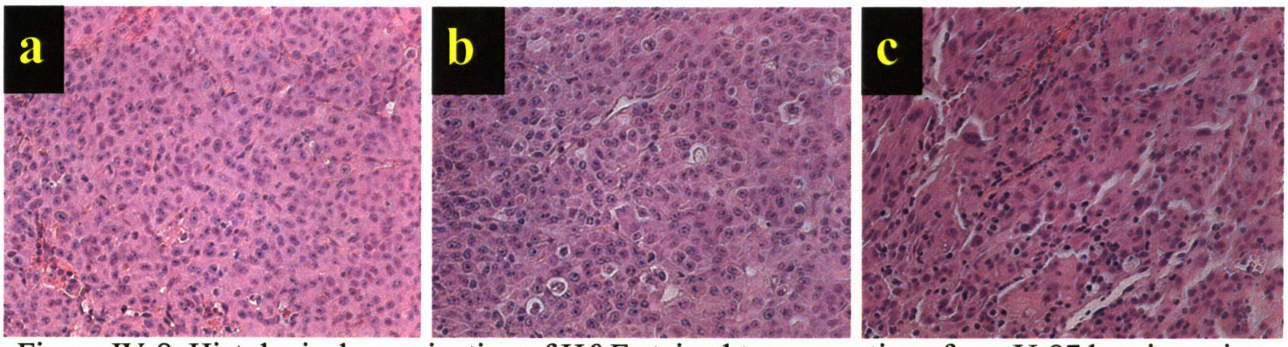

Figure IV-8. Histological examination of H&E stained tumor sections from U-87 bearing mice. Tumors were harvested a week after the second injection from mice treated with : a) saline (control); b) free methotrexate ; c) conjugate MTX-PVGLIG-dextran.

As in the case of HT-1080, the anti-tumor effect from the conjugate MTX-PVGLIG-dextran in the U-87 model was evident by a reduced proliferative index compared to the control and free methotrexate treated groups (Figure IV-9). There appeared to be some reduction in the blood vessel density in the conjugate-treated tumor section (Figure IV-10). However, the difference was not sufficient to let us draw a definite conclusion about the anti-angiogenesis property of the conjugate. More experiments are needed to address this potential of the conjugate.

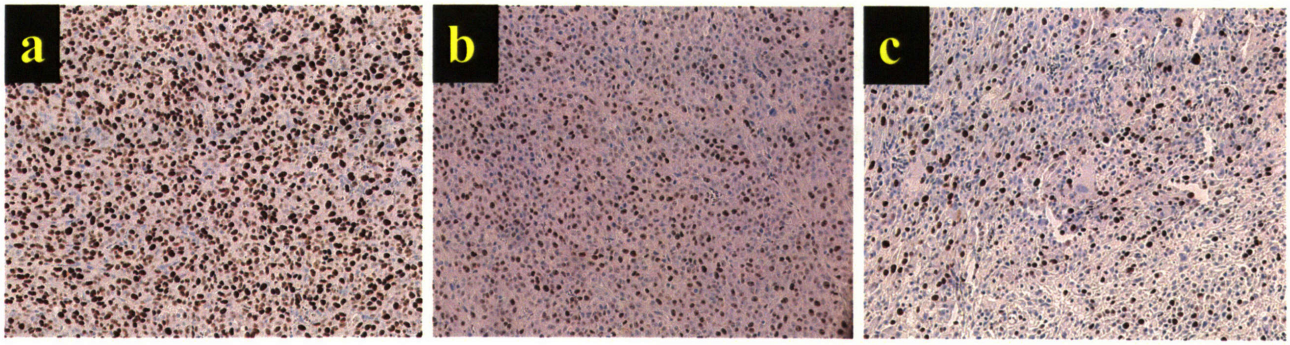

Figure IV-9. Histological examination of Ki67 stained tumor sections from U-87 bearing mice. Tumors were harvested a week after the second injection from mice treated with : a) saline (control); b) free methotrexate ; c) conjugate MTX-PVGLIG-dextran. Brown colorations indicate the presence of proliferative cells.

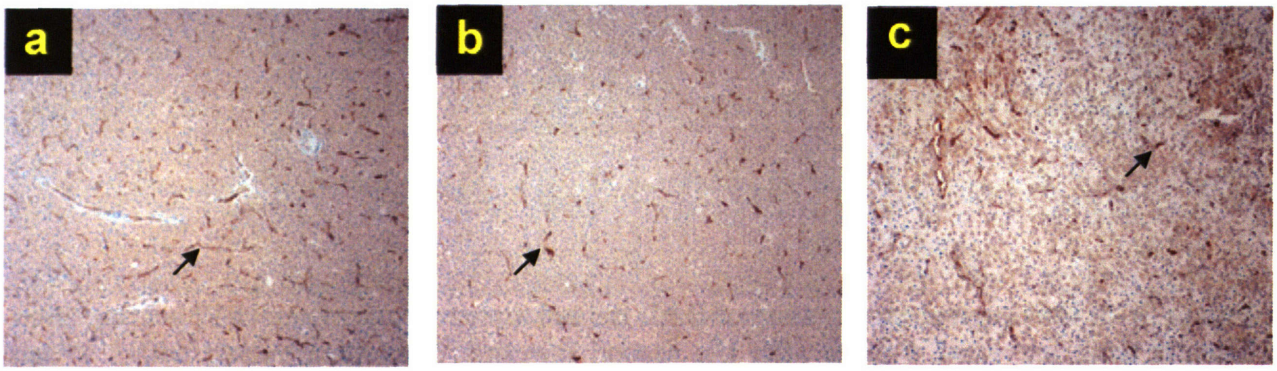

Figure IV-10. Histological examination of CD34 stained tumor sections from U-87 bearing mice. Tumors were harvested a week after the second injection from mice treated with : a) saline (control); b) free methotrexate ; c) conjugate MTX-PVGLIG-dextran. Examples of brown stained blood vessels are pointed by arrows.

In RT-112 bearing mice, neither methotrexate nor the conjugate MTX-PVGLIG-dextran had any significant effect in suppressing tumor growth, as shown in Figure IV-11. The two-tailed t-tests between the treatment groups and the control groups gave p= 0.48 and 0.30 respectively. RT-112 tumor grew much slower than HT-1080 and U-87. At one week after the 3rd injection, the tumor size of the control group averaged 541±161 cm^3 in RT-112 bearing mice whereas the tumor size averaged 2569±427 cm^3 in the control group of HT-1080 bearing mice. Treatment with MTX-GIVGPL-dextran did not result in a significant anti-tumor effect (p=0.079, two-tailed t-test compared with the control) but severe toxicity was again observed after the 1st injection. The study with this MMP-insensitive conjugate was aborted on day 6 for the same reasons as aforementioned studies.

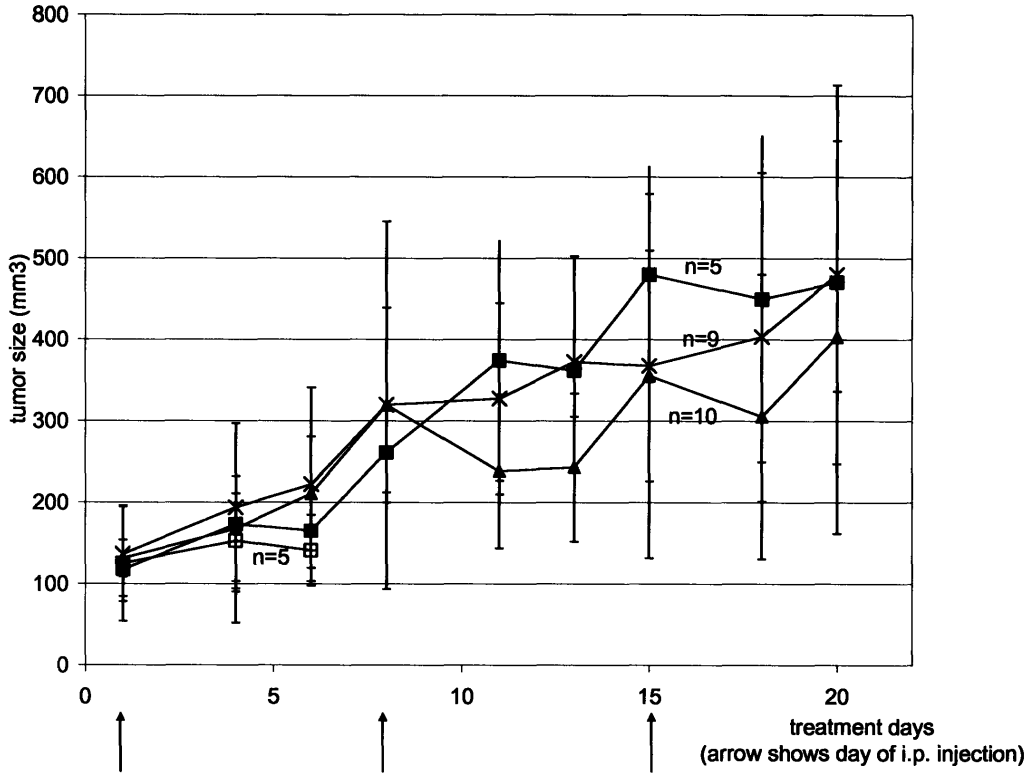

Figure IV-11. Tumor progression in RT-112 bearing mice witht different treatments: free methotrexate (■), MTX-PVGLIG-Dextran (▲), MTX-GIVGPL-Dextran (□) and phosphate buffered saline control (×).Equivalent dosage of methotrexate at 50 mg/kg of mouse body weight was used at each i.p. injection.

The RT-112 bladder tumor in all treatment groups consisted of an epithelial tumor with predominantly transitional features, but with focal glandular formation. There was no significant difference between the control group and the various treatment groups from the standpoint of the histological evaluation (Figure IV-12).

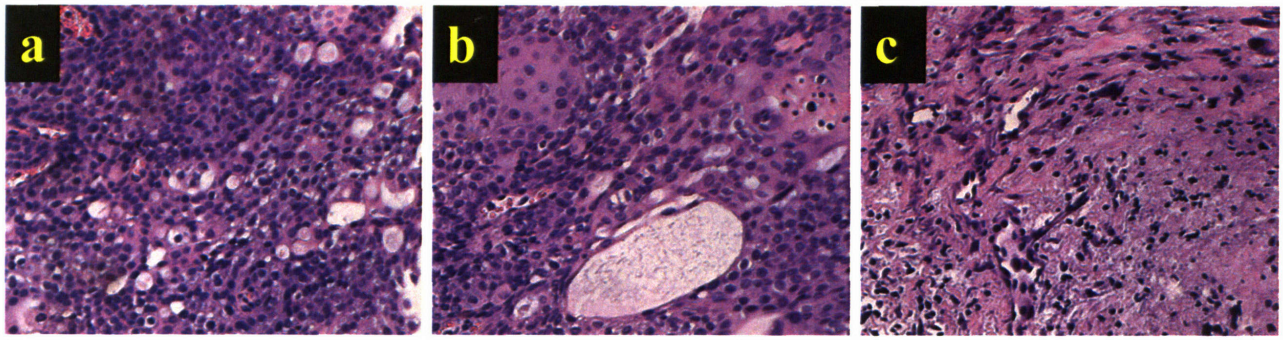

Figure IV-12. Histological examination of H&E stained tumor sections from RT-112 bearing mice. Tumors were harvested a week after the third injection from mice treated with : a) saline (control); b) free methotrexate ; c) conjugate MTX-PVGLIG-dextran.

Examination of Ki67 staining consistently showed that the proliferative index was similar among the control, the free methotrexate-treated and the conjugate-treated groups (Figure IV-13). Compared to HT-1080 and U-87, the control tumor of RT-112 had a lower proliferative index (Figure IV-5a, Figure IV-9a, Figure IV-13a). CD34 staining was obscured by the cross-staining on tumor cells (Figure IV-14). As in the previous mouse models, we could not draw a conclusion about the anti-angiogenesis property of the conjugate based on the histological examination.

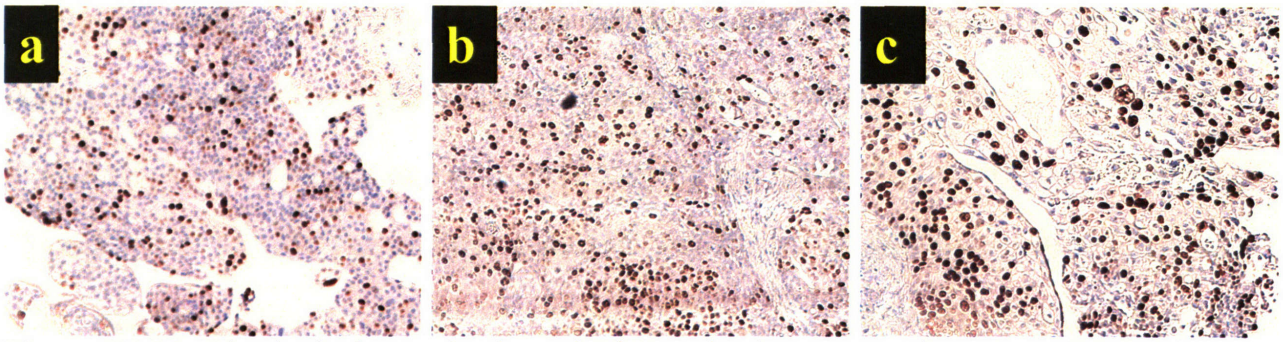

Figure IV-13. Histological examination of Ki67 stained tumor sections from RT-112 bearing mice. Tumors were harvested a week after the third injection from mice treated with : a) saline (control); b) free methotrexate ; c) conjugate MTX-PVGLIG-dextran. Brown colorations indicate the presence of proliferative cells.

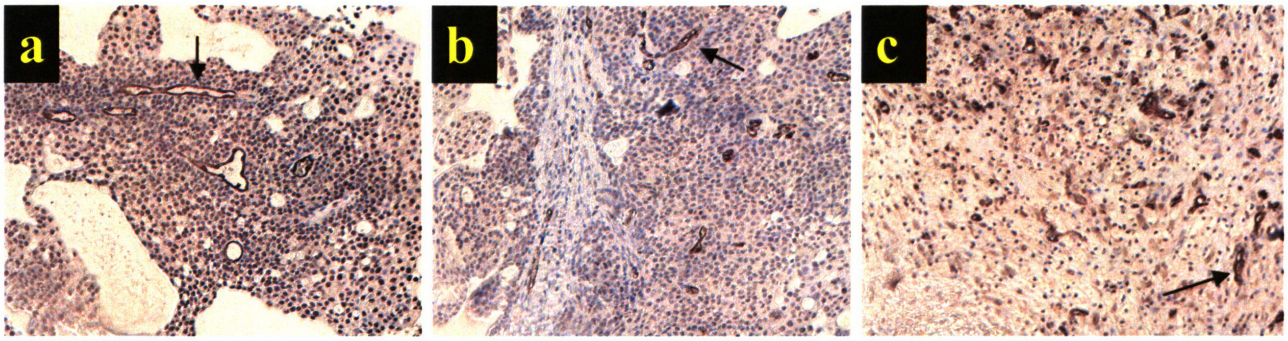

Figure IV-14. Histological examination of CD34 stained tumor sections from RT-112 bearing mice. Tumors were harvested a week after the third injection from mice treated with : a) saline (control); b) free methotrexate ; c) conjugate MTX-PVGLIG-dextran. Examples of brown stained blood vessels are pointed by arrows.

Study on systemic side effects

The body weight of the mice was monitored as an indicator of systemic toxicity. To ensure that the modified dextran carrier of the conjugates did not induce toxicity, mice were injected with carboxymethyl dextran that was charge neutralized with ethanolamine during the pilot study (data not shown). A week after three injections, the body weight increased slightly by 7.8% ±4.8%. The lack of any toxic response supported that the modified dextran was biocompatible. One week after multiple injections with the MMP-sensitive conjugate MTX-PVGLIG-dextran, we observed a small decrease in body weight in the HT-1080 (-11±1.8%) and U-87 (-1.3±1.6%) bearing mice. In RT-112 bearing mice, the body weight increased at the end of the study (+8.6±2.5%). These weight changes were not significantly different from the groups receiving phosphate buffered saline as a control or with free methotrexate injections. The most drastic weight loss was observed in the groups treated with MTX-GIVGPL-dextran, the conjugates with the scrambled peptide linkers insensitive to MMP. In all three tumor models, the

mice receiving only single injection of MTX-GIVGPL-dextran suffered 15--25% weight loss (Table IV-4). The mice were severely hypoactive and their hair was ruffled, significantly worse than the control or the free methotrexate group. As a result, they were sacrificed on day 6 post treatment because of the drug-related toxicity.

Table IV-4. Summary of side effects due to treatment with free methotrexate, MTX-PVGLIG-dextran, MTX-GIVGPL-dextran and saline (control)

	%Body weight change[a]		Drug-related toxic response in small intestine	Drug-related toxic response in bone marrow
Phosphate-buffered saline (Control)	H[b]	-4.5% (± 2.6%)	None	None
	U[c]	-1.5% (± 3.0%)	None	[e]
	R[d]	+10% (± 3.7%)	None	None
Free methotrexate	H	-16% (± 2.3%)	None-to-minimal	None
	U	+4.0%(± 2.8%)	None-to-minimal	[e]
	R	+10% (± 3.7%)	None	None
Conjugate MTX-PVGLIG-dextran	H	-11% (± 1.8%)	None-to-minimal	None
	U	-1.3% (± 1.6%)	None-to-minimal	[e]
	R	+8.6%(± 2.5%)	None	None
Conjugate MTX-GIVGPL-dextran	H	-18% (± 3.0%)	Moderate	Moderate-to-severe
	U	-23% (± 1.9%)	Moderate	[e]
	R	-21%(± 1.6%)	Moderate	Moderate-to-severe

[a] The body weight at the last day of the study- a week after the last injection- was compared with the initial body weight on the treatment start date.

[b,c,d] Abbreviations for the three tumor models: H=HT-1080; U=U-87; R=RT-112

[e] Bone marrow tissues were not sampled from U-87 bearing mice

The side effects were further evaluated by histological examinations of the major tissues, including small intestine, bone marrow, liver, kidney, spleen and skin. Regardless of the type of tumor model, there was moderate-to-severe toxicity in the small intestines and the bone marrows in all of the mice treated with the MMP-insensitive conjugate MTX-GIVGPL-dextran (Table IV-4). The drastic weight loss and these tissue damages showed that MTX-GIVGPL-dextran caused toxicity, independent of the MMP expression level of the tumor model.

The histologic changes in the small intestine of MTX-GIVGPL-dextran treated mice consisted of epithelial necrosis with focal regenerative changes, and occasional degeneration of the muscularis without evidence of frank perforation. There were only a limited number of cases with minimal small intestinal toxicity in the mice treated with the MTX-PVGLIG-dextran or with free methotrexate, consisting of regenerative changes in the epithelium and increased chronic inflammation in the lamina propria. In most cases, the small intestines appeared healthy and similar to the control mice treated with saline (Figure IV-15 and Appendix A).

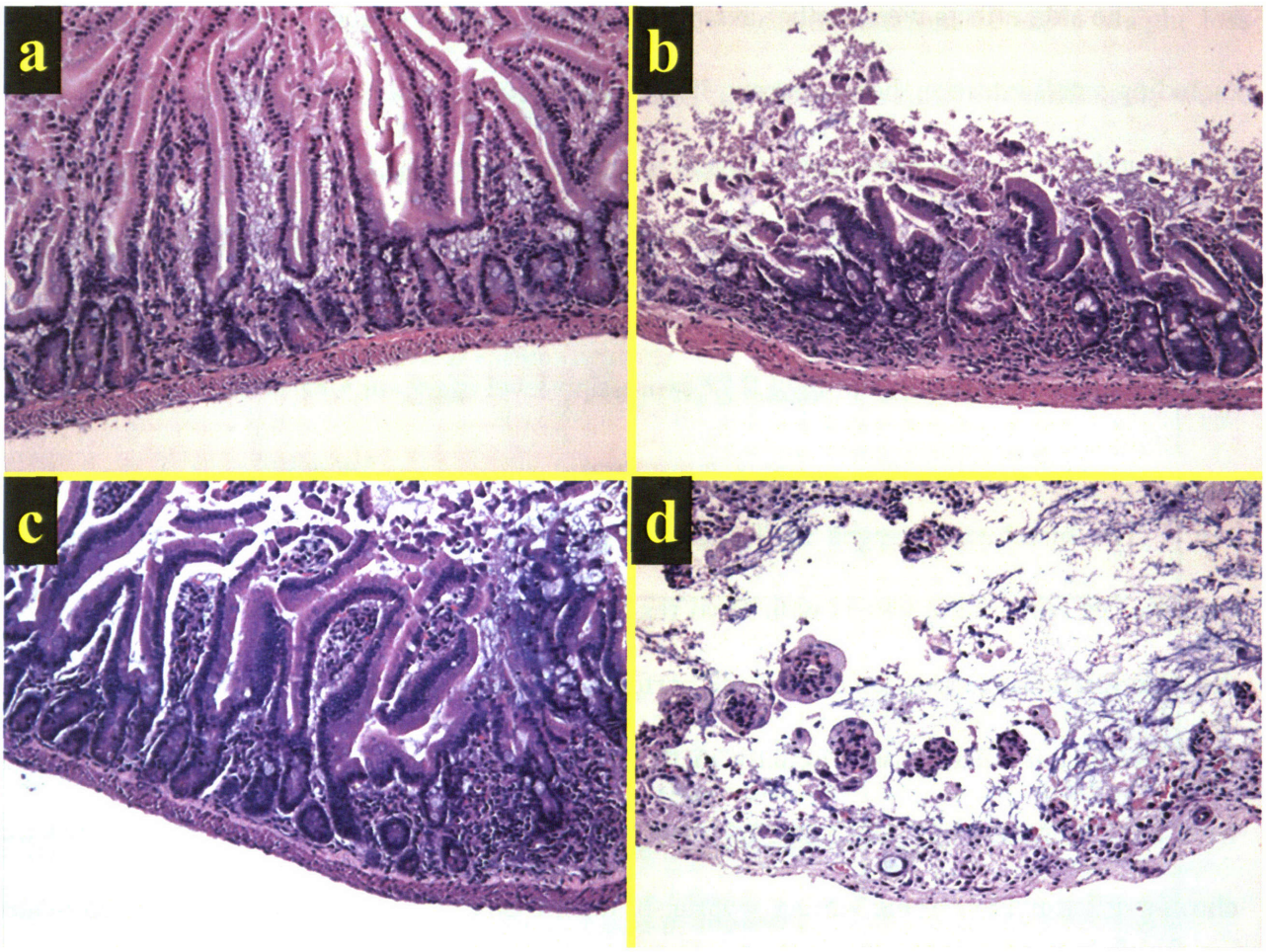

Figure IV-15. Histological examination of the small intestine sections from HT-1080 bearing mice. Tissues were harvested from mice treated with: a) 3 injections of saline (control); b) 3 injections of free methotrexate ; c) 3 injections of conjugate MTX-PVGLIG-dextran; d) 1 injection of conjugate MTX-GIVGPL-dextran.

In the bone marrow, there was necrosis and hemorrhage with a loss of all hematopoetic lineages in the MTX-GIVGPL-dextran treated mice. These signs of tissue damage were absent in the mice treated with saline, free methotrexate or MTX-PVGLIG-dextran (Figure IV-16 and Appendix B).

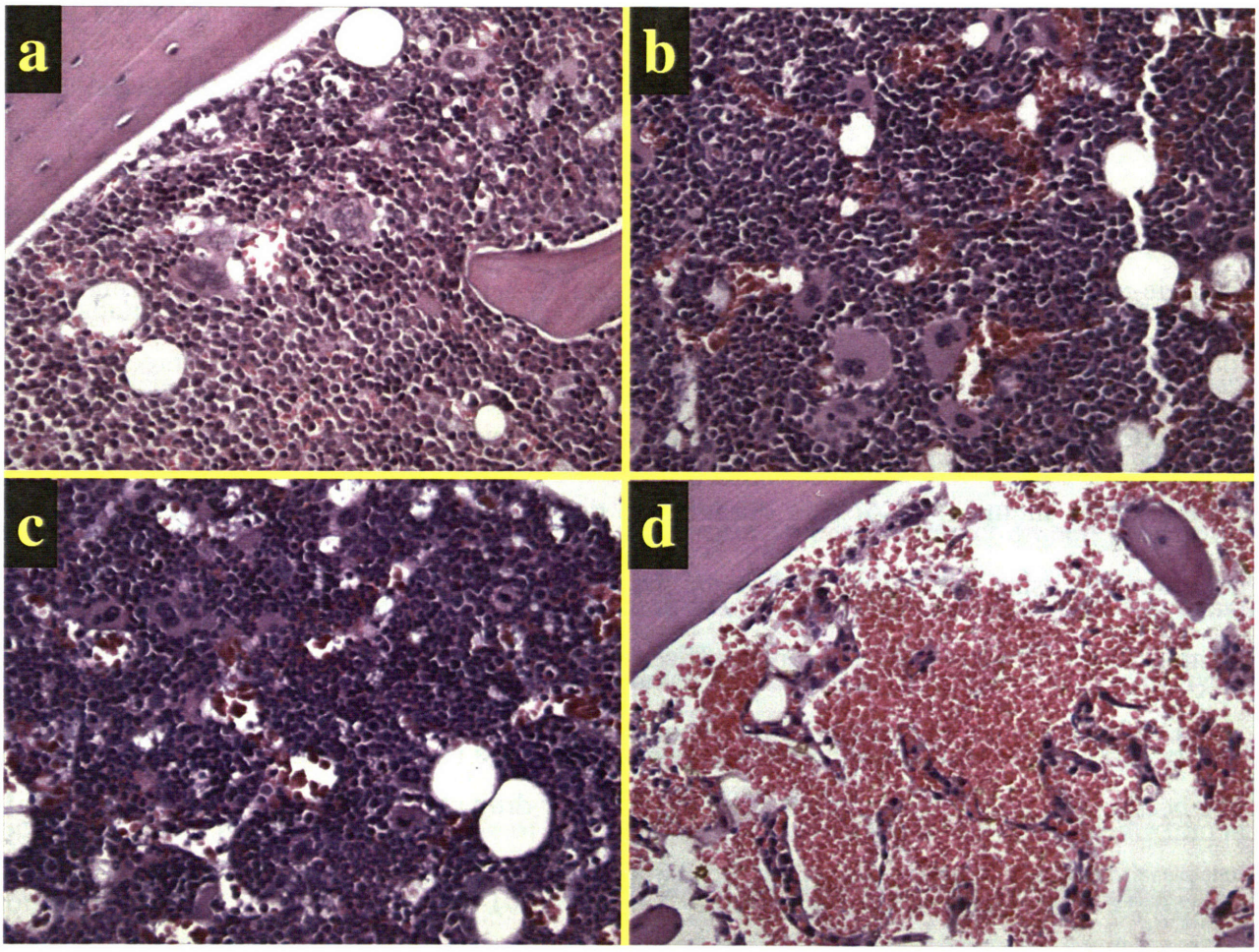

Figure IV-16. Histological examination of the bone marrow sections from HT-1080 bearing mice. Tissues were harvested from mice treated with : a) 3 injections of saline (control); b) 3 injections of free methotrexate ; c) 3 injections of conjugate MTX-PVGLIG-dextran; d) 1 injection of conjugate MTX-GIVGPL-dextran.

Liver (Appendix C), kidney (Appendix D), spleen (Appendix E) and skin (Appendix F) appeared healthy in all treatment groups. There was occasional non-specific mild extramedullary hematopoiesis in the liver and spleen.

Discussion

The primary goal in this study was to evaluate the anti-tumor efficacy of the new dextran-peptide-methotrexate conjugate in an *in vivo* model system. Based on the pilot experiments, the dose of 50mg methotrexate eq./kg of body weight administrated weekly up to three times was selected. This dosage equals half the maximum tolerated dose found by Burger using free methotrexate in mice [13]. At this dosage, we did not detect any therapeutic effect for free methotrexate using our animal models. On the other hand, the MTX-PVGLIG-dextran conjugate demonstrated an increased anti-tumor efficacy without any significant side effect in HT-1080 and U-87 bearing mice. The inhibition in tumor growth (by 83% in both models) was on par with the best results found in the literature on the polymer-drug conjugate investigation (Table IV-1). Since the potency of the released MTX-peptide analog was two orders of magnitude lower than free methotrexate, this promising result suggested that the conjugate had a significantly higher tumor targeting ratio.

The superior anti-tumor efficacy could possibly be due to the prolonged circulation of methotrexate as a result of passive targeting. In its free form, methotrexate is cleared rapidly from the body by the kidney[14]. The dextran carrier we selected for conjugation with the drug has a nominal molecular weight of 70,000 Da. Reports from Kopecek's group and others have shown that the renal excretion limit is about 40,000 Da[15]. Our conjugate is intentionally sized above this threshold. The tumor targeting ratio could also be potentially enhanced by the mediation of

MMPs. These tumor-associated enzymes could release more active peptide-methotrexate from the conjugate at the tumor tissue.

We attempted to shed some light on the targeting mechanism by comparing the *in vivo* observations among tumor models with different levels of MMP expression. Out of the three tumor models, only RT-112 did not show any treatment effect by the MTX-PVGLIG-dextran conjugate. It was also the cell line with the lowest level of MMP expression. As an anti-metabolite, methotrexate must be released from the carrier to exert its effect on cell growth by inhibiting DNA synthesis. The release can happen in two ways: 1) by non-specific endocytosis, as conjugates are internalized by cells and methotrexate can be released by either acid hydrolysis or lysosomal enzyme digestion or 2) by MMP cleavage of the peptide linker in the extracellular vicinity of tumor tissue. The latter route of localized drug release from MTX-PVGLIG-dextran is not as probable in RT-112 as in HT-1080 or U-87, due to their differential MMP expression levels. However, RT-112 also differs from HT-1080 and U-87 in its *in vivo* growth kinetics, so the lack of treatment effect may not be solely due to the low expression of MMP-2 and MMP-9 in RT-112. The treatment effectiveness of the conjugate was accompanied by a reduction in proliferative index. This is in agreement with the pharmacological action of methotrexate, which hinders proliferation by inhibiting DNA synthesis through its binding of dihydrofolate reductase. As the mechanism to suppress tumor growth is related to the inhibition of tumor cell proliferation[14], if the tumor model is not highly proliferative, as in the case of RT-112, the therapeutic effect of free methotrexate or the conjugate will be limited.

The new conjugate, MTX-PVGLIG-dextran, was well tolerated by the mice under the current treatment regime. The weight drop was minor, and histological examination of the major organs and tissues did not find any significant toxicity. In clinical uses, free methotrexate is known to cause side effects in the gastrointestinal tract and in the bone marrow[14]. In our study, the mice treated by free methotrexate at the designated dosage did not show any severe drug-related toxicity. However, some HT-1080 and RT-112 bearing mice died from unknown reasons prior the completion of the free methotrexate treatment. These accounted for approximately 13% of the total number in the methotrexate group and we did not observe any similar case in the saline control group.

The severe and acute drug-related toxicity caused by the MMP-insensitive conjugate, MTX-GIVGPL-dextran, was surprising. This conjugate resulted in more than 20% weight drop causing us to sacrifice the mice after only the first injection. Severe necrosis within the small bowel and bone marrow was present. This form differs from the well-tolerated MTX-PVGLIG-dextran only in the sequence of amino acids in the peptide linker. Without an MMP-sensitive linker, MTX-GIVGPL-dextran was predicted to have a lower anti-tumor efficacy because of its inability to release active peptide-methotrexate. However, it seemed capable of inhibiting tumor growth, despite the fact that the study ended prematurely due to drug-related toxicity. Differences between the two types of the conjugates in systemic side effects suggest that MMP-independent release from MTX-GIVGPL-dextran is possible.

From our *in vivo* study, it was evident that MTX-PVGLIG-dextran is a promising vehicle to achieve tumor-targeted delivery of methotrexate in MMP-overexpressing models. However, it

was unclear if and how the difference in drug-related toxicity was related to the MMP specificity of the linkers. Further studies in assessing the biodistribution of the conjugate and the drug release profile should be useful in understanding the targeting mechanism of the new conjugate.

References

1. Noguchi A, Takahashi T, Yamaguchi T, Kitamura K, Takakura Y, Hashida M, Sezaki H. Tumor-Localization and Invivo Antitumor-Activity of the Immunoconjugate Composed of Anti-Human Colon Cancer Monoclonal-Antibody and Mitomycin C-Dextran Conjugate. *Japanese Journal of Cancer Research* 1991;82(2):219-26.

2. Duncan R, Seymour LW, O'Hare KB, Flanagan PA, Wedge S, Hume IC, Ulbrich K, Strohalm J, Subr V, Spreafico F. Preclinical evaluation of polymer-bound doxorubicin. *Journal of Controlled Release* 1992;19(1-3):331-46.

3. Nogusa H, Yano T, Kajiki M, Gonsho A, Hamana H, Okuno S. Antitumor effects and toxicities of carboxymethylpullulan-peptide-doxorubicin conjugates. *Biological & Pharmaceutical Bulletin* 1997;20(10):1061-65.

4. Song YH, Onishi H, Nagai T. Pharmacokinetic Characteristics and Antitumor-Activity of the N-Succinyl-Chitosan Mitomycin-C Conjugate and the Carboxymethyl-Chitin Mitomycin-C Conjugate. *Biological & Pharmaceutical Bulletin* 1993;16(1):48-54.

5. Rosowsky A, Forsch R, Uren J, Wick M. Methotrexate Analogs .14. Synthesis of New Gamma-Substituted Derivatives as Dihydrofolate-Reductase Inhibitors and Potential Anticancer Agents. *Journal of Medicinal Chemistry* 1981;24(12):1450-55.

6. Hoes CJT, Grootoonk J, Duncan R, Hume IC, Bhakoo M, Bouma JMW, Feijen J. Biological Properties of Adriamycin Bound to Biodegradable Polymeric Carriers. *Journal of Controlled Release* 1993;23(1):37-54.

7. Chau Y, Tan FE, Langer R. Synthesis and characterization of dextran-peptide-methotrexate conjugates for tumor targeting via mediation by matrix metalloproteinase II and matrix metalloproteinase IX. *Bioconjugate Chemistry* 2004;15(4):931-41.

8. Peters CA, Freeman MR, Fernandez CA, Shepard J, Wiederschain DG, Moses MA. Dysregulated proteolytic balance as the basis of excess extracellular matrix in fibrotic disease. *Am J Physiol Regul Integr Comp Physiol* 1997;272(6):R1960-65.

9. Lu WS, Zhou XP, Hong B, Liu HM, Yue ZJ. Suppression of invasion in human U87 glioma cells by adenovirus-mediated co-transfer of TIMP-2 and PTEN gene. *Cancer Letters* 2004;214(2):205-13.

10. Nutt JE, Durkan GC, Mellon JK, Lunec J. Matrix metalloproteinases (MMPs) in bladder cancer: the induction of MMP9 by epidermal growth factor and its detection in urine. *Bju International* 2003;91(1):99-104.

11. Emmertbuck MR, Emonard HP, Corcoran ML, Krutzsch HC, Foidart JM, Stetlerstevenson WG. Cell-Surface Binding of Timp-2 and Pro-Mmp-2/Timp-2 Complex. *Febs Letters* 1995;364(1):28-32.

12. Okada Y, Gonoji Y, Naka K, Tomita K, Nakanishi I, Iwata K, Yamashita K, Hayakawa T. Matrix Metalloproteinase-9 (92-Kda Gelatinase Type-Iv Collagenase) from Ht-1080 Human Fibrosarcoma Cells - Purification and Activation of the Precursor and Enzymatic-Properties. *Journal of Biological Chemistry* 1992;267(30):21712-19.

13. Burger AM, Hartung G, Stehle G, Sinn H, Fiebig HH. Pre-clinical evaluation of a methotrexate-albumin conjugate (MTX-HSA) in human tumor xenografts in vivo. *International Journal of Cancer* 2001;92(5):718-24.

14. Chamber BA, Ryan DP, Paz-Ares L, Garcia-Carbonero R, Calabresi P. In: Hardman JG, Limbird LE, Gilman AG, eds. Goodman and Gilman's The Pharmacological Basis of Therapeutics: The McGraw-Hill Companies, Inc., 2001:1389.

15. Putnam D, Kopecek J. Polymer conjugates with anticancer activity Biopolymers II, vol. 122, 1995:55-123.

CHAPTER V : BIODISTRIBUTION STUDY WITH NEW DEXTRAN-PEPTIDE-METHOTREXATE CONJUGATES

Introduction

As described in Chapter IV, we observed that the new conjugate with a MMP-sensitive linker, MTX-PVGLIG-dextran, demonstrated a superior anti-tumor effect compared to free drug (methotrexate). In our working hypothesis, the improved efficacy is a result of the passive and active targeting capabilities of the new conjugate. Unlike the MMP-sensitive conjugate, we found that the MMP-insensitive conjugate caused severe side effects. The targeting mechanism of the new conjugate and the cause of side effects are the topics of investigation in this chapter.

In passive targeting, the drug molecules can circulate in the blood plasma for a prolonged period of time as a result of their conjugation to a polymer backbone, presumably due to reduced clearance by the kidney and the liver. The plasma drug concentration is maintained above the therapeutic concentration longer and the conjugate is allowed additional time to reach the targeted tissues. Maeda has discovered the effect called enhanced permeation and retention (EPR), which describes the preferential accumulation of large macromolecules in the tumor tissues. Because of the pathophysiology of tumor tissues, which includes leaky blood vessels and poor lymphatic drainage, high molecular weight conjugates can theoretically permeate better into the solid tumor and remain at the tumor site [1].

Traditionally, the design criteria of the linker between the drug and the polymer are: 1) the linker is stable during storage and remains intact in the general circulation; and 2) it is able to be cleaved to release the drug after the conjugate is internalized into the cell. The latter requirement has prompted the development of acid-labile linkers cleavable by low pH and peptide linkers cleavable by ubiquitous intracellular enzymes such as lysosomal enzymes[2]. The function of actively targeting the delivery to the diseased tissues has been carried out by homing signals such as monoclonal antibodies and antigens for specific receptors[3 4 5 6]. We have proposed a linker that is sensitive to disease-associated enzymes. These enzymes are characteristic of the immediate extracellular environment of the target tissue. In the context of tumor targeting, a linker labile to tumor-associated enzymes can potentially provide a means for site-specific drug delivery. For our conjugate, the linker joining methotrexate to the dextran backbone has been optimized for cleavage by matrix-metalloproteinases[7-9]. These enzymes are overexpressed in a number of cancers[10, 11 12 13 14 15] and are implicated with various functions for the growth and metastasis of tumor cells[16].

We intended to verify and measure the extent of passive and active targeting by assessing the plasma pharmacokinetics and tissue distribution in mice with MMP-overexpressing tumor xenografts. To address our questions regarding passive targeting and EPR effect, we compared the conjugates with free drug. To gauge the effects of MMPs in mediating drug release from our conjugates, we compared the MMP-sensitive conjugate (MTX-PVGLIG-dextran) with the MMP-insensitive conjugate (MTX-

GIVGPL-dextran). We attempted to find supporting evidence for our hypothesis that enzymes other than MMPs are involved in causing the discrepancy in drug-related toxicity between the two types of conjugates.

Materials and Methods

Methotrexate was ordered from Sigma. The two conjugates, MTX-PVGLIG-dextran and MTX-GIVGPL-dextran were prepared as described[9].

Human xenograft tumor models in mice were established as described[17], and were in accordance to the guidelines of the Animal Care Committee at the Massachusetts Institute of Technology. HT-1080 bearing mice with tumor size of 500-1500mm^3 were injected i.p. with either methotrexate, MTX-PVGLIG-dextran or MTX-GIVGPL-dextran at 50mg MTX eq./kg mouse body weight. One group of mice receiving MTX-PVGLIG-dextran was also injected with minocyclin at 50mg/kg twice daily starting from the day before the conjugate injection. Blood and major tissues were harvested from at least three mice were used for each specified time point.

Tissue homogenate was obtained by homogenizing the thawed tissue in a cold buffer (0.5M sucrose, 20mM Tris, 5.5mM EDTA with complete protease inhibitor (Roche Cat. No. 1873580) and pH adjusted to 7.5) at 25% w/w and centrifuging at 16000g at 8°C for 10 minutes. The supernatant was retained. Tissue homogenate and plasma samples from mice injected with the two conjugates were further processed with a membrane device to separate the uncleaved conjugate from the released methotrexate-peptide.

Blood plasma was diluted 10-fold and heart homogenate was diluted 5-fold with a buffer (same composition as the homogenization buffer) at room temperature. The diluted sample was centrifuged in a Microcon with 10,000 MWCO (Millipore) at 14000g for 30 minutes at room temperature. This step was repeated 3 times and the retentate chamber was replenished with the buffer after each spin. Filtrate from the first two spins, containing methotrexate-peptide, which was smaller than the cutoff of the membrane, was pooled for measurement. Retentate obtained after the last spin contained the uncleaved conjugate and was also measured for the methotrexate equivalent concentration.

Other types of tissue homogenate were first precipitated by adding an equal volume of acetonitrile and centrifuging at 13000rpm for 10 min at room temperature. The supernatant was processed with a membrane ultrafiltration device, Ultrafree-MC with 10,000 MWCO (Millipore), by spinning 2 times at 5600g for 60 minutes at room temperature. A solution of 1:1 acetonitrile: homogenization buffer was used to replenish the retentate chamber after each spin. Filtrate from the first spin and the retentate after the last spin was measured for the methotrexate equivalent concentrations.

The concentrations of methotrexate, methotrexate-peptide and dextran-peptide-methotrexate conjugate were measured by the TDxFLx® system using the reagents for methotrexate quantitation (Abbott Laboratory). The instrument made use of a technology combining fluorescence polarization and competitive binding immunoassay [18]. To obtain the concentration of methotrexate-peptide and dextran-peptide-methotrexate, we

multiplied the TDx readouts by 1.8 and 2.0 respectively. These conversion factors were obtained by a linear regression between the TDx readouts and the known concentrations of these two types of samples. The formulae used to calculate values found in the current report were listed below.

% conjugate = Percentage of equivalent methotrexate found in uncleaved conjugate
= concentration of conjugate / (concentration of methotrexate-peptide + concentration of conjugate) x 100%

Total methotrexate equivalent concentration in tissue (from mice injected with free methotrexate) = homogenate reading x 4

Total methotrexate equivalent concentration in plasma (from mice injected with free methotrexate) = plasma reading

Total methotrexate equivalent concentration in tissue (from mice injected with conjugate) = homogenate reading x 4 x (% conjugate x 2.0 + (1.0-% conjugate) x 1.8)

Total methotrexate equivalent concentration in plasma (from mice injected with conjugate) = homogenate reading x (% conjugate x 2.0 + (1.0-% conjugate) x 1.8)

The half-life of elimination of the two conjugates in plasma was estimated by assuming a one-compartment model with first-order absorption and first-order elimination (Figure V-1).

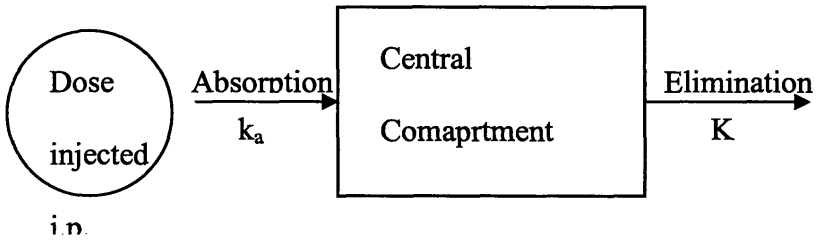

Figure V-1. Classic one-compartmental model for the evaluation of plasma pharmacokinetics of the polymer-peptide-drug conjugates

The integrated equation of this model is:

$$C_p = \frac{Dk_a}{V_d(k_a - K)}\left(e^{-Kt} - e^{-k_a t}\right)$$

Where C_p represents the drug concentration in plasma, D represents the total dosage, V_d represents the volume of distribution, k_a equals the absorption rate constant and K equals the elimination rate constant. In the usual case when $k_a > K$, the second exponential term becomes negligible at large time t. K can be obtained from the linear regression of the terminal linear portion of the semi-log graph plotting drug concentration versus time. The half-life of circulation for the two conjugates was calculated by $t_{1/2} = 0.693 / K$. The area-under-curve (AUC) was calculated using the trapezoidal rule.

Results

To explain the observations we made regarding the anti-tumor efficacy and the systemic toxicity, we measured the biodistribution of three different types of dosage forms in HT-1080 bearing mice: free methotrexate, the MMP-sensitive conjugate, and the MMP-insensitive conjugate. HT-1080 is a fibrosacroma known to overexpress MMP-2 and MMP-9 and we confirmed its expression levels in a previous experiment (Chapter IV). Our detection method allowed us to distinguish between the uncleaved conjugate and the cleavage product in blood plasma and tissue homogenate.

Figure V-2 presents the plasma pharmacokinetics of the free methotrexate and the two conjugates. By two hours after free methotrexate injection, most of the dose was cleared from the body. The area-under-curve (AUC) for free methotrexate was 64 μM-h and was significantly lower than either conjugate: 2.24 x 10^4 μM-h for MTX-PVGLIG-dextran and 1.90 x 10^4 μM-h for MTX-GIVGPL-dextran. The concentration-time curves for the two conjugates with different peptide linkers were similar. The maximum plasma concentration occurred at approximately 5 hours post i.p. injection. The plateau at the maximum lasted to about 24 hours post injection. The regression on the data in the terminal portion yielded $C_p(\mu M) = 470.18e^{-0.021t(hr)}$ for MTX-PVGLIG-dextran and $C_p(\mu M) = 517.74e^{-0.023t(hr)}$ for MTX-GIVGPL-dextran. Thus the half life of elimination was 32.5 hours for the former and 30.3 hours for the later conjugate. For both conjugates,

the dosage forms remained intact in the circulation. More than 99% of the methotrexate equivalent was found in the uncleaved conjugate form up to at least 72 hours post injection.

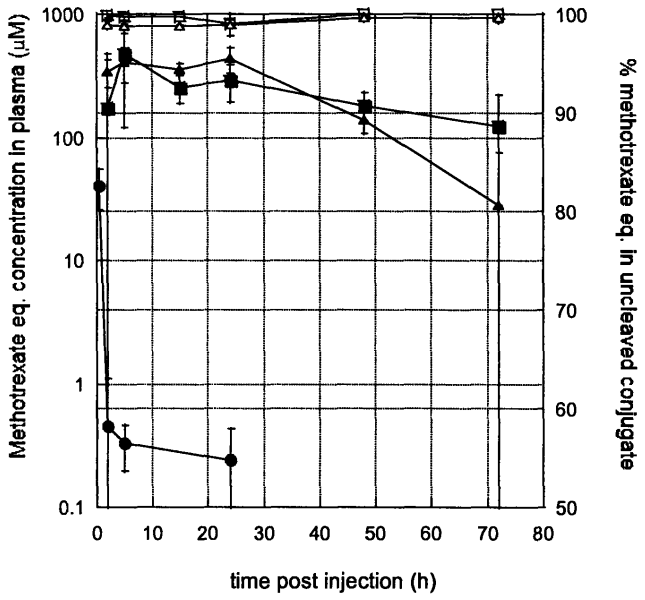

Figure V-2. Plasma pharmacokinetics of methotrexate, conjugate MTX-PVGLIG-dextran and conjugate MTX-GIVGPL-dextran. Shown in this figure is the concentration of methotrexate equivalent in mice injected with free methotrexate (●), MTX-PVGLIG-dextran (■) and MTX-GIVGPL-dextran (▲). The percentage of methotrexate found in uncleaved conjugate is plotted for MTX-PVGLIG-dextran (□) and MTX-GIVGPL-dextran(Δ).

The tissue distribution of the free methotrexate and the two conjugates at 5 and 24 hours post injection are compared in Figure V-3, Figure V-4 and Figure V-5. The concentrations in the tissues reflected the concentrations in the plasma. Not surprisingly, the drug concentrations within the tumor tissues and the major organs, including heart, liver, kidney, lung, small intestines, were much lower for the free methotrexate than for the two conjugates. The tissue distributions for the conjugates differing in peptide linkers

were similar. For both types of conjugates, the total methotrexate eq. at the tumor tissue was significantly higher than the free drug. The accumulation differed by two orders of magnitude at 5h and 24h post injection.

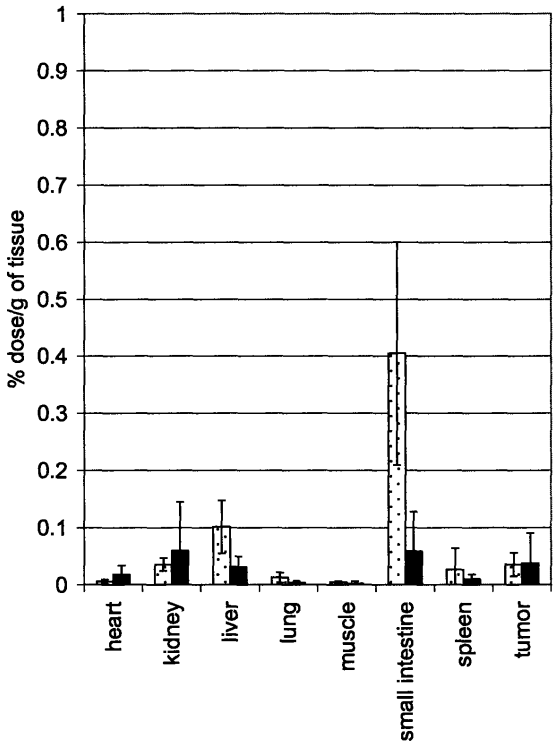

Figure V-3. Tissue distribution of methotrexate in mice receiving free methotrexate, at 5 hours (▒)and 24 hours (■) post injection.

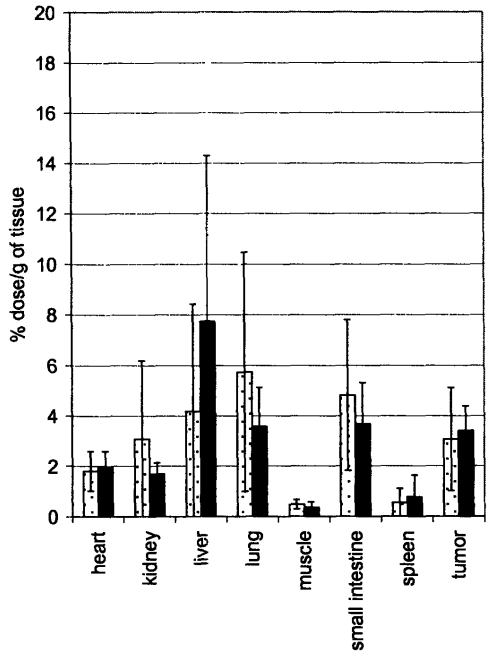

Figure V-4. Tissue distribution of methotrexate equivalent in mice receiving MTX-PVGLIG-dextran, at 5 hours (▒) and 24 hours (■) post injection.

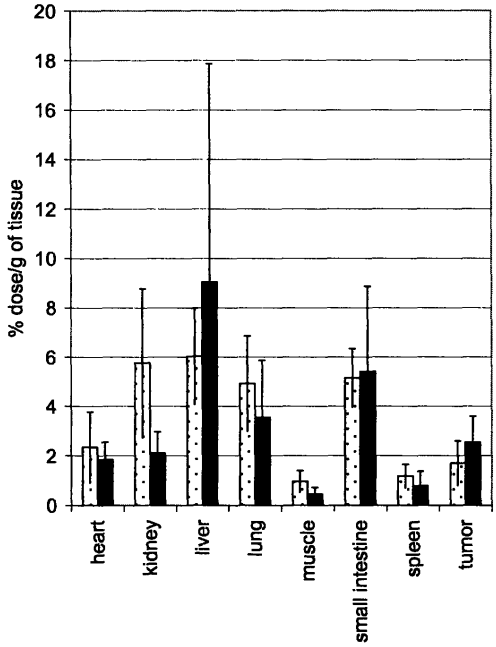

Figure V-5. Tissue distribution of methotrexate equivalent in mice receiving MTX-GIVGPL-dextran, at 5 hours (▒) and 24 hours (■) post injection.

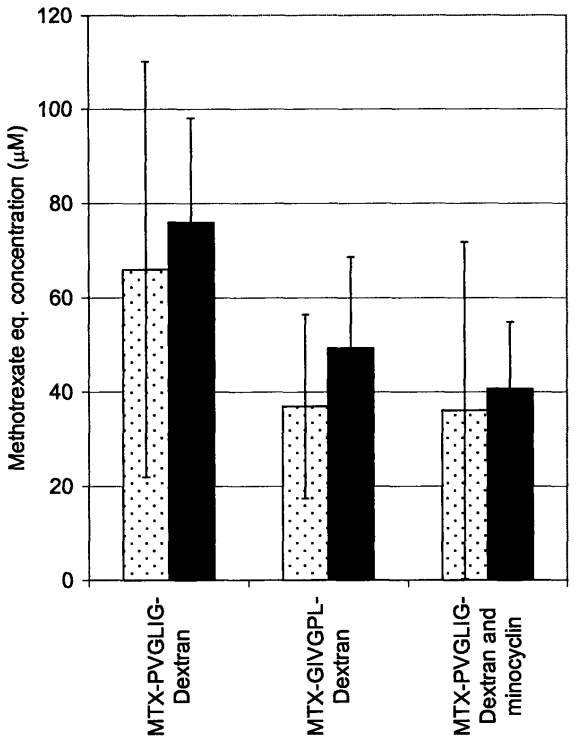

Figure V-6. Comparison of tumor accumulation in mice receiving the two different conjugates, at 5 hours (▒) and 24 hours (■) post injection. One group tested with MMP-sensitive conjugate MTX-PVGLIG-dextran also received injection of minocyclin, an MMP inhibitor.

Slightly more accumulation in the tumor was found with MTX-PVGLIG-dextran than with MTX-GIVGPL-dextran (Figure V-6). The difference was 1.8 fold at 5h ($p=0.12$) and 1.5 fold at 24h ($p=0.075$). This difference disappeared when the mice receiving MTX-PVGLIG-dextran injections were also treated with minocyclin, a broad inhibitor on MMP. This suggested that the higher tumor accumulation of the MMP-sensitive conjugate compared to the MMP-insensitive conjugate was a result of the enzymatic release from MMP.

Although the MTX-PVGLIG-dextran is highly sensitive in releasing peptide-MTX in the presence of MMP-2 and MMP-9 *in vitro*[9], we noted that more than half of the MMP-sensitive conjugate in the tumor tissue remained in an uncleaved form up to 48 hours after injection (Figure V-7).

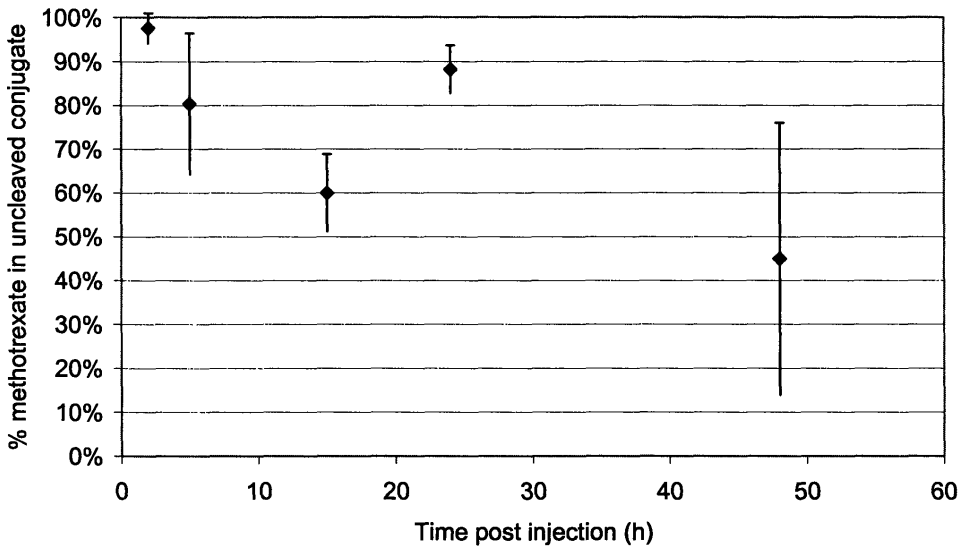

Figure V-7. Proportion of conjugate MTX-PVGLIG-dextran remaining uncleaved in the tumor tissues of HT-1080 bearing mice.

Nevertheless, the amount of peptidyl methotrexate released by the conjugate MTX-PVGLIG-dextran was sufficient to inhibit tumor growth *in vivo* (Chapter IV). We found that from 5 to 48 hours post injection, the concentration of the peptidyl methotrexate released from this conjugate remained at or above 10μM (Figure V-8), the IC_{50} concentration of MTX-PVG in a HT-1080 cell culture assay (Chapter III). At the current dosage of 50mg MTX eq./kg, the conjugate is able to attain a therapeutic

concentration during this time frame. The allows methotrexate to exert its pharmacological action to reduce the proliferative index of the tumor cells [17].

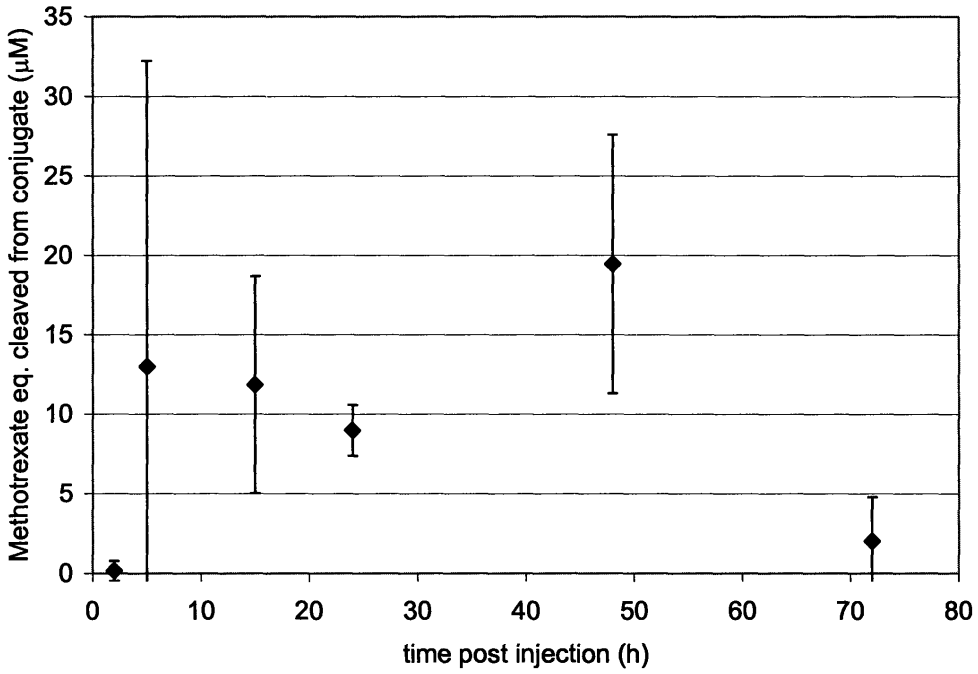

Figure V-8. Concentration of peptidyl methotrexate released from the conjugate MTX-PVGLIG-dextran post injection in HT-1080 bearing mice.

Besides answering questions about the targeting mechanism to achieve anti-tumor efficacy, the biodistribution study is instructive in explaining the side effects described in Chapter IV. Clinically, methotrexate is known to cause side effects in the gastrointestinal tract. Although we only observed mild damage to the small intestine in the free methotrexate treated mice, the small intestine was the major site of accumulation of the free drug (Figure V-3). The amount of drug peaked at this tissue rapidly after injection,

at around 0.5 hour (Figure V-9a). The drug concentration in the small intestine, the major site of side effects, was compared with the drug concentration in the tumor, the target site of the chemotherapy (Figure V-9). For the free methotrexate, the ratio of AUC of small intestine to tumor = 4.3. This ratio was significantly higher than the corresponding value for the two conjugates. (1.23 for MTX-PVGLIG-dextran and 1.65 for MTX-GIVGPL-dextran). As shown in Chapter IV, free methotrexate at this dosage did not have any significant anti-tumor effect. One might expect that if the dosage were to increase to a therapeutic level, severe toxicity would be expected in the small intestine due to the skewed distribution present in this tissue.

In the small intestines, the two conjugates were comparable in their total methotrexate equivalent accumulations and their concentration-time profiles. The tissue concentration peaked at 5 hours post injections and remained at the maximum plateau until 24 hours before it slowly declined (Figure V-9b,c). However, the proportion of conjugate remaining uncleaved was dependent on the sequence of the peptide linker of the conjugate (Table V-1). A higher percentage of the conjugates with the PVGLIG linkers were cleaved. MMPs are not known to be present in the bowel and the injection of minocyclin did not change our experimental observation. These led us to hypothesize that the discrepancy in drug-related toxicity resulting from the two conjugates was due to their different susceptibility to enzymes other than MMP. Note that the assay differentiated uncleaved conjugate and released drug based on size separation, so the exact form of the released drug was not known. The possible entities included methotrexate-peptide analogs of varying number of amino acids and free methotrexate.

a)

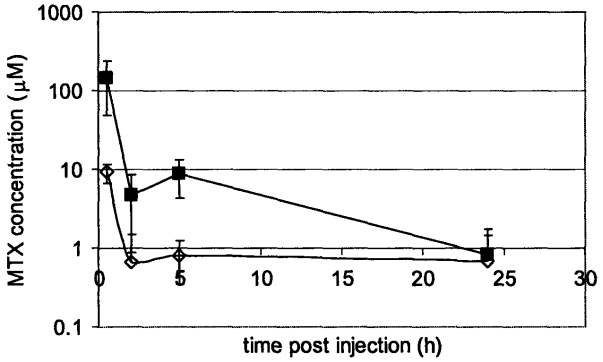

b)

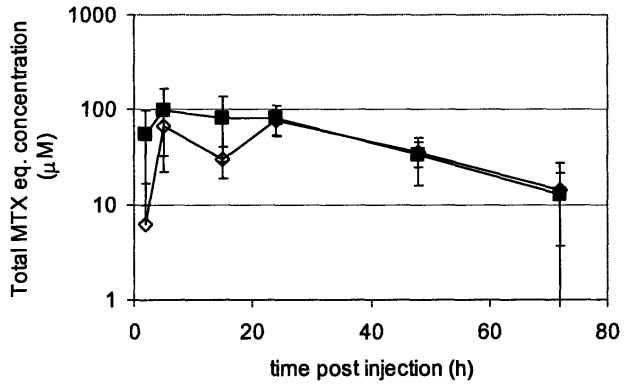

c)

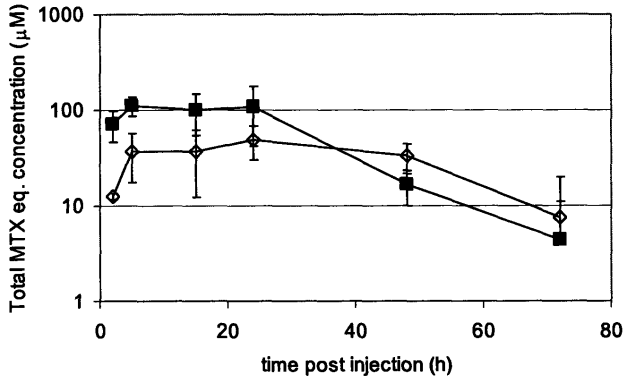

Figure V-9. Comparison of the total methotrexate concentration in the small intestine (■) and the tumor tissue (◊) in HT-1080 bearing mice injected with a) free methotrexate, b) MTX-PVGLIG-dextran and c) MTX-GIVGPL-dextran.

Table V-1. Comparison of accumulation of total methotrexate equivalent and the percentage in uncleaved conjugate form in the small intestine at 5h and 24h post injection

	Injection	MTX eq.in small intestine (μM)	percentage of MTX in uncleaved conjugate
T=5h	MTX-PVGLIG-dextran	99±67	0.80±0.91
	MTX-GIVGPL-dextran	111±26	28±22
	MTX-PVGLIG-dextran + minocyclin	173±37	1.1±1.7
T=24h	MTX-PVGLIG-dextran	81±28	1.4±1.4
	MTX-GIVGPL-dextran	108±66	8.9±6.9
	MTX-PVGLIG-dextran + minocyclin	118±47	0.31±0.32

As we reported previously, the cytotoxicity of methotrexate was decreased by two orders of magnitude when the free drug was covalently linked to Pro-Val-Gly (Chapter III)[9]. MTX-PVG was the product released from the conjugate MTX-PVGLIG-dextran in the presence of MMP-2 or MMP-9. When we compared the cytotoxicity of MTX-peptide with varying number of amino acids: MTX-G, MTX-GI and MTX-GIV (**Figure V-10**), we found that the reduction in the potency of the free methotrexate increased with the number of amino acids attached to the free methotrexate.

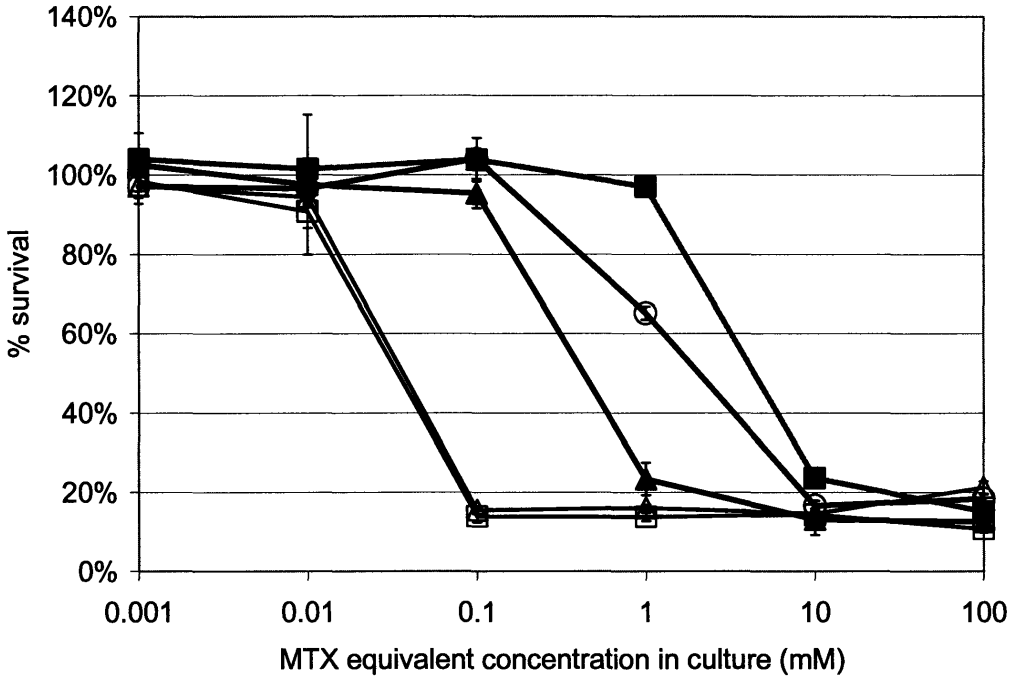

Figure V-10. Cytotoxicity of methotrexate and different types of methotrexate-peptide analogs: MTX (Δ), MTX-G (□), MTX-GI (o), MTX-GIV (▲) and MTX-PVG (■). The test was performed in HT-1080 cell culture.

Discussion

This biodistribution study was carried out to examine the targeting mechanism of the new dextran-peptide-methotrexate conjugate. By comparing the plasma pharmacokinetics of free methotrexate to the MMP-sensitive conjugate, MTX-PVGLIG-dextran, and MMP-insensitive conjugate, MTX-GIVGPL-dextran (Figure V-2), we confirmed that the conjugates demonstrated passive targeting. While methotrexate is mainly cleared from the body through the urine [19], the high molecular weight dextran carrier we selected for conjugation was able to reduce renal excretion and increase circulation time. Independent of the peptide linker sequence, the conjugates remained uncleaved in the blood stream for a prolonged period of time. Even when the peptide linker is labile to MMPs and possibly other endopeptidases in the bloodstream, the presence of some serum proteins, such as α-macroglobulin, may act as inhibitors to these enzymes [20]. The peptide linker is flanked on the terminals by methotrexate and dextran. These moieties should also protect the peptide from the attack of exopeptidases. This explained the observation that the drugs remained attached to the dextran carrier for at least 3 days in the plasma, enabling a prolonged circulation time and increased tissue accumulation.

The higher plasma concentration of MTX eq. resulted in higher concentrations in the tissues and contributed to the increase in the tumor targeting ratio --- the amount of drug localized to the tumor site normalized by the dosage (Figure V-3, Figure V-4 and Figure V-5). Despite the difference in the peptide linkers, the features designed for

passive targeting, including size and hydrophilicity, are the same for both conjugates. These features also help to achieve tumor targeting by the EPR effect. In comparing the ratio of AUC of the tumor to the small intestine, we observed a favorable shift towards the tumor for both conjugates (Figure V-9). The enhancement of tumor targeting ratio of both conjugates relative to the free drug illustrates the advantages of passive targeting and EPR effects.

As shown in Figure V-6, MTX-PVGLIG-dextran, the MMP-sensitive conjugate, surpassed MTX-GIVGPL-dextran, the MMP-insensitive conjugate, in the drug accumulation in the tumor tissue without statistical significance. The new conjugate therefore achieved selective delivery to the tumor tissue mainly by passive targeting and the EPR effects, and MMP-mediated release was not the primary targeting mechanism. Although the conjugate MTX-PVGLIG-dextran is highly sensitive to MMP-2 and MMP-9 in releasing MTX-PVG *in vitro* (Chapter III) [9], tumor-specific delivery of peptidyl methotrexate mediated by MMP was not significant *in vivo*. We can think of two possible explanations. First, we consider the competition of non-specific drug uptake. At the tumor tissue, drug uptake can happen through two processes. Regardless of the linker specificity, conjugates can be internalized by the tumor cells via non-specific endocytosis. For the conjugates with MMP-sensitive linkers, enzyme-mediated release of the peptidyl methotrexate provides a different venue for site-specific delivery. The relative importance of these two processes depends on their relative rates. The enzymatic release rate by MMP can be modeled by the Michaelis Menten mechanism. The rate plateaus to $k_{cat} \bullet E_o$ as the conjugate concentration increases. (k_{cat} is the turnover rate

from substrate-enzyme complex to product and E_0 is the enzyme concentration of MMP.) Fluid-phased endocytotic uptake can be modeled as a first-order process and its rate thus increases linearly with the conjugate concentration. At low conjugate concentration, the rate of MMP-mediated release is higher and therefore has a more prominent role. At high conjugate concentration, the reverse is true. In our animal study, a high dosage (50mg MTX eq./kg) is administrated because MTX-PVG has reduced potency compared to free methotrexate[9]. This high dosage may have caused the endocytotic uptake to dominate over the MMP-mediated release.

Second, we consider the heterogeneity and complexity of the tumor environment *in vivo*. The activity of MMPs is regulated by host inhibitors such as TIMPs [20] and the spatial distribution of MMPs within the tumor tissue may not be even. Our conjugate, because of the large size, may not be able to penetrate the tumor tissue evenly[21]. Together, these can cause the conjugate MTX-PVGLIG-dextran to demonstrate a lower sensitivity in the mouse model. As a supporting consideration, we observed that most of the methotrexate remained attached to the dextran carrier in the tumor tissue for at least two days after the injection (Figure V-7).

Although the amount of total methotrexate eq. in the small intestine between the two types of conjugates was similar, we found that the percentage cleavage was significantly different (Table V-1). Furthermore, the potency of the release product from the conjugate varied significantly based on the number of amino acids attached (Figure V-10). These results confirm our earlier suspicion that enzymes other than MMPs in the

normal tissues (such as the small intestine) are involved. The significant difference in the side effects found in the bowel could have resulted in the release of more potent toxic products (methotrexate-peptide with shorter peptide) from one conjugate but not the other. There are many endopeptidases and exopeptidases that are present in the small intestine[22] which can potentially cleave the conjugate MTX-GIVGPL-dextran to release the active component. Enzymes such as elastase, carboxypeptidase and aminopeptidase are possibly involved but we are unable to pinpoint the key enzyme with our current method.

References

1. Maeda H. SMANCS and polymer-conjugated macromolecular drugs: advantages in cancer chemotherapy. *Advanced Drug Delivery Reviews* 2001;46(1-3):169-85.

2. Putnam D, Kopecek J. Polymer conjugates with anticancer activity Biopolymers II, vol. 122, 1995:55-123.

3. Li C. Poly(L-glutamic acid) - anticancer drug conjugates. *Advanced Drug Delivery Reviews* 2002;54(5):695-713.

4. Lu ZR, Kopeckova P, Kopecek J. Polymerizable Fab ' antibody fragments for targeting of anticancer drugs. *Nature Biotechnology* 1999;17(11):1101-04.

5. Flanagan PA, Duncan R, Subr V, Ulbrich K, Kopeckova P, Kopecek J. Evaluation of Protein-N-(2-Hydroxypropyl)Methacrylamide Copolymer Conjugates as Targetable Drug-Carriers .2. Body Distribution of Conjugates Containing Transferrin, Antitransferrin Receptor Antibody or Anti-Thy 1.2 Antibody and Effectiveness of Transferrin-Containing Daunomycin Conjugates against Mouse L1210 Leukemia Invivo. *Journal of Controlled Release* 1992;18(1):25-37.

6. Lu YJ, Low PS. Folate-mediated delivery of macromolecular anticancer therapeutic agents. *Advanced Drug Delivery Reviews* 2002;54(5):675-93.

7. Chau Y, Langer RS. Important factors in designing targeted delivery of cancer therapeutics via MMP-2 mediation. *Journal of Controlled Release* 2003;91(1-2):239-40.

8. Chau Y, D. P, Dang N, Tan F, Langer R: Investigation of new tumor-targeting conjugates with MMP sensitive linkers *Controlled Release Society Annual Meeting* 2004.

9. Chau Y, Tan FE, Langer R. Synthesis and characterization of dextran-peptide-methotrexate conjugates for tumor targeting via mediation by matrix metalloproteinase II and matrix metalloproteinase IX. *Bioconjugate Chemistry* 2004;15(4):931-41.

10. Davies B, Miles DW, Happerfield LC, Naylor MS, Bobrow LG, Rubens RD, Balkwill FR. Activity of Type-IV Collagenases in Benign and Malignant Breast Disease. *British Journal of Cancer* 1993;67(5):1126-31.

11. Hamdy FC, Fadlon EJ, Cottam D, Lawry J, Thurrell W, Silcocks PB, Anderson JB, Williams JL, Rees RC. Matrix Metalloproteinase-9 Expression in Primary Human Prostatic Adenocarcinoma and Benign Prostatic Hyperplasia. *British Journal of Cancer* 1994;69(1):177-82.

12. Levy AT, Cioce V, Sobel ME, Garbisa S, Grigioni WF, Liotta LA, Stetlerstevenson WG. Increased Expression of the Mr 72,000 Type-IV Collagenase in Human Colonic Adenocarcinoma. *Cancer Research* 1991;51(1):439-44.

13. Naylor MS, Stamp GW, Davies BD, Balkwill FR. Expression and Activity of MMPs and Their Regulators in Ovarian-Cancer. *International Journal of Cancer* 1994;58(1):50-56.

14. Davies B, Waxman J, Wasan H, Abel P, Williams G, Krausz T, Neal D, Thomas D, Hanby A, Balkwill F. Levels of Matrix Metalloproteases in Bladder-Cancer Correlate with Tumor Grade and Invasion. *Cancer Research* 1993;53(22):5365-69.

15. Derrico A, Garbisa S, Liotta LA, Castronovo V, Stetlerstevenson WG, Grigioni WF. Augmentation of Type-Iv Collagenase, Laminin Receptor, and Ki67 Proliferation Antigen Associated with Human Colon, Gastric, and Breast-Carcinoma Progression. *Modern Pathology* 1991;4(2):239-46.

16. Egeblad M, Werb Z. New functions for the matrix metalloproteinases in cancer progression. *Nature Reviews Cancer* 2002;2(3):161-74.

17. Chau Y, Padera RF, Dang NM, Langer R. Anti-tumor efficacy of a novel polymer-peptide-drug conjugate in human tumor xenograft models. *Submitted to International Journal of Cancer* 2005.

18. Dandliker SB, Kelly RJ, Dandliker J, et.al. Fluorescence polarization immunoassay. Theory and experimental method. *Immunochemistry* 1973;10:219-27.

19. Chamber BA, Ryan DP, Paz-Ares L, Garcia-Carbonero R, Calabresi P. In: Hardman JG, Limbird LE, Gilman AG, eds. Goodman and Gilman's The Pharmacological Basis of Therapeutics: The McGraw-Hill Companies, Inc., 2001:1389.

20. Woessner JF, Nagase H. Matrix Metalloproteinases and TIMPs. New York: Oxford university press, 2000.

21. Jain RK. Delivery of molecular and cellular medicine to solid tumors. *Advanced Drug Delivery Reviews* 2001;46(1-3):149-68.

22. Alpers DH. Digestion and Absorption of Carbohydrates and Proteins. In: Johnson LR, Christensen J, Jackson MJ, Jacobson ED, Walsh JH, eds. Physiology of the Gastrointestinal Tract, ed. Second Edition, vol. 2 New York: Raven Press, 1987:1469.

Chapter VI : OPPORTUNITIES FOR ENZYMATIC MEDIATIONS IN BIOMEDICAL APPLICATIONS

Introduction

We have designed a novel polymer-drug conjugate containing linkers cleavable by disease-associated enzymes. As an example, we synthesized and characterized dextran-peptide-chemotherapeutic conjugates to improve anticancer treatment by targeted delivery. The concept of using disease-associated enzymes as mediators to elicit biologically relevant responses is applicable for designing new drug delivery vehicles in addition to polymer-drug conjugates, as well as for devising other biomedical applications. Because of the strong correlation of MMPs with cancer progression, these enzymes have been studied widely in the past two decades. The work in this dissertation has joined a number of research groups to pioneer biomedical applications using MMP activation. In this chapter, the potentials of enzymatic mediations are illustrated by the examples employing MMP-based activation. In addition to helping us to improve the design of a drug-delivery vehicle to make better use of an enzyme's activity, these examples also let us perceive the future opportunites of MMP-mediated applications.

The MMP family consists of at least 25 zinc-dependent endoproteinases, most of which were discovered in the past decade[1] (Table VI-1). These matrix-metalloproteinases together can break down all the major proteins comprising the ECM and the basement

membrane. The common names of some of these MMPs, such as collagenase and gelatinase, indicate the natural substrates for these proteases. In the quest of understanding the roles of these enzymes in tumor progression, a myriad of substrates other than the ECM, such as growth factors, angiogenic factors and syndecans[1, 2], were found for these enzymes. In addition to cancer, these enzymes play major roles in biological processes wherein tissue remodeling is essential. They are involved in normal processes such as wound healing and embryo development. In pathological processes, they are associated with inflammation and unchecked tissue remodeling, and are found dysregulated in diseases such as cancer, cardiovascular diseases, and arthritis. Because of the important roles of MMPs in these processes, they can be exploited in various applications for attaining regulation of biological processes, providing therapy and obtaining diagnosis.

Table VI-1. The matrix-metalloproteinase family[1]

MMP designation	Structural class	Common name(s)
MMP-1	Simple hemopexin domain	Collagenase-1, interstitial collagenase, fibroblast collagenase, tissue collagenase
MMP-2	Gelatin-binding	Gelatinase A, 72-kDa gelatinase, 72-kDa type IV collagenase, neutrophil gelatinase
MMP-3	Simple hemopexin domain	Stromelysin-1, transin-1, proteoglycanase, procollagenase-activating protein
MMP-7	Minimal domain	Matrilysin, matrin, PUMP1, small uterine metalloproteinase
MMP-8	Simple hemopexin domain	Collagenase-2, neutrophil collagenase, PMN collagenase, granulocyte collagenase
MMP-9	Gelatin-binding	Gelatinase B, 92-kDa gelatinase, 92-kDa type IV collagenase
MMP-10	Simple hemopexin domain	Stromelysin-2, transin-2
MMP-11	Furin-activated and secreted	Stromelysin-3
MMP-12	Simple hemopexin domain	Metalloelastase, macrophage elastase, macrophage metalloelastase
MMP-13	Simple hemopexin domain	Collagenase-3
MMP-14	Transmembrane	MT1-MMP, MT-MMP-1
MMP-15	Transmembrane	MT2-MMP, MT-MMP-2
MMP-16	Transmembrane	MT3-MMP, MT-MMP-3
MMP-17	GPI-linked	MT4-MMP, MT-MMP-4
MMP-18	Simple hemopexin domain	Collagenase-4 (Xenopus; no human homologue known)
MMP-19	Simple hemopexin domain	RASI-1, MMP-18
MMP-20	Simple hemopexin domain	Enamelysin
MMP-21	Vitronectin-like insert	Homologue of Xenopus XMMP
MMP-22	Simple hemopexin domain	CMMP (chicken, no human homologue known)
MMP-23	Type II transmembrane	Cysteine array MMP (CA-MMP), femalysin, MIFR, MMP-21/MMP-22
MMP-24		MT5-MMP, MT-MMP-5
MMP-25	Transmembrane	MT6-MMP, MT-MMP-6, leukolysin
MMP-26	GPI-linked	Endometase, matrilysin-2
MMP-27	Simple hemopexin domain	
MMP-28	Furin-activated and secreted	Epilysin
No designation	Simple hemopexin domain	Mcol-A (Mouse)
No designation	Simple hemopexin domain	Mcol-B (Mouse)
No designation	Gelatin-binding	75-kDa gelatinase (chicken)

Development of inhibitors against MMPs for cancer therapy

The development of inhibitors against MMPs for cancer therapy was sparked by the strong correlation between MMPs and tumor progression. Initially, the assumption was that the primary roles of MMPs were to break down the basement membrane and the ECM, and hence were important especially in tumor expansion and invasion during the late stage and during metastasis. More functions of the MMPs have been discovered suggesting their involvement at an earlier stage and at multiple levels, such as generating growth signals and releasing angiogenesis factors[1].

In animal models, the inhibition of MMPs by small molecules or by gene knockout results in significant anti-tumor efficacy. The chemical inhibitors of MMPs were quickly tested in clinical trials in the early 1990s, when only 3 MMPs were found and much less was known about these enzymes. The disappointing results of these clinical trials and the lessons learnt from the early developments are found in a number of good reviews[3-5]. In hindsight, one can attribute three causes for the results of the clinical trials: 1) the failure to recognize that MMP inhibitors can moderate the diseases in multiple stages and that treatment at an early stage can potentially confer more benefits than at a late stage; 2) the failure to recognize that inhibitors have cross reactivity against enzymes essential for normal functions and thus induce side effects (for example, mucoskeletal inflammation is caused by the unintentional inhibition of ADAMs- a disintegrin and metalloproteinases); 3) the lack of a detection method for establishing the effectiveness of the treatment and thereby the lack of appropriate measures to determine the optimal

dosages. Despite these initial disappointments, the lessons learnt should give a good direction to the future development of MMP inhibitors. Furthermore, because of the immense interest to develop synthetic inhibitors against MMPs, the substrate specificity of these enzymes has been studied extensively. This knowledge is applicable for developing MMP-mediated applications.

Drug delivery vehicles with MMP-cleavable linkers

MMP inhibitors are cytostatic but not cytotoxic against cancer cells. To effectively kill cancer cells without damaging normal tissues, MMP-mediated cytotoxicity is an appealing solution considering that MMPs are overexpressed in many types of cancer and their levels are generally lower in healthy tissues. A general strategy to achieve MMP-mediated cytotoxicity is the incorporation of an MMP-cleavable linker in a delivery vehicle. This linker serves as a switch such that the therapeutics remain inactive until proteolysis by an MMP. The different approaches discussed in this section are illustrated in Figure VI-1.

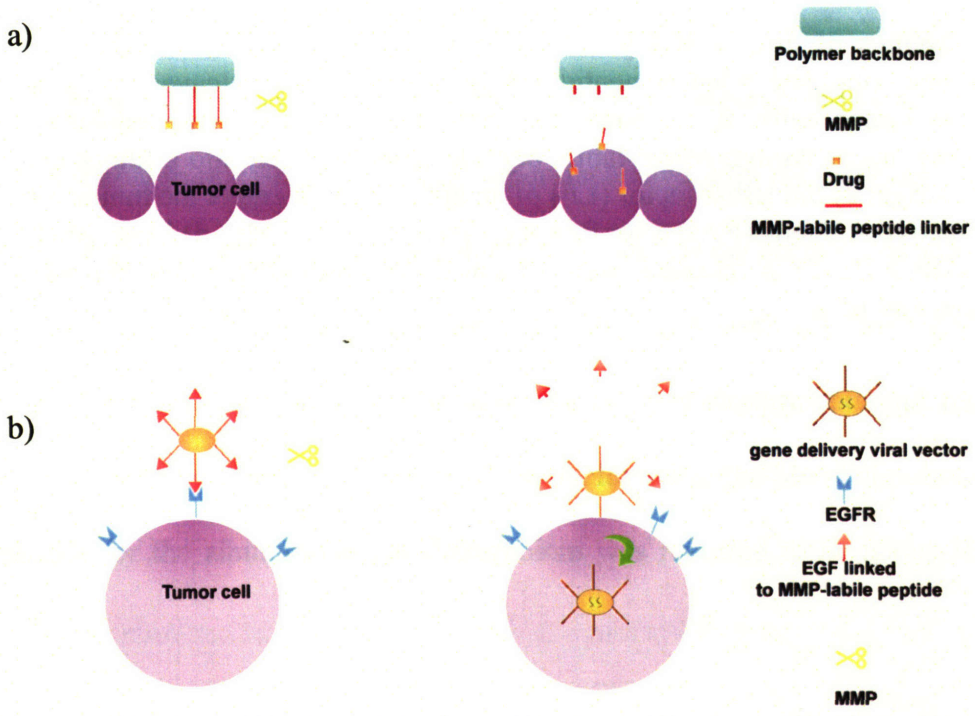

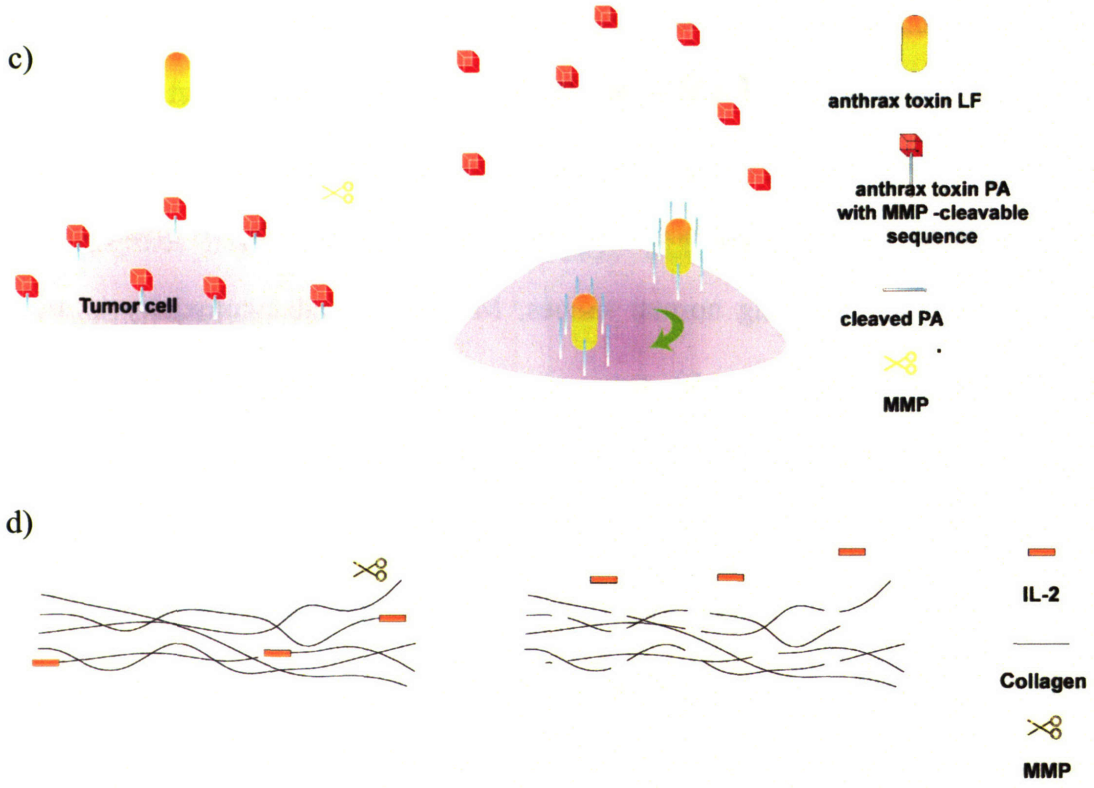

Figure VI-1. Schematics of drug delivery vehicles with MMP-cleavable linkers: a) a polymer-peptide-drug conjugate releases peptidyl-drug after the MMP cleavage to exert cytotoxic effect on tumor cells; b) a retroviral gene delivery vector with epidermal growth factor (EGF) linked though MMP-labile peptide is internalized into a tumor cell after the MMP cleavage; c) the lethal factor (LF) of an anthrax toxin enters the tumor cell by binding to protective antigens (PAs) after PAs are cleaved by an MMP; d) Upon MMP cleavage, Interleukin-2 (IL-2) is released from a local depot consisting of the chimeric proteins of collagen and IL-2

Polymer-drug conjugates have shown promise in delivering small molecular weight chemotherapeutics to solid tumors. These soluble conjugates can increase the half-life of therapeutics, improve the solubility of attached drugs and increase the targeting ratio through enhanced permeation and retention (as we have discussed in the previous chapters). Oligopeptide sequences have been investigated as the potential linkers between drugs and polymers. GFLG is the most widely published one, a linker that can be cleaved by ubiquitous lysosomal enzymes such as cathepsin B to liberate the free drugs. We and others have attempted to exploit MMPs to mediate drug release in order to enhance targeting to MMP-expressing tumors (Figure VI-1a).

We have synthesized two types of conjugates: carboxymethyl-peptide-doxorubicin and dextran-peptide-methotrexate. Both are sensitive towards MMP-2 and MMP-9 and able to release peptide-drugs when incubated with the enzymes[6, 7]. Mansour has prepared an albumin-peptide-doxorubicin that can release peptide-doxorubicin when digested by MMP-2 [8]. These conjugates are stable in serum: our conjugates remain uncleaved for at least 24 hours when tested by *in vitro* experiments and the dextran-peptide-methotrexate conjugates remain >99% uncleaved in the blood circulation *in vivo*; the half-life for the albumin-peptide-doxorubicin was reported to be about 16 hours *in vitro*.

Injection of the conjugates via the i.v. or i.p. route resulted in superior anti-tumor effects in MMP-producing tumor models in mice[8, 9]. However, it is inconclusive whether MMP-mediation is the dominant targeting mechanism of the albumin-peptide-doxorubicin conjugate as Mansour's study did not compare the MMP-sensitive conjugate with the MMP-insensitive conjugate, nor did the *in vivo* experiments contrast the results in a MMP-producing tumor model with a MMP-negative model. When comparing the MMP-sensitive dextran-peptide-methotrexate conjugate with the MMP-insensitive conjugate, we found that the later exhibited an anti-tumor effect despite being more toxic systemically[9] (Chapter IV). This prompted us to perform a biodistribution study to compare the MMP-sensitive, the MMP-insensitive conjugate and the free drug. We observed a comparable increase in half-life of the two conjugates compared to the free drug; but we did not observe any significant difference in the tumor accumulation of peptidyl-drugs between the two conjugates (Chapter V). We have concluded that the MMP-sensitive dextran-peptide-methotrexate conjugate targets primarily by passive targeting and enhanced permeation and retention, with MMP-mediated release playing a modest role.

The challenge of achieving MMP-mediated release from a polymer-drug conjugate is that the MMP-sensitive peptide linker can be possibly cleaved by other enzymes *in vivo*. Presumably upon endocytosis, the conjugate enters the lysosomal compartment, where many proteases are present. Although the peptide linker is designed to be most sensitive to MMPs, it is not exclusively labile to the targeted enzyme and can be a substrate for lysosomal proteases, usually having broad substrate requirements. We

have incubated our MMP-sensitive conjugate with a mixture of lysosomal enzymes and found that peptidyl-drug and free drug can be released (data not shown). This release mechanism enables the conjugate to have a cytotoxic effect without the involvement of MMPs. Another difficulty is due to the substrate requirement of P3 to P3' sites for the recognition by MMP-2 or MMP-9. As a result, peptidyl-drug instead of the original free drug is liberated from the aforementioned conjugates after enzymatic cleavage. The attachment of several amino acids significantly reduced the potency of the drug. Mansour suggested that after the initial cleavage by MMP-2, other proteases removed the remaining amino acids to liberate the free doxorubicin. But his data also showed that free doxorubicin was liberated even when MMP-2 was inhibited. The need of non-targeted proteases to release the free drug weakens the effect of tumor targeting by MMP-mediated release.

Nevertheless, there are other approaches of MMP-mediated delivery that yield higher specificity. Peng first described a retroviral gene delivery system that targeted epidermal fibroblast growth factor receptor (EGFR) whose infectivity depended on MMPs[10] (Figure VI-1b). The epidermal growth factor (EGF) was displayed on the viral particle via an MMP-cleavable linker. The viral vectors could bind to EGFR on the cell surface but could not enter the cell, as the receptor did not support the steps to allow for the viral entry. In the presence of MMPs, EGF was cleaved from the viral particle and the viral infectivity was restored. The linker was cleavable by both the extracellular MMP-2 and the transmembrane MT1-MMP, and the authors pointed out that the enzymes bound

on the cell membrane could play a more significant role through a co-culture experiment. The vector with the MMP-cleavable linker preferentially infected the MMP-expressing cells over the non-expressing cells when both types of cells were grown in the same culture dish. Such selectivity should be caused by the enzymatic cleavage at the cell surface and the subsequent internalization of the virus.

Another example of MMP-mediated cancer therapy is found in a new toxin prodrug[11](Figure VI-1c). This strategy involves an engineered two-part anthrax toxin. The cytotoxicity of the anthrax toxin lethal factor (LF) is dependent on the binding to the heptamer formed by the protective antigens (PAs) and the subsequent internalization of the complex. The PAs bind to the host cell surface but do not associate to form a channel until they are cleaved by the cell surface furin or furin-like proteases. Here, the furin protease cleavage site was mutated to an MMP-2 and MMP-9 cleavable sequence. The combination of the mutated PA and LF showed selective cytotoxicity in cells overexpressing the MMPs. More interestingly, it spared the normal cells co-cultured with the MMP-expressing tumor cells. This specificity requires that the productive enzymatic cleavage that enables the internalization of LF to happen at the cell surface. The membrane-bound MT-MMPs or soluble MMPs that remain bound to the cell surface (through molecules such as MT1-MMP and adhesion receptors) are very likely involved in the MMP-mediated activation.

Both aforementioned examples showing MMP-mediated specificity rely on cell surface events and are linked to the MMP cleavage at the membrane. There are four

known membrane bound MMPs (MT1-,2-,3- and 4-MMP). Some excreted MMPs are anchored to the cell surface by cell-bound molecules, including MT1-MMP, αvβ3 integrin and CD44[12-14]. The MMP activity on the cell surface, which may help the cancer cells to establish an invasive front, is more concentrated than that in the interstitial fluid and can be exploited to cleave the polymer-peptide-drug conjugate. To further improve the conjugate's specificity, we propose to target the conjugate to the tumor cell surface by attaching to the conjugate a non-internalizing ligand that recognizes a specific receptor on the tumor cell. This type of ligand, such as a monovalent fragment of an anti-tumor antibody[15], helps to concentrate the polymer-drug conjugates to the tumor site, and also places the conjugates in close proximity to the MMPs at the cell surface, increasing the probability of the conjugates to be cleaved by MMPs rather than by other interstitial proteases or intracellular enzymes.

Although the specificity of the more recently discovered MT-MMPs is less extensively studied, targeting these membrane bound enzymes may have an additional advantage in designing a polymer-peptide-drug conjugate. The consensus sequence recognized by MT1-MMP includes the substrate sites of P3—P1'[16], instead of the P3—P3' requirement by MMP-2 and -9. The smaller number of amino acids adjacent to the scissile bond means that the liberated drug from the conjugate is more similar to the original form and the drug potency should be less likely reduced.

Besides mediating targeting for a systemic delivery vehicle, MMP activity can be employed as a release mechanism for a local delivery system (Figure VI-1d). However,

there are not as many reports in the later category. The example here uses a natural substrate for MMP as a depot for local release. Hayashi constructed a chimeric protein joining Interleukin-2 (IL-2) and type III collagen[17]. IL-2 is a potent chemokine, considered useful for cancer immunotherapy, and its function includes stimulating the proliferation of antitumor effector cells. However, IL-2 has a short half-life and toxic side effects if administered at a high dosage. It was reasoned that the new chimeric protein can form fibrils like regular collagen, thus shielding and protecting the linked IL-2. As a proof of concept, he showed that the chimeric was able to liberate biologically active IL-2 using a bacterial collagenase. This type of construct has the potential of providing a local delivery of IL-2 at the tumor site, where MMPs are available to digest the collagen and release the IL-2.

So far, targeted delivery of therapeutics via MMP mediation has been focused on cancer treatment. There are many new opportunities for expanding this concept to other diseases in which MMPs have major roles. MMPs are associated with cardiovascular diseases. Dysregulation of these enzymes are associated with atherosclerosis and heart failure. MMP-1 and MMP-13 are up-regulated during the left ventricular myocardial remodeling in congestive heart failure[18]. In atherosclerosis, the inflammation at the site of atherosclerotic plaque recruits the macrophages expressing MMP-1,-8,-13, enzymes capable of degrading the collagen fibrils. In addition, MMP-2 and MMP-9 are up-regulated to degrade gelatin after the fibrils unwind. These MMP activities presumably cause the rupture of the plaque and the progression the disease[19]. MMPs are also implicated in the development of arthritis: in both osteoarthritis and rheumatoid arthritis.

The overexpression of MMP-1 and MMP-13 are involved in breaking down the cartilage at the affected joint[20]. With the hypothesis that MMP activity is correlated with disease progression, a local depot that has an MMP-activatable switch can deliver therapeutics on demand.

Disease imaging with MMP-activatable probes

The poor design of some earlier MMP inhibitor clinical trials was partly due to the lack of a suitable surrogate marker, making it impossible to gauge enzyme activity in response to a treatment. Inside the body, MMPs are tightly regulated on both the transcriptional and translational levels. After the MMPs are expressed, their activities are kept in check with the endogenous inhibitors such as TIMPs and α2-macroglobulins[21]. The pathological process is characterized by the dysregulation of one or more of these processes, resulting in a net deviation in MMP activity away from normal. These changes in enzymatic activity are excellent indicators of the prognosis of cancer and other diseases. It is now known that MMPs are involved at the early stages of cancer progression[1]; monitoring MMP activity can potentially give early diagnosis. All of these reasons call for the development of smart probes for the *in vivo* imaging of MMPs.

A smart probe increases or decreases a detectable signal as a result of a biological event carried out by the molecule of interest. To detect MMPs, this event is their proteolysis of the peptide or protein substrates. The proteolytic event is essential to the biological function of the enzyme, whether it is the breaking down of the ECM or the activation of a growth factor.

Table VI-2. Cleavage-site motifs for six MMPs[22]

Enzyme	Common name	Cleavage position P5	P4	P3	P2	P1	P1'	P2'	P3'
MMP-7	Matrilysin	P (1.4) I (1.3)	V (1.4) I (1.4) R (1.3)	P (1.6) V (1.6) I (1.5)	L (1.7) M (1.6) Y (1.4)	S (1.8) E (1.6) N (1.3) A (1.3)	L (8.4) I (3.6) M (2.5)	V (1.7) T (1.7) I (1.5) M (1.5) K (1.5) R (1.3)	M (1.5) Y (1.3) Q (1.3)
MMP-1	Collagenase-1	V (1.8) I (1.4)	V (1.4)	P (2.3)	M (1.5) Y (1.4) L (1.4) E (1.4)	S (2.2) N (1.8) A (1.8)	M (4.9) I (3.8) L (3.1)	M (1.7) I (1.5) K (1.4) R (1.3)	A (2.0) G (1.8) S (1.6)
MMP-2	Gelatinase A	D (1.4) L (1.3) F (1.3) N (1.3) I (1.3)	I (1.4) V(1.3)	P (1.7) V (1.6) I (1.5)	V (1.3) A (1.3)	S (1.9) G (1.4) A (1.4) E (1.3)	L (4.2) M (2.8) I (2.6) Y (1.9) F (1.8)	R (1.5) Y (1.5) K (1.4) M (1.4) I (1.4) V (1.4)	S (2.2) A (2.1) G (2.1)
MMP-9	Gelatinase B	V (1.4)	V (1.3)	P (2.5) V (1.6)	L (1.6) Y (1.3)	S (1.8)	L (3.4) M (2.6) I (2.6) Y (2.1) F (1.3)	R (1.4) T (1.4) Y (1.4) V (1.3) I (1.3)	S (1.9) A (1.8) G (1.6)
MMP-3	Stromelysin-1	N (1.3) I (1.3)	K (1.6) V (1.4) I (1.4) R (1.4)	P (2.5) V (1.4) I (1.4)	F (1.5) Y (1.5) L (1.4) M (1.3) A (1.3)	S (1.6) E (1.4)	M (3.5) I (2.9) L (2.5) Y (2.4) F (2.1)	M (1.9) K (1.8) I (1.7) R (1.6)	M (1.6) A (1.3)
MMP-14	MT1-MMP	F (1.5) L (1.4) D (1.3) I (1.3) V (1.3)	I (1.6) K (1.4) V (1.3) D (1.3)	P (2.0) V (1.4)	X	S (1.8) A (1.4)	L (3.5) I (2.2) M (2.2) Y (1.4) F (1.4)	R (1.4) K (1.3) Y (1.3)	M (1.4) A (1.4)

The first type of MMP-activatable probe uses the phenomenon of fluorescence resonance energy transfer (FRET) to suppress the signals, which are liberated upon the cleavage of the peptides recognizable by the specific MMPs. McIntyre and colleagues developed a smart probe to detect MMP-7[23], an enzyme found in benign intestinal tumors and tumors of the colon and the breast. For this probe, fluorescein and tetramethylrhodamine dyes were attached to a PAMAM (polyamido amino) dendrimer (Figure VI-2a). The emission spectrum of fluorescein overlaps with the excitation spectrum of tetramethylrhodamine, thus the fluorescein signal is suppressed and the tetramethylrhodamine signal serves as an internal reference. Fluorescein is covalently linked to the polymer via a peptide linker labile to MMP-7. Upon cleavage, the fluorescein signal increases significantly. The limit of using a UV-excitable probe, as in the previous example, comes mainly from the interference of the host tissues. To solve this problem, Weissleder's group has pioneered the use of near-infrared fluorescent fluorophores (NIRF) for probing MMP activity *in vivo* (Figure VI-2b). For example, Cy5 dyes are attached via MMP-2 and -9 cleavable peptides to a linear PEG-grafted polylysine backbone[24]. Cy5 are self-quenching probes and so the proteolysis of MMP-2 or -9 are required to produce an amplified signal. The group developed this probe with the intention to provide a surrogate marker for MMP inhibitor treatment. They demonstrated that the treatment with a MMP inhibitor (prinomastat) resulted in a reduction in the *in vivo* signal in the MMP-2 and -9 expressing tumor, thereby providing a readout about the effectiveness of the inhibitor.

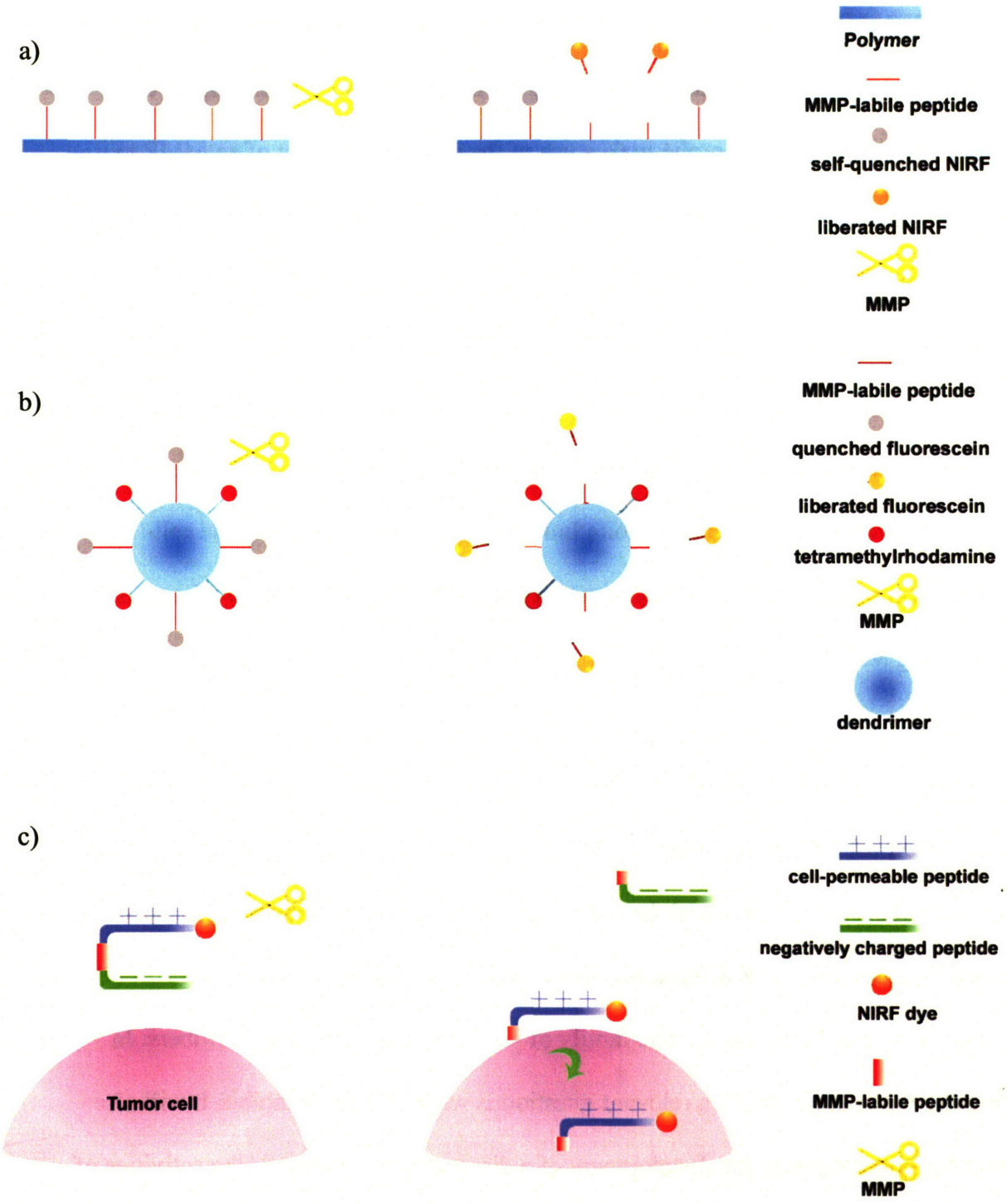

Figure VI-2. Schematics of MMP-activatable imaging probes: a) Fluorescein dyes are freed upon MMP cleavage from the dendrimer with bound tetramethylrhodamine molecules resulting in fluorescein signals; b) NIRF dyes are self-quenched when joined to a polymer backbone and are liberated upon the MMP proteolysis; c) Cell-permeable peptide carries the NIRF probe into intracellular space after being released from the linkage with a peptide containing multiple negative charges

The first type of probe uses a polymeric carrier to enhance the circulation half-life. The proteolytic event is required to amplify the signal. To increase the signal to noise ratio, the second type of probe makes use of the proteolytic event of an MMP to increase the intracellular accumulation of dyes, which are otherwise cleared rapidly from the body. This approach, developed by Jiang and co-workers, is illustrated in

Figure VI-2c [25]. A cell-permeable peptide is a part of this probe, a sequence to bring a NIRF probe inside a cell. The cell-permeable peptide is highly positively charged and its internalization capability is abolished by covalently joining to a highly negatively charged peptide via a MMP-2 and -9 labile linker. The probe is restored to the cell-permeable form by proteolytic activity; hence it is selectively internalized by the cells overexpressing MMPs.

As discussed earlier, MMPs are implicated in a number of major diseases. In addition to their role in imaging cancer, MMP-activatable probes should be useful for the diagnosis of other MMP-associated diseases. As MMP inhibitors are being developed to treat these diseases, an MMP-activatable probe is important for monitoring the effectiveness of MMP inhibition. The family of MMPs consists of many members. In selecting the therapeutic target, a relevant question is which MMP to inhibit. It will also be useful for understanding the development of a disease if we can image the activities of different members of MMPs with multiple probes, or better yet, with a single probe containing multiple channels. The major challenge is that the cleavable peptide for one member of MMP is also a substrate for a different member, albeit at a lower rate. As

shown in Turk's report, the consensus sequences for some MMPs are digested at a rate on the same order of magnitude by other MMPs [22] (Table VI-3).

Table VI-3. Kinetic parameters for the cleavage of a series of consensus peptides by six MMPs[22]

	Peptide substrate k_{cat}/K_m ($M^{-1}s^{-1}$)						
Enzyme	**Collagen GPQG-IACQ**	**MMP-1 consensus VPMS-MRGG**	**MMP-2 consensus IPVS-LRSG**	**MMP-3 consensus RPFS-MIMG**	**MMP-7 consensus VPLS-LTMG**	**MMP-9 consensus VPLS-LYSG**	**MT1-MMP consensus IPES-LRAG**
MMP-1	27.4 ± 0.9	1,600 ± 100	98 ± 7	440 ± 20	300 ± 50	2,100 ± 300	870 ±30
MMP-2	10,100 ± 400	24,000 ± 1000	82,000 ± 6000	4,600 ± 500	13,200 ± 400	61,000 ± 4000	24,000 ± 3000
MMP-3	160 ± 40	3,900 ± 400	2,300 ± 100	6,900 ± 200	2,400 ± 200	1,390 ± 30	1,500 ±100
MMP-7	180 ± 20	7,900 ± 900	9,700 ± 400	12,000 ± 1500	120,000 ± 20,000	22,000 ± 3000	12,000 ± 600
MMP-9	8,400 ± 200	51,000 ±3000	11,500 ± 300	21,000 ± 4000	20,000 ± 1000	49,000 ± 3000	12,600 ± 800
MT1-MMP	3,600 ± 200	6,100 ± 300	4,300 ±300	3,700 ± 300	10,300 ±700	5,500 ± 300	6,900 ± 500

MMP-responsive material for tissue engineering

A more recent application making use of the MMP-mediation is found in the field of tissue engineering. The design of a biomimetic material for tissue regeneration has been of great interest to many research groups. In the natural environments, cells are surrounded by the extracellular matrix and the process of morphogenesis involves the degradation and deposition of the extracellular matrix. The active remodeling of the ECM during tissue regeneration shares some similarities with the process of tumor expansion. MMPs, whose members can degrade all major components of the ECM, are key proteases in breaking down ECM to make room for the growing tissues. The ability to grow vascularized tissues is at the heart of tissue engineering. We have learnt from cancer biology that MMPs are implicated in tumor angiogenesis, whose activities release growth factors such as VEGF and expose cryptic angiogenic epitopes in the collagen[1]. In the context of tissue engineering, *in vitro* experiments have demonstrated the importance of several MT-MMPs with blood vessel growth and tube formation[26-28]. In addition to providing the mechanical support, ECM is now considered a reservoir of signals that direct growth and differentiation of the growing tissue. These signals are released in a cell-mediated manner, by the proteases anchored on the cell membrane or in the interstitial space. Since ECM components are the natural substrates for MMPs, their roles in regulating morphogenic cues are important[2].

Natural materials derived from the ECM are popular for building tissue engineering scaffolds. Collagen and fibrin, for example, have found uses in bone[29], cartilage[30] and skin repair[31]. They can be degraded by an MMP-mediated process. However, problems such as immunogenicity and disease transmission have caused concerns for their clinical use. Synthetic materials such as PLGA circumvent these issues. However, they are usually degraded by hydrolysis and do not reflect the natural process of tissue remodeling.

Hubbell's lab has pioneered a new class of synthetic materials that mimic the MMP-driven degradation of the ECM. They developed a network of PEG crosslinked by oligopeptides that are substrates for MMPs (Figure VI-3a). An example of this type of PEG gel, with covalently linked RGD-containing peptides as cell attachment signals and embedded bone morphogenic protein (BMP), was tested *in vivo* for bone healing[32].They demonstrated *in vitro* that this new gel was susceptible to MMP-1 and the rate of degradation increased with enzyme concentration. When fibroblasts were seeded on the gel, invasion fronts were observed as the cells penetrated. Localized instead of bulk degradation of the gel occurred. This cell-derived degradation process is similar to the intrinsic ECM remodeling process. This concept has also been applied to an injectable hydrogel that exhibits phase transition behavior around lower critical solution temperature (LCST)[33]. Kim and Healy reasoned that when the cartilage was replaced by the bone during the endochnodral bone formation, type-II collagen was likely degraded by the MMP-13 secreted by the osteoblasts. They prepared a poly(N-isopropylacrylamide-co-acrylic acid) hydrogel crosslinked by MMP-13 labile peptides,

and demonstrated weight loss from the gel as a result of the enzymatic degradation by a collagenase.

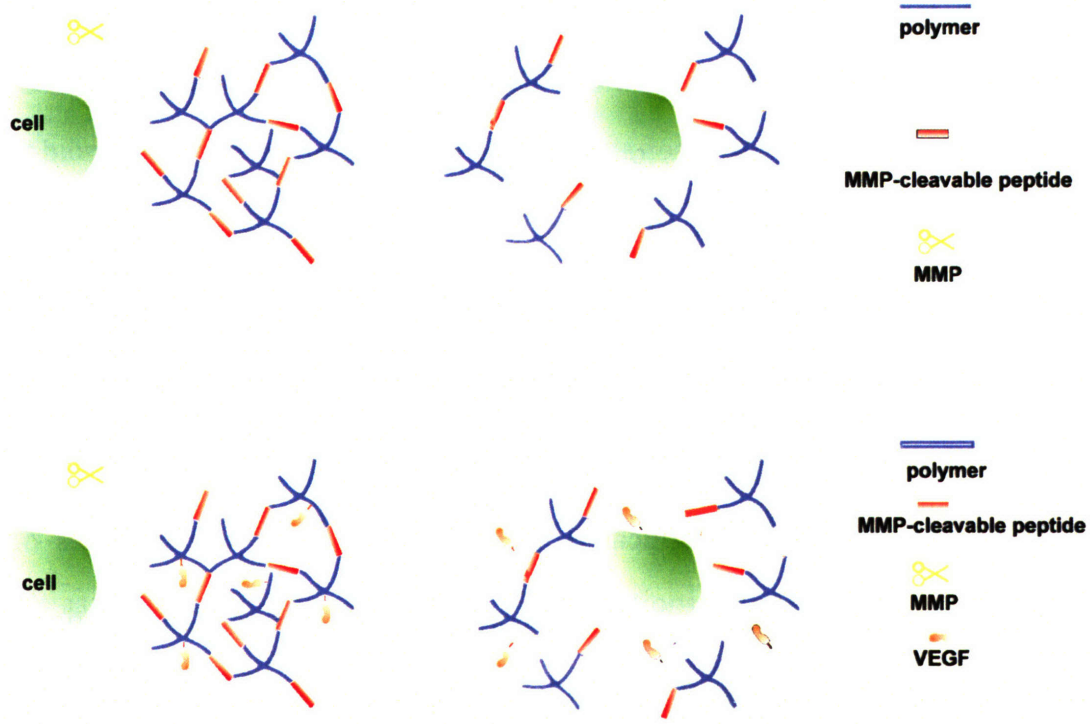

Figure VI-3. Schematics of MMP-responsive material as tissue engineering scaffolds: a) polymer chains are crosslinked with MMP-labile sequences and the network is degraded upon MMP digestion; b) growth factors are covalently bound to the synthetic polymeric scaffold with MMP-cleavable peptides and the cell-demanded release of the growth factors is achieved by the proteolytic digestion of MMP

In addition to invading the ECM, the cell-derived MMPs release various growth factors during the morphogenic process. Vascular endothelial growth factors (VEGF) are important molecules for inducing angiogenesis as they promote the growth of endothelial cells. Several isoforms of VEGF bind tightly to the heparin sulfate proteoglycans of the ECM[34]. MMP-9 and other MMPs are shown to be able to mobilize the matrix-bound VEGF[35]. To imitate this phenomenon, Hubbell's lab covalently linked VEGF to the PEG hydrogel with an MMP-sensitive linker[36] (Figure VI-3b) . They hypothesized that as the

cells migrate into the PEG gel, the release of VEGF is triggered by the cell-derived MMP and localized angiogenesis takes place. They demonstrated that, using a CAM assay (embryonic chick choriallontoic membrane assay), angiogenesis occurred at the gel-membrane interface. They also showed that vascularized tissue formed within the VEGF-containing gel when implanted subcutaneously in rats.

Unlike VEGF, which remains biologically active when bound to the ECM, transforming growth factor-β (TGF- β) is presented as a latent complex bound to the ECM though its latency-associated peptide (LAP)[37]. A number of MMPs (MMP-2,-9,-13, and MT1-MMP) are shown to be critical in activating TGF- β at various stages of morphogenic development[38, 39]. TGF- β is an important factor with multiple functions, including the synthesis of ECM[40]. If dysregulated, TGF- β contributes to the pathological process that comprises of excessive ECM deposition, such as scarring and fibrosis[41]. On the other hand, a controlled ECM synthesis by the seeded cells is necessary in tissue regeneration. It is attractive to consider mimicking the MMP-mediated activation of TGF- β in a tissue engineering scaffold. The proteolysis events of MMPs play many roles in regulating the components of ECM. They also affect how the cells interface with the surrounding matrix, by cleaving the heparan sulfate proteoglycans on the cell surface which interact with the ECM molecules[42]. On the other hand, ECM molecules can control the expression of MMPs via binding to the cell surface heparan sulfate proteoglycans[43]. Further understanding of the biological consequences of these processes, their effects on cellular differentiation and tissue architecture, should provide useful guidelines to enhance biomimectic material design employing MMPs as mediators.

Concluding remarks

Exploiting disease-associated enzymes as mediators is a versatile tool useful in different biomedical applications. The elegance of this concept is that it relies on a simple event: the proteolysis of a target enzyme. The widely studied MMPs are interesting disease-associated enzymes. They are involved in tissue remodeling and many pathological processes. Their roles have expanded beyond weakening the mechanical strength of the ECM to releasing important cellular signals and providing biochemical feedback between the cells and their environments. MMPs have shown tremendous potentials as mediators in various biomedical applications. We have surveyed the fields of MMP inhibitor therapy, MMP-triggered drug delivery, MMP-activated imaging and MMP-responsive biomaterial for tissue engineering. Since the pathological processes share the common theme of MMP dysregulation, the useful application for one disease – whether it is MMP inhibitor treatment, imaging or drug delivery – is relevant and transferable to another disease indication. Significant cross-talking is not only possible but is synergetic between different biomedical applications. The quest of more specific substrates for different MMPs is obviously essential for developing MMP inhibitors as therapeutics, at the same time the results should enable the design of better imaging probes and drug delivery vehicles mediated by specific MMPs. There are overlaps in the strategies for making use of MMPs in targeted imaging and targeted drug delivery. Besides the difference in dose requirement, the major discrepancy is that imaging is concerned with a snapshot in time and drug delivery considers the cumulative effect over

time. In addition, MMP-mediated release of signaling molecules on cellular demand is an appealing approach for tissue engineering. Biomaterials developed for this purpose can also find applications as local drug delivery depots for the treatment of diseases which are localized in nature, including but not limited to cardiovascular diseases and arthritis.

References

1. Egeblad M, Werb Z. New functions for the matrix metalloproteinases in cancer progression. *Nature Reviews Cancer* 2002;2(3):161-74.

2. Mott JD, Werb Z. Regulation of matrix biology by matrix metalloproteinases. *Current Opinion in Cell Biology* 2004;16(5):558-64.

3. Coussens LM, Fingleton B, Matrisian LM. Cancer therapy - Matrix metalloproteinase inhibitors and cancer: Trials and tribulations. *Science* 2002;295(5564):2387-92.

4. Overall CM, Lopez-Otin C. Strategies for MMP inhibition in cancer: Innovations for the post-trial era. *Nature Reviews Cancer* 2002;2(9):657-72.

5. Zucker S, Cao J, Chen WT. Critical appraisal of the use of matrix metalloproteinase inhibitors in cancer treatment. *Oncogene* 2000;19(56):6642-50.

6. Chau Y, Langer RS. Important factors in designing targeted delivery of cancer therapeutics via MMP-2 mediation. *Journal of Controlled Release* 2003;91(1-2):239-40.

7. Chau Y, Tan FE, Langer R. Synthesis and characterization of dextran-peptide-methotrexate conjugates for tumor targeting via mediation by matrix metalloproteinase II and matrix metalloproteinase IX. *Bioconjugate Chemistry* 2004;15(4):931-41.

8. Mansour AM, Drevs J, Esser N, Hamada FM, Badary OA, Unger C, Fichtner I, Kratz F. A new approach for the treatment of malignant melanoma: Enhanced antitumor efficacy of an albumin-binding doxorubicin prodrug that is cleaved by matrix metalloproteinase 2. *Cancer Research* 2003;63(14):4062-66.

9. Chau Y, Padera RF, Dang NM, Langer R. Anti-tumor efficacy of a novel polymer-peptide-drug conjugate in human tumor xenograft models. *Submitted to International Journal of Cancer* 2005.

10. Peng KW, Morling FJ, Cosset FL, Murphy G, Russell SJ. A gene delivery system activatable by disease-associated matrix metalloproteinases. *Human Gene Therapy* 1997;8(6):729-38.

11. Liu SH, Netzel-Arnett S, Birkedal-Hansen H, Leppla SH. Tumor cell-selective cytotoxicity of matrix metalloproteinase-activated anthrax toxin. *Cancer Research* 2000;60(21):6061-67.

12. Yu Q, Stamenkovic I. Localization of matrix metalloproteinase 9 to the cell surface provides a mechanism for CD44-mediated tumor invasion. *Genes & Development* 1999;13(1):35-48.

13. Polette M, Birembaut P. Membrane-type metalloproteinases in tumor invasion. *International Journal of Biochemistry & Cell Biology* 1998;30(11):1195-202.

14. Brooks PC, Stromblad S, Sanders LC, vonSchalscha TL, Aimes RT, StetlerStevenson WG, Quigley JP, Cheresh DA. Localization of matrix metalloproteinase MMP-2 to the surface of invasive cells by interaction with integrin alpha v beta 3. *Cell* 1996;85(5):683-93.

15. Carrel F, Amstutz H, NovakHofer I, Schubiger PA. Evaluation of radioiodinated and radiocopper labeled monovalent fragments of monoclonal antibody chCE7 for targeting of neuroblastoma. *Nuclear Medicine and Biology* 1997;24(6):539-46.

16. Ohkubo S, Miyadera K, Sugimoto Y, Matsuo K, Wierzba K, Yamada Y. Identification of substrate sequences for membrane type-1 matrix metalloproteinase using

bacteriophage peptide display library. *Biochemical and Biophysical Research Communications* 1999;266(2):308-13.

17. Hayashi M, Tomita M, Yoshizato K. Interleukin-2-collagen chimeric protein which liberates interleukin-2 upon collagenolysis. *Protein Engineering* 2002;15(5):429-36.

18. Spinale FG, Gunasinghe H, Sprunger PD, Baskin JM, Bradham WC. Extracellular degradative pathways in myocardial remodeling and progression to heart failure. *Journal of Cardiac Failure* 2002;8(6):S332-S38.

19. Libby P. Inflammation in atherosclerosis. *Nature* 2002;420(6917):868-74.

20. Vincenti MP, Brinckerhoff CE. Transcriptional regulation of collagenase (MMP-1, MMP-13) genes in arthritis: integration of complex signaling pathways for the recruitment of gene-specific transcription factors. *Arthritis Research* 2002;4(3):157-64.

21. Woessner JF, Nagase H. Matrix Metalloproteinases and TIMPs. New York: Oxford university press, 2000.

22. Turk BE, Huang LL, Piro ET, Cantley LC. Determination of protease cleavage site motifs using mixture-based oriented peptide libraries. *Nature Biotechnology* 2001;19(7):661-67.

23. McIntyre JO, Fingleton B, Wells KS, Piston DW, Lynch CC, Gautam S, Matrisian LM. Development of a novel fluorogenic proteolytic beacon for in vivo detection and imaging of tumour-associated matrix metalloproteinase-7 activity. *Biochemical Journal* 2004;377:617-28.

24. Bremer C, Tung CH, Weissleder R. In vivo molecular target assessment of matrix metalloproteinase inhibition. *Nature Medicine* 2001;7(6):743-48.

25. Jiang T, Olson ES, Nguyen QT, Roy M, Jennings PA, Tsien RY. Tumor imaging by means of proteolytic activation of cell-penetrating peptides. *Proceedings of the National Academy of Sciences of the United States of America* 2004;101(51):17867-72.

26. Plaisier M, Kapiteijn K, Koolwijk P, Fijten C, Hanemaaijer R, Grimbergen JM, Mulder-Stapel A, Quax PHA, Helmerhorst FM, van Hinsbergh VWM. Involvement of membrane-type matrix metalloproteinases (MT-MMPs) in capillary tube formation by human endometrial microvascular endothelial cells: Role of MT3-MMP. *Journal of Clinical Endocrinology and Metabolism* 2004;89(11):5828-36.

27. Collen A, Hanemaaijer R, Lupu F, Quax PHA, van Lent N, Grimbergen J, Peters E, Koolwijk P, van Hinsbergh VWM. Membrane-type matrix metalloproteinase-mediated angiogenesis in a fibrin-collagen matrix. *Blood* 2003;101(5):1810-17.

28. Lafleur MA, Handsley MM, Knauper V, Murphy G, Edwards DR. Endothelial tubulogenesis within fibrin gels specifically requires the activity of membrane-type-matrix metalloproteinases (MT-MMPs). *Journal of Cell Science* 2002;115(17):3427-38.

29. Uludag H, D'Augusta D, Golden J, Li J, Timony G, Riedel R, Wozney JM. Implantation of recombinant human bone morphogenetic proteins with biomaterial carriers: A correlation between protein pharmacokinetics and osteoinduction in the rat ectopic model. *Journal of Biomedical Materials Research* 2000;50(2):227-38.

30. Okamoto T, Yamamoto Y, Gotoh M, Liu D, Kihara M, Kameyama K, Hayashi E, Nakamura K, Yamauchi A, Huang CL, Yokomise H, Yamamoto M, et al. Cartilage regeneration using slow release of bone morphogenetic protein-2 from a gelatin sponge to treat experimental canine tracheomalacia: A preliminary report. *Asaio Journal* 2003;49(1):63-69.

31. Horch RE, Bannasch H, Stark GB. Transplantation of cultured autologous keratinocytes in fibrin sealant biomatrix to resurface chronic wounds. *Transplantation Proceedings* 2001;33(1-2):642-44.

32. Lutolf MP, Lauer-Fields JL, Schmoekel HG, Metters AT, Weber FE, Fields GB, Hubbell JA. Synthetic matrix metalloproteinase-sensitive hydrogels for the conduction of tissue regeneration: Engineering cell-invasion characteristics. *Proceedings of the National Academy of Sciences of the United States of America* 2003;100(9):5413-18.

33. Kim S, Healy KE. Synthesis and characterization of injectable poly(N-isopropylacrylamide-co-acrylic acid) hydrogels with proteolytically degradable cross-links. *Biomacromolecules* 2003;4(5):1214-23.

34. Park JE, Keller GA, Ferrara N. Vascular Endothelial Growth-Factor (Vegf) Isoforms - Differential Deposition into the Subepithelial Extracellular-Matrix and Bioactivity of Extracellular Matrix-Bound Vegf. *Molecular Biology of the Cell* 1993;4(12):1317-26.

35. Belotti D, Paganoni P, Manenti L, Garofalo A, Marchini S, Taraboletti G, Giavazzi R. Matrix metalloproteinases (MMP9 and MMP2) induce the release of vascular endothelial growth factor (VEGF) by ovarian carcinoma cells: Implications for ascites formation. *Cancer Research* 2003;63(17):5224-29.

36. Zisch AH, Lutolf MP, Ehrbar M, Raeber GP, Rizzi SC, Davies N, Schmokel H, Bezuidenhout D, Djonov V, Zilla P, Hubbell JA. Cell-demanded release of VEGF from synthetic, biointeractive cell-ingrowth matrices for vascularized tissue growth. *Faseb Journal* 2003;17(13).

37. Annes JP, Munger JS, Rifkin DB. Making sense of latent TGF beta activation. *Journal of Cell Science* 2003;116(2):217-24.

38. D'Angelo M, Sarment DP, Billings PC, Pacifici M. Activation of transforming growth factor beta in chondrocytes undergoing endochondral ossification. *Journal of Bone and Mineral Research* 2001;16(12):2339-47.

39. Mu DZ, Cambier S, Fjellbirkeland L, Baron JL, Munger JS, Kawakatsu H, Sheppard D, Broaddus VC, Nishimura SL. The integrin alpha v beta 8 mediates epithelial homeostasis through MT1-MMP-dependent activation of TGF-beta 1. *Journal of Cell Biology* 2002;157(3):493-507.

40. Verrecchia F, Mauviel A. Transforming growth factor-beta signaling through the Smad pathway: Role in extracellular matrix gene expression and regulation. *Journal of Investigative Dermatology* 2002;118(2):211-15.

41. Ihn H. Pathogenesis of fibrosis: role of TGF-beta and CTGF. *Current Opinion in Rheumatology* 2002;14(6):681-85.

42. Endo K, Takino T, Miyamori H, Kinsen H, Yoshizaki T, Furukawa M, Sato H. Cleavage of syndecan-1 by membrane type matrix metalloproteinase-1 stimulates cell migration. *Journal of Biological Chemistry* 2003;278(42):40764-70.

43. Utani A, Momota Y, Endo H, Kasuya Y, Beck K, Suzuki N, Nomizu M, Shinkai H. Laminin alpha 3 LG4 module induces matrix metalloproteinase-1 through mitogen-activated protein kinase signaling. *Journal of Biological Chemistry* 2003;278(36):34483-90.

APPENDIX A : Histological illustrations of small intestines from tumor-bearing mice undergone different treatments

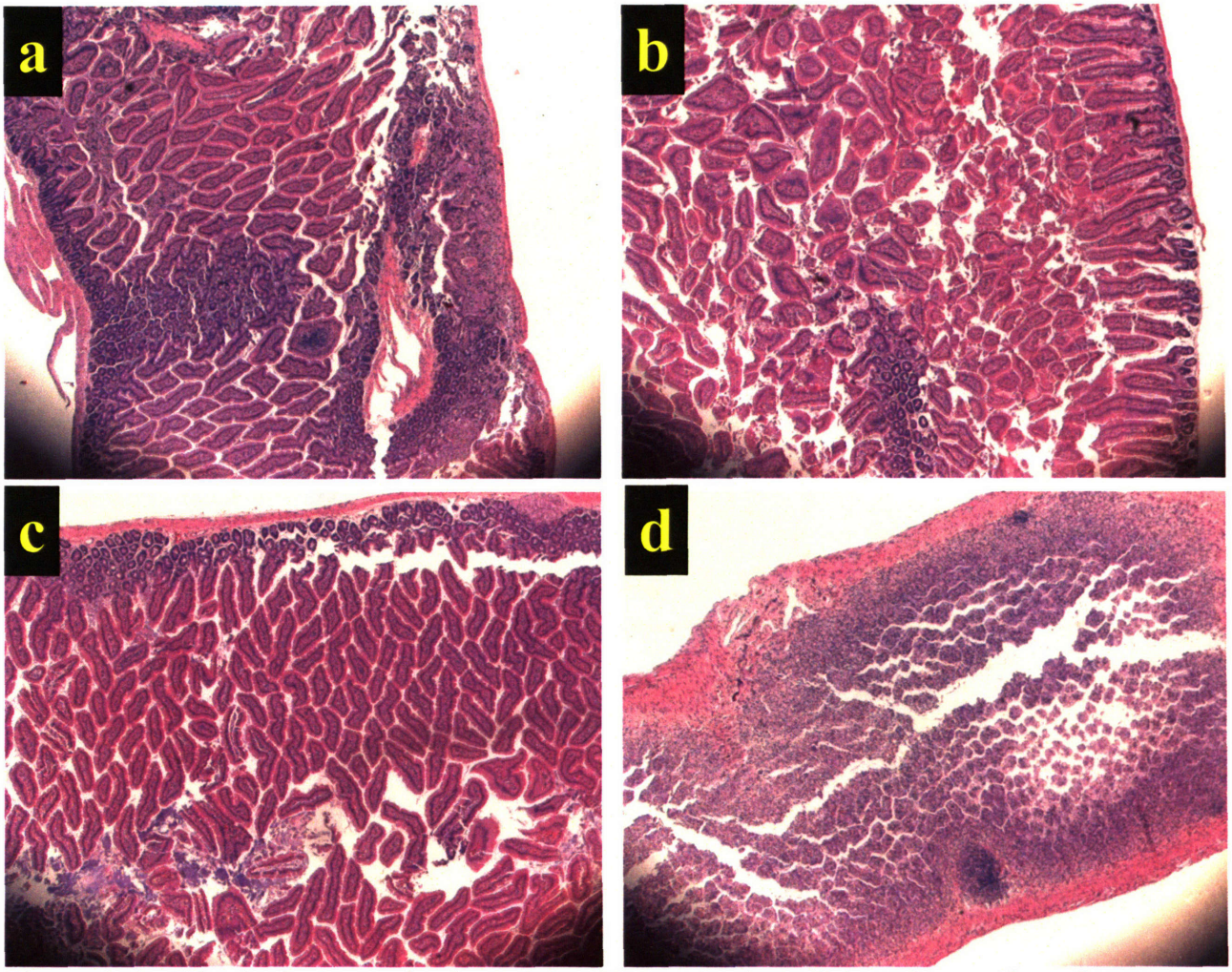

Figure A-1. Histological examination of the H&E stained small intestine sections from U-87 bearing mice. Tissues were harvested from mice treated with : a) 2 injections of saline (control); b) 2 injections of free methotrexate ; c) 2 injections of conjugate MTX-PVGLIG-dextran; d) 1 injection of conjugate MTX-GIVGPL-dextran.

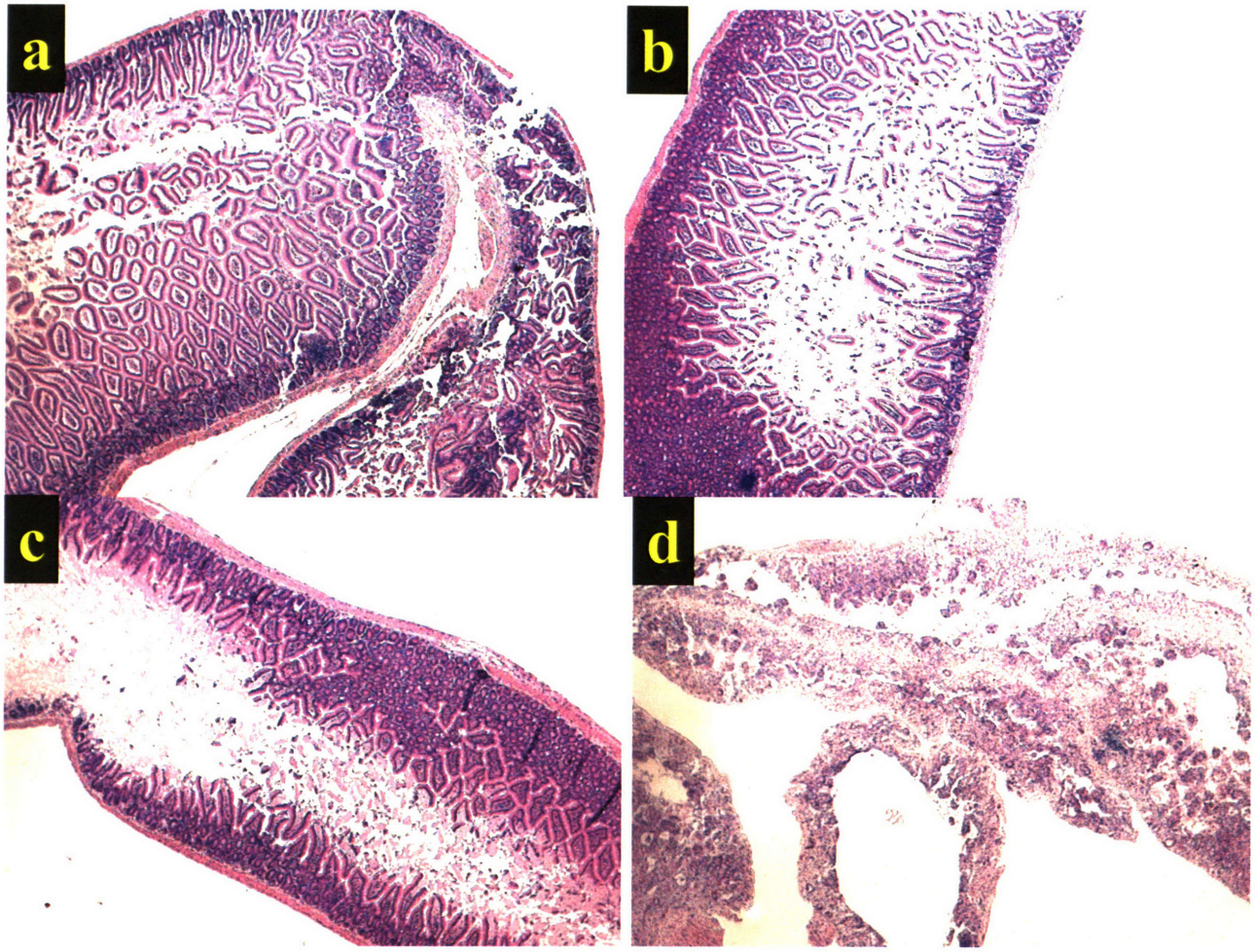

Figure A-2. Histological examination of the H&E stained small intestine sections from RT-112 bearing mice. Tissues were harvested from mice treated with : a) 3 injections of saline (control); b) 3 injections of free methotrexate ; c) 3 injections of conjugate MTX-PVGLIG-dextran; d) 1 injection of conjugate MTX-GIVGPL-dextran.

APPENDIX B : Histological illustrations of bone marrows from tumor-bearing mice undergone different treatments

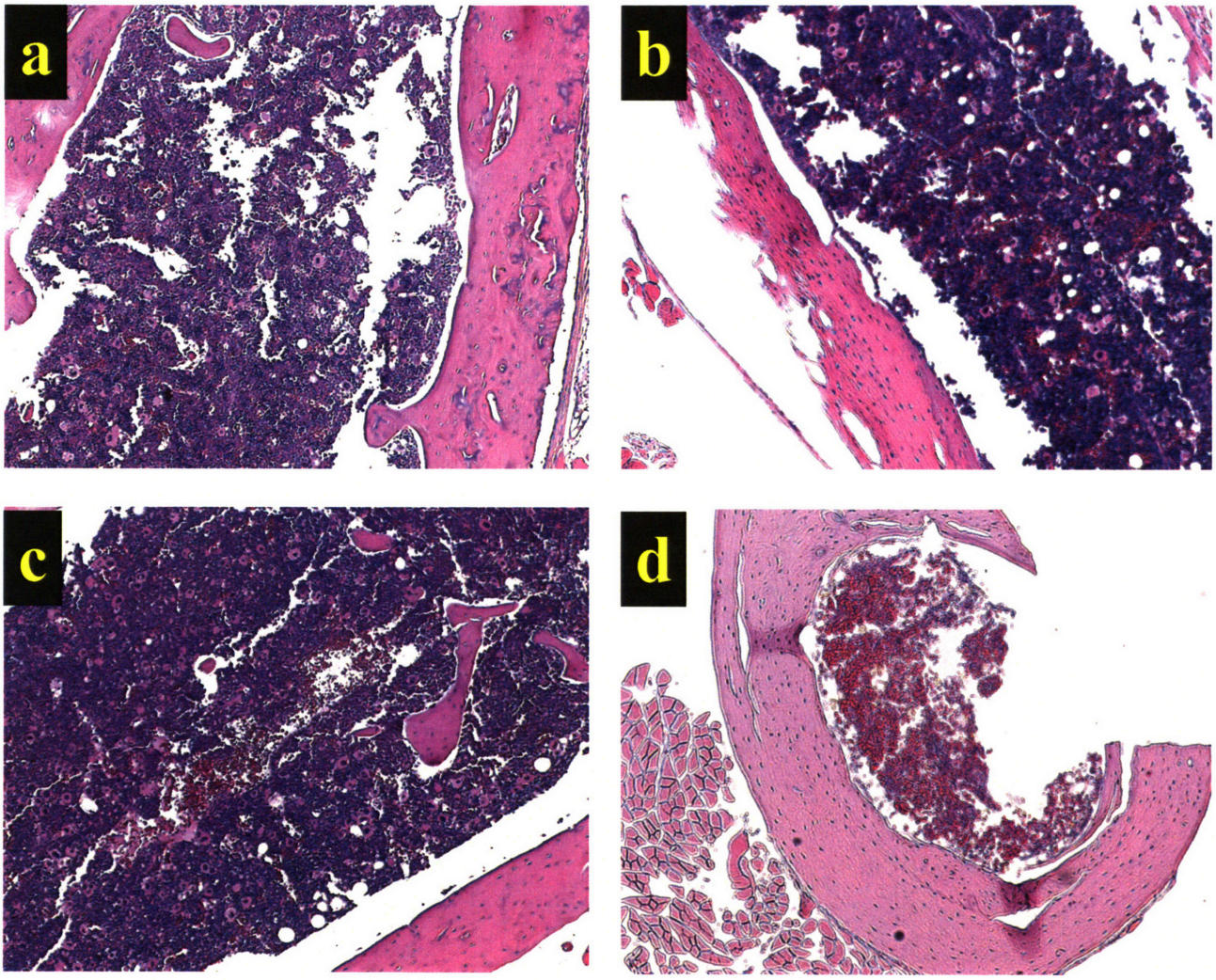

Figure B-1.Histological examination of the H&E stained bone marrow sections from RT-112 bearing mice. Tissues were harvested from mice treated with : a) 3 injections of saline (control); b) 3 injections of free methotrexate ; c) 3 injections of conjugate MTX-PVGLIG-dextran; d) 1 injection of conjugate MTX-GIVGPL-dextran.

APPENDIX C : Histological illustrations of livers from tumor-bearing mice undergone different treatments

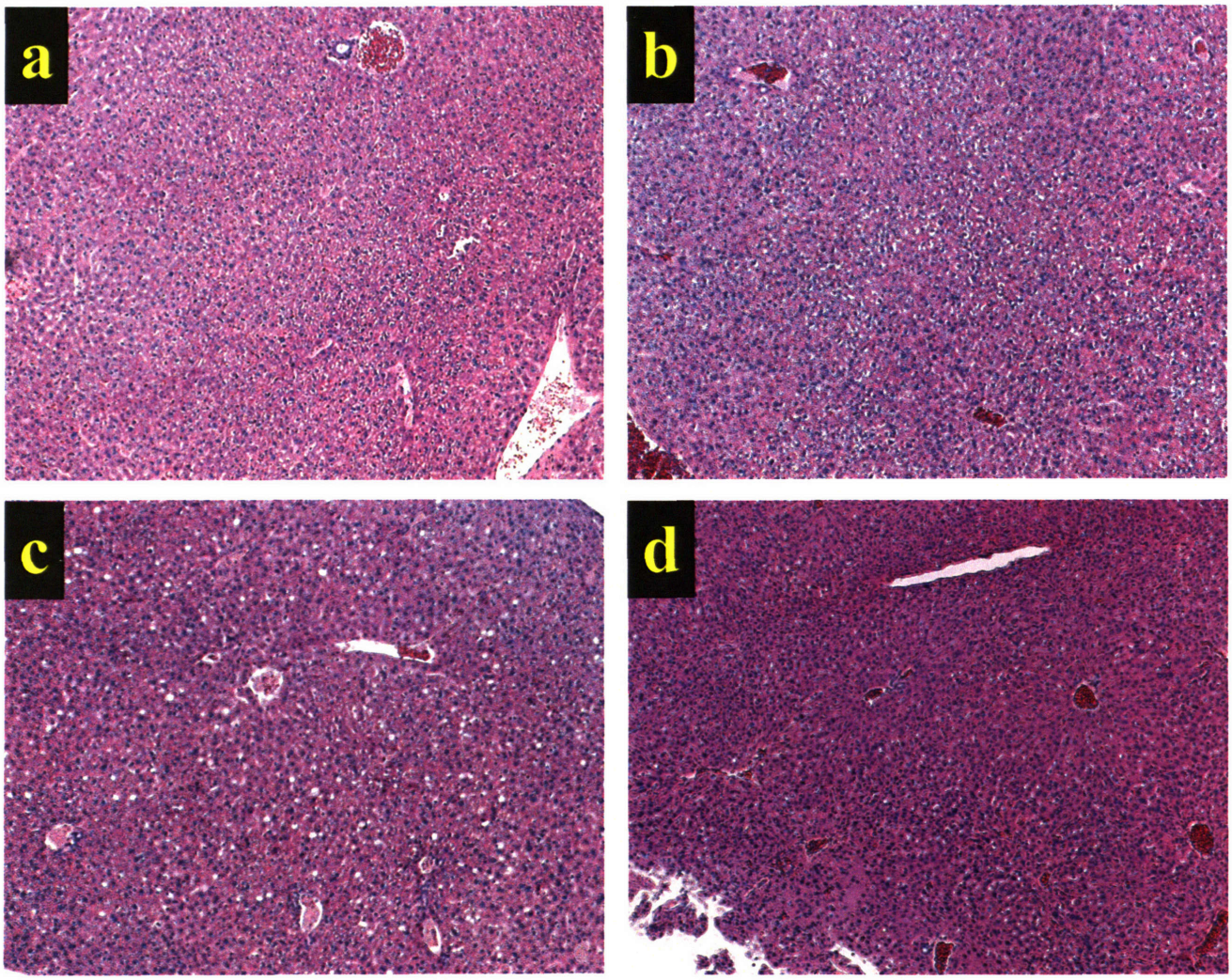

Figure C-1. Histological examination of the H&E stained liver sections from RT-112 bearing mice. Tissues were harvested from mice treated with : a) 3 injections of saline (control); b) 3 injections of free methotrexate ; c) 3 injections of conjugate MTX-PVGLIG-dextran; d) 1 injection of conjugate MTX-GIVGPL-dextran.

APPENDIX D : Histological illustrations of kidneys from tumor-bearing mice undergone different treatments

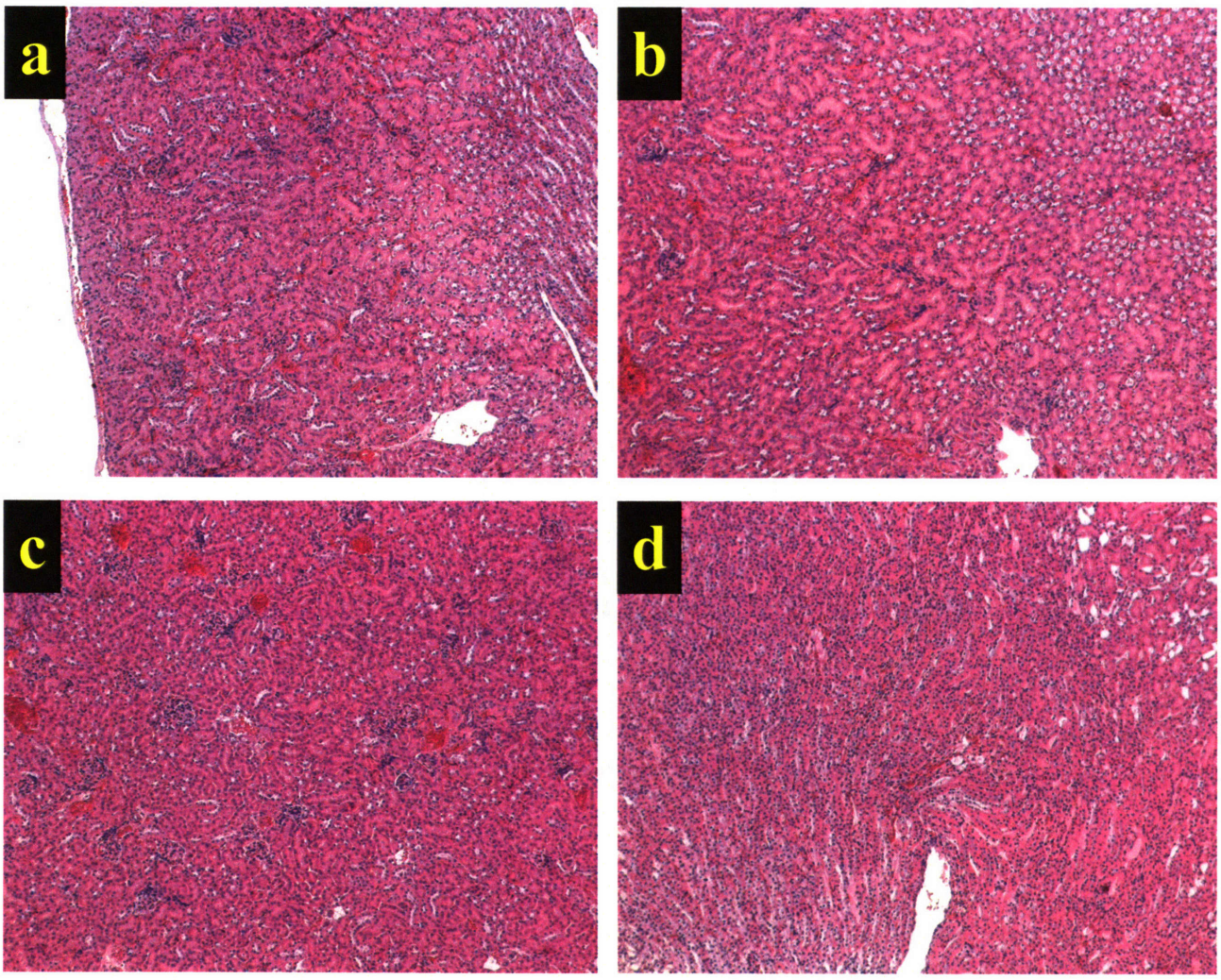

Figure D-1. Histological examination of the H&E stained kidney sections from HT-1080 bearing mice. Tissues were harvested from mice treated with : a) 3 injections of saline (control); b) 3 injections of free methotrexate ; c) 3 injections of conjugate MTX-PVGLIG-dextran; d) 1 injection of conjugate MTX-GIVGPL-dextran.

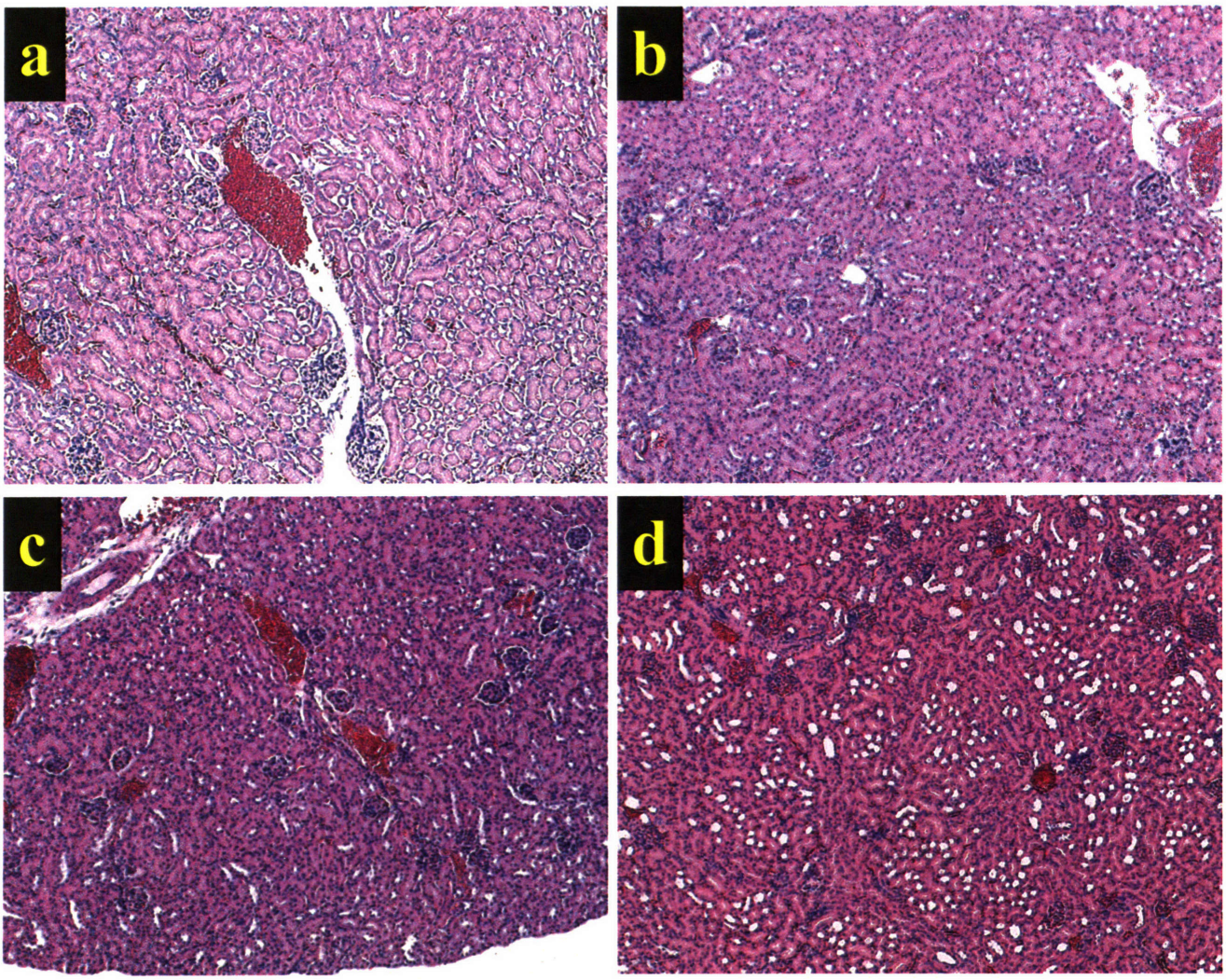

Figure D-2. Histological examination of the H&E stained kidney sections from RT-112 bearing mice. Tissues were harvested from mice treated with : a) 3 injections of saline (control); b) 3 injections of free methotrexate ; c) 3 injections of conjugate MTX-PVGLIG-dextran; d) 1 injection of conjugate MTX-GIVGPL-dextran.

APPENDIX E : Histological illustrations of spleens from tumor-bearing mice undergone different treatments

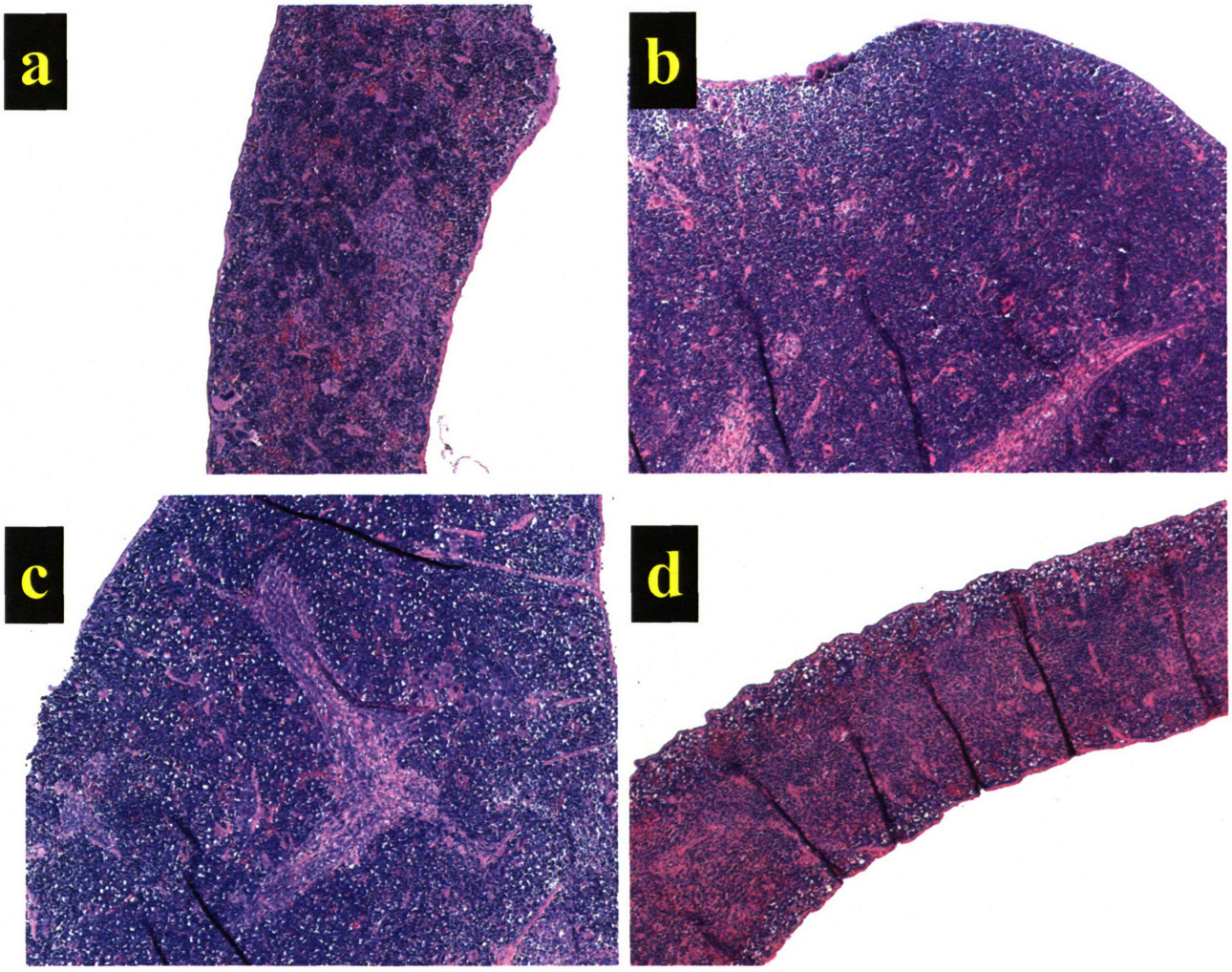

Figure E-1. Histological examination of the H&E stained spleen sections from HT-1080 bearing mice. Tissues were harvested from mice treated with : a) 3 injections of saline (control); b) 3 injections of free methotrexate ; c) 3 injections of conjugate MTX-PVGLIG-dextran; d) 1 injection of conjugate MTX-GIVGPL-dextran.

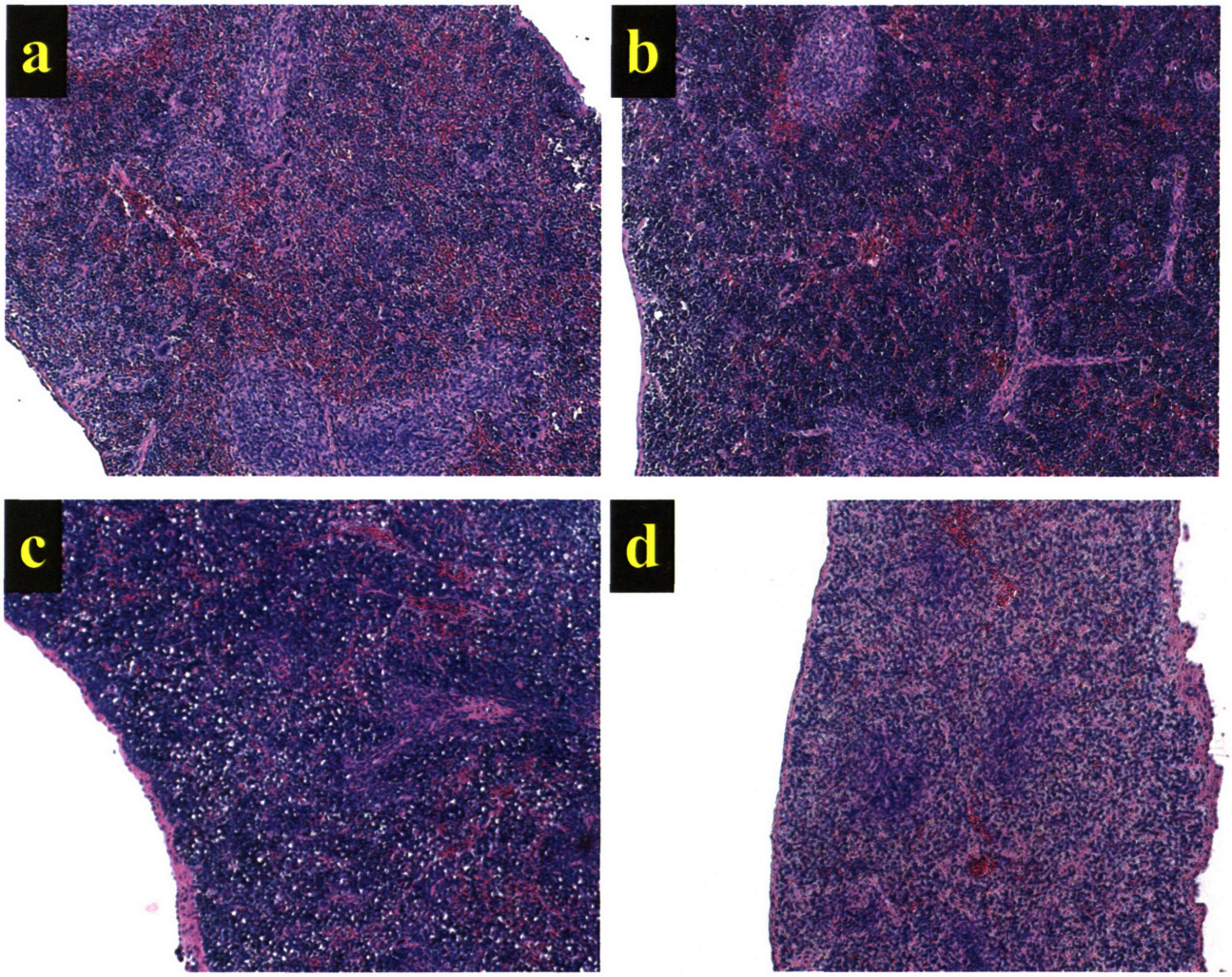

Figure E-2. Histological examination of the H&E stained spleen sections from RT-112 bearing mice. Tissues were harvested from mice treated with : a) 3 injections of saline (control); b) 3 injections of free methotrexate ; c) 3 injections of conjugate MTX-PVGLIG-dextran; d) 1 injection of conjugate MTX-GIVGPL-dextran.

APPENDIX F : Histological illustrations of skin from tumor-bearing mice undergone different treatments

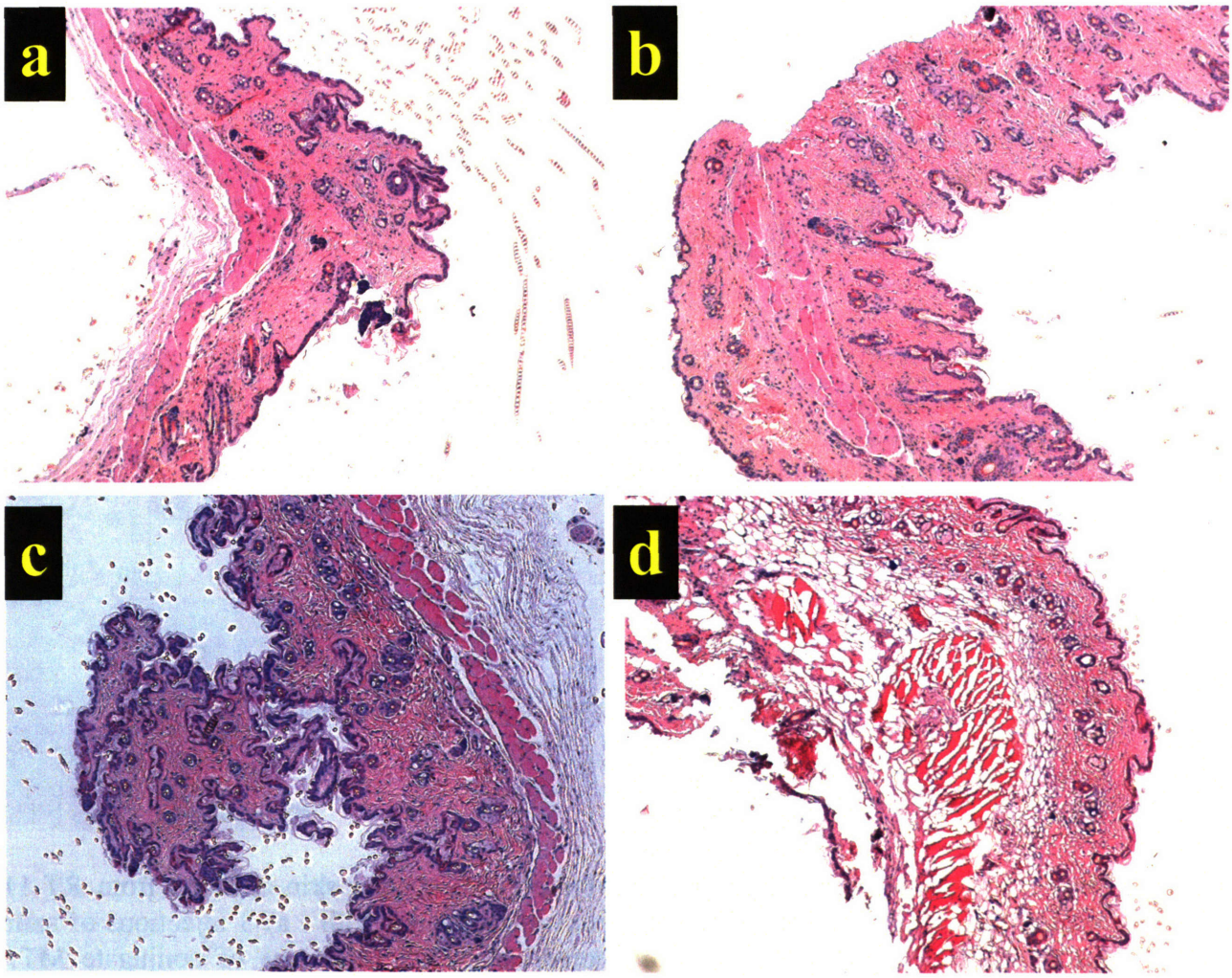

Figure F-1. Histological examination of the H&E stained skin sections from HT-1080 bearing mice. Tissues were harvested from mice treated with : a) 3 injections of saline (control); b) 3 injections of free methotrexate ; c) 3 injections of conjugate MTX-PVGLIG-dextran; d) 1 injection of conjugate MTX-GIVGPL-dextran.

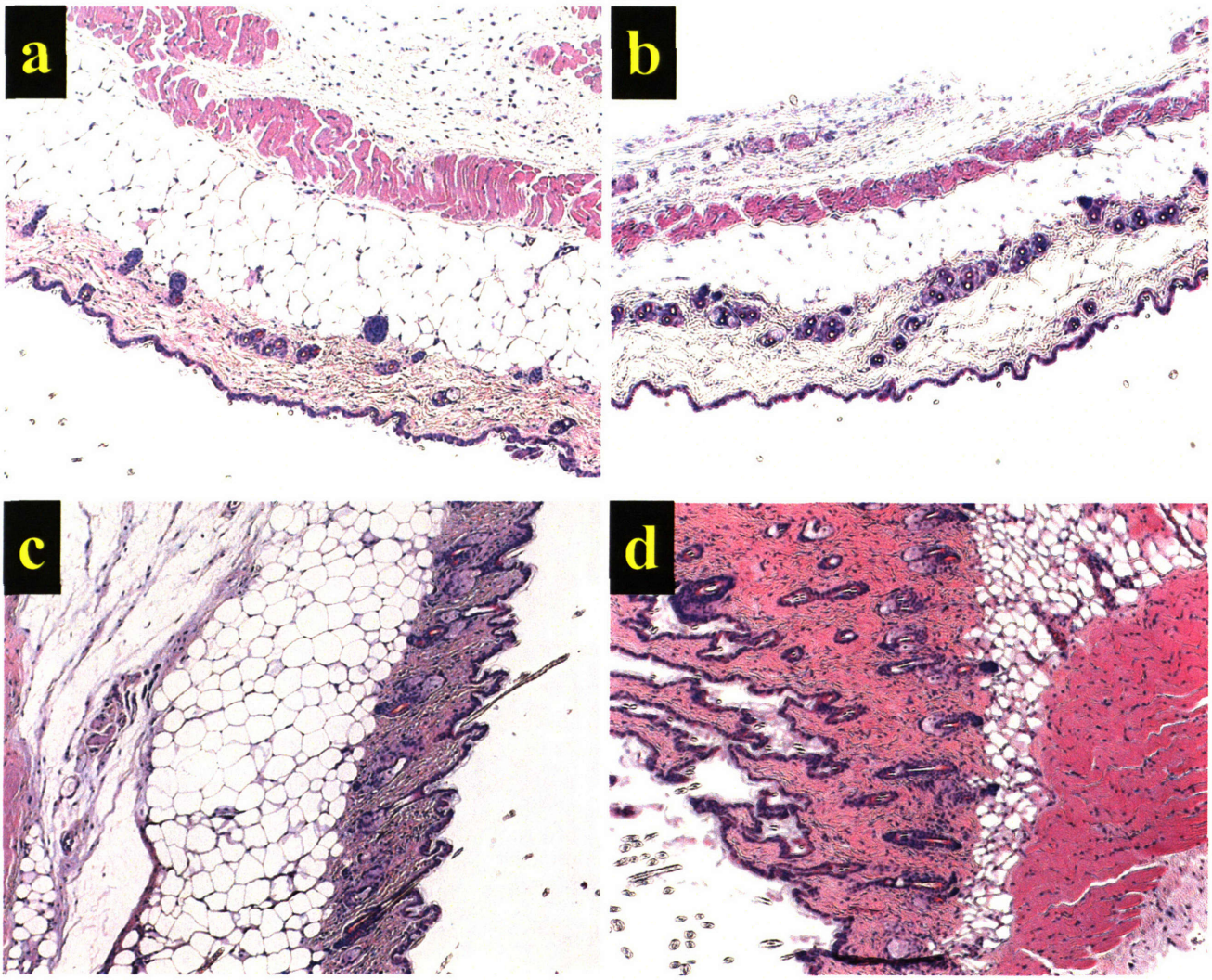

Figure F-2. Histological examination of the H&E stained skin sections from RT-112 bearing mice. Tissues were harvested from mice treated with : a) 3 injections of saline (control); b) 3 injections of free methotrexate ; c) 3 injections of conjugate MTX-PVGLIG-dextran; d) 1 injection of conjugate MTX-GIVGPL-dextran

5413-19